



第二章 表面等离激元的发展、前沿及应用

2.1 表面等离激元发展简史 (1-43)

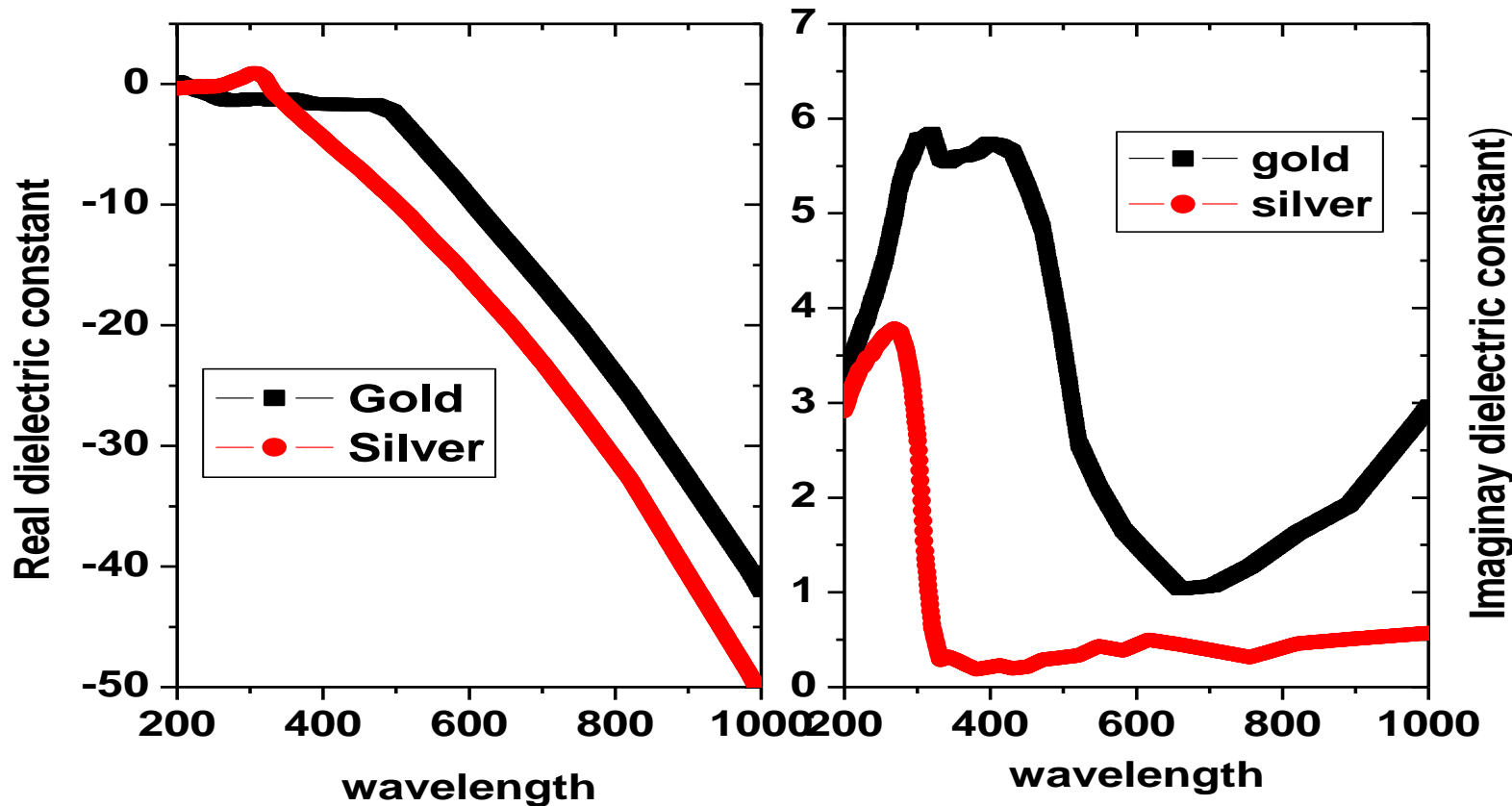
2.2 表面等离激元的应用

2.2.1 表面等离激元 (SPP) 波导 (45-65)

2.2.2 表面等离激元共振 (SPR) 及应用 (67-96)

2.2.3 周期性结构中SPP性质 (98-112)

金和银的介电常数值

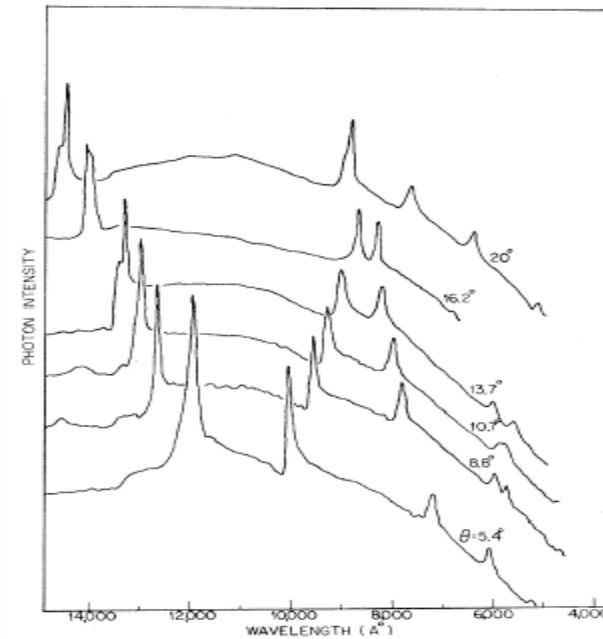
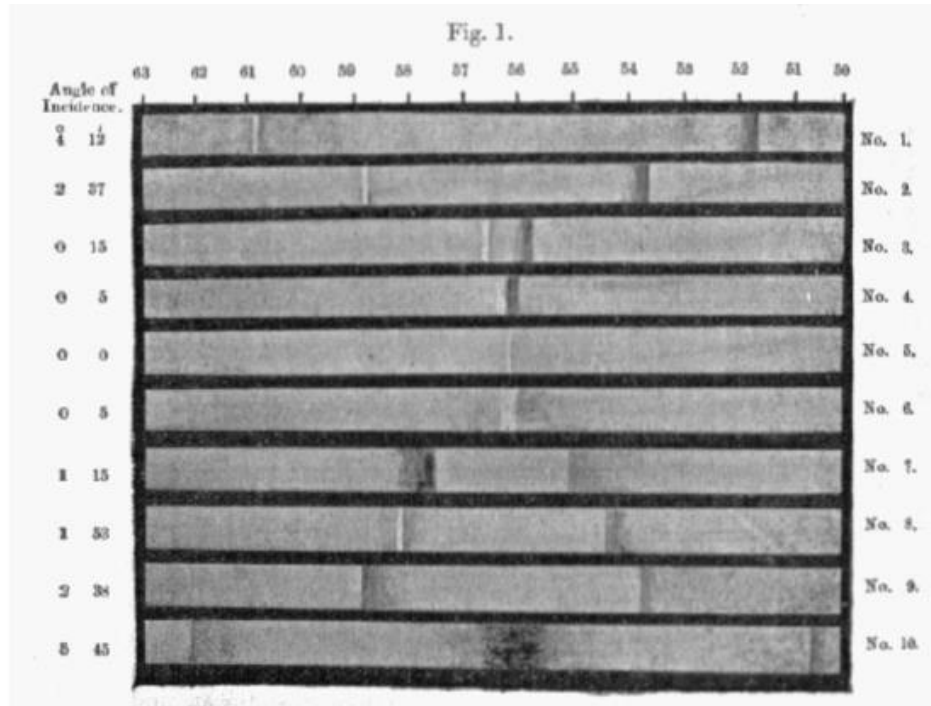


Optical Constants of the Noble Metals

P. B. Johnson and R. W. Christy PRB, 6, 4370 (1972).

2.1 表面等离激元发展简史（按年代）

Wood's anomalies, 1902



On a Remarkable Case of Uneven Distribution of Light in a Diffraction Grating Spectrum

R W Wood 1902 *Proc. Phys. Soc. London* 18 269

SURFACE-PLASMON RESONANCE EFFECT IN GRATING DIFFRACTION

RITCHIE RH, ARAKAWA ET, COWAN JJ, et al (1968) *PRL*, 21, 1530.

Mie theory , 1908

Exact solution of **sphere**, spherical symmetry structure
Absorption, scattering, and extinction

Zenneck (1907) & Sommerfeld (1909)

Demonstrated (theoretically) that radio frequency surface EM waves occur at the boundary of two media when one medium is either a "lossy" dielectric, or a metal, and the other is a loss-free medium.

They also suggested that it is the "lossy" (imaginary) part of the dielectric function that is responsible for binding the EM wave to the interface.

Fano (1939)

Suggested that surface EM waves were responsible for the striking anomalies in the continuous source diffraction spectra of metallic gratings - **'Wood's Anomalies'**

According to Fano : Surface EM wave, at metal-air interfaces, are evanescent waves whose wave vectors are greater than those of the incident and diffracted bulk EM waves, and that the grating augments the wave vector of the incident EM waves enabling them to couple with the surface EM waves.

Fano suggested:

1. surface EM waves at lossy-dielectric-air interfaces at radio frequencies (Zenneck-Sommerfeld waves)
2. surface EM waves at metal-air interfaces in the optical region (Fano modes)
3. loss-free dielectric/air interfaces (Brewster angle EM waves)

"represent for media of different electrical properties the same singular case defined by the same mathematical equation."

Ritchie (1957)

Demonstrated theoretically the existence of Surface plasma excitations (surface plasmons) at a metal surface.

Stern (1958)

Showed (theoretically) that surface EM waves at a metallic surface involved EM radiation coupled to surface plasmons.

Derived, for the first time, the dispersion relations for surface EM waves at metal surfaces.

Powell & Swan (1960)

Observed the excitation of **surface plasmons** at metal interfaces using electrons.

Otto (1968)

Devised the ATR (prism coupling) method for the coupling of bulk EM waves (optical) to surface EM waves.

Kretschmann (1971)

Modified the Otto geometry is now the most widely used device geometry.

Knoll (1989)

Introduced the technique of Surface Plasmon Microscopy

Extraordinary optical transmission

T.W.Ebbesen group , 1998

Start point of SPP

Bottleneck: low light transmittivity of apertures smaller than the wavelength of incident photon

Hole arrays in silver film:
metal film thickness t
Periodicity of holes a_0
Scale of holes d

Results:

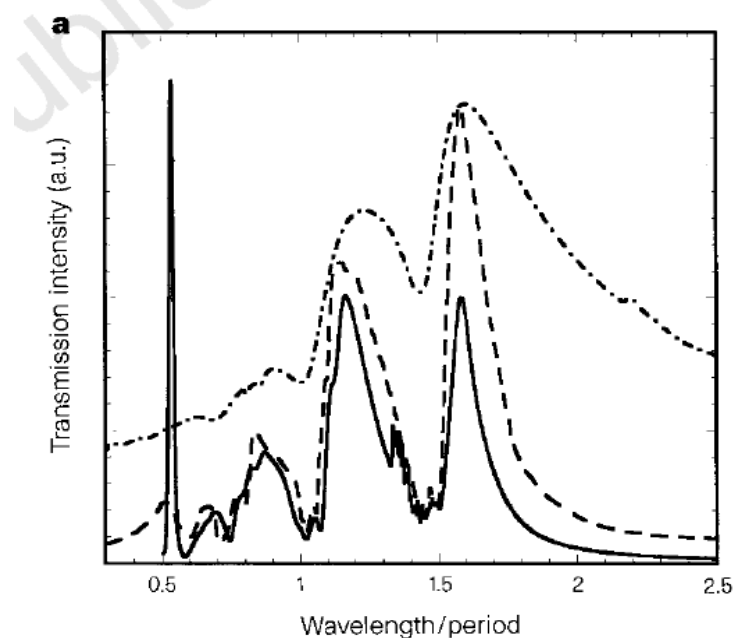
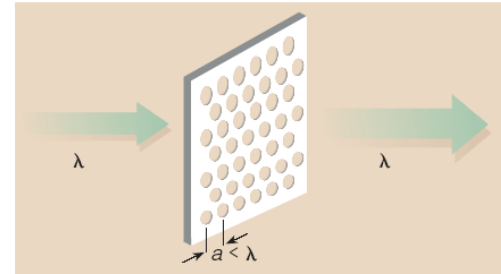
Extraordinary transmission

Maximum at $\lambda/d \sim 10$

Influence of t (in APL)

Explanation:

Coupling of light and plasmons



Beaming light from a bull's eyes structure

T.W.Ebbesen group , 2002

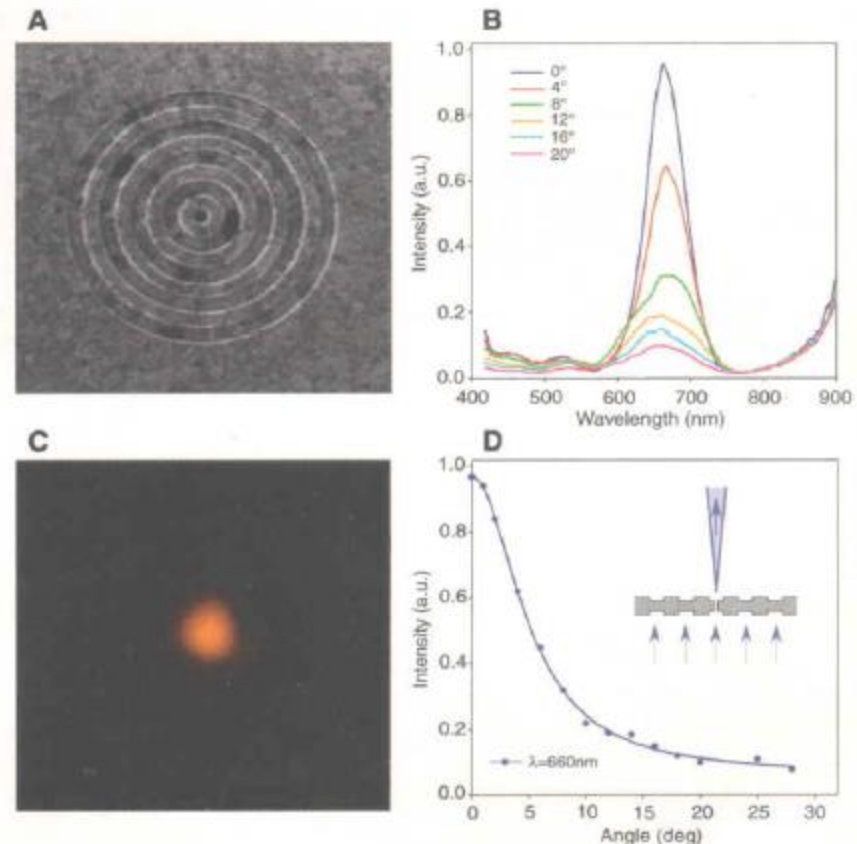
Progress work

To solve: light diffracts in all directions when an aperture is small.

Bull's eye of Ag film:
thickness 300nm
Groove periodicity 500nm
And depth 60nm
Hole diamter 250nm

Results:
Beaming light

Explanation:
Coupling of light and plasmons



Plasmon-assisted transmission of entangled photons

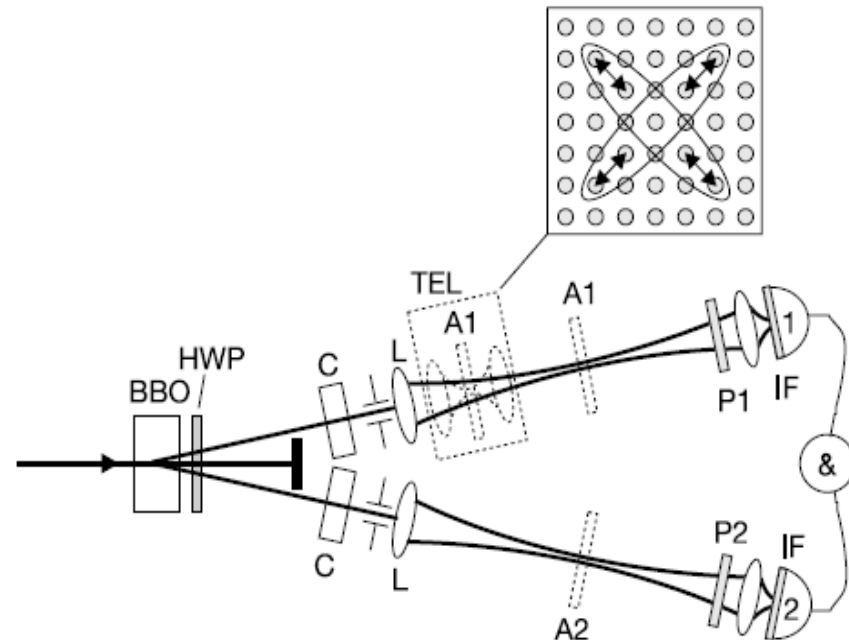
E. Altwiescher et al, 2002

Application work

Aim to: Investigate the effects of nanostructured metal on entangled photons.

Results:

Such arrays convert photons into surface-plasmon —**optically excited compressive charge density waves** — which tunnel through the holes before reradiating as photons.



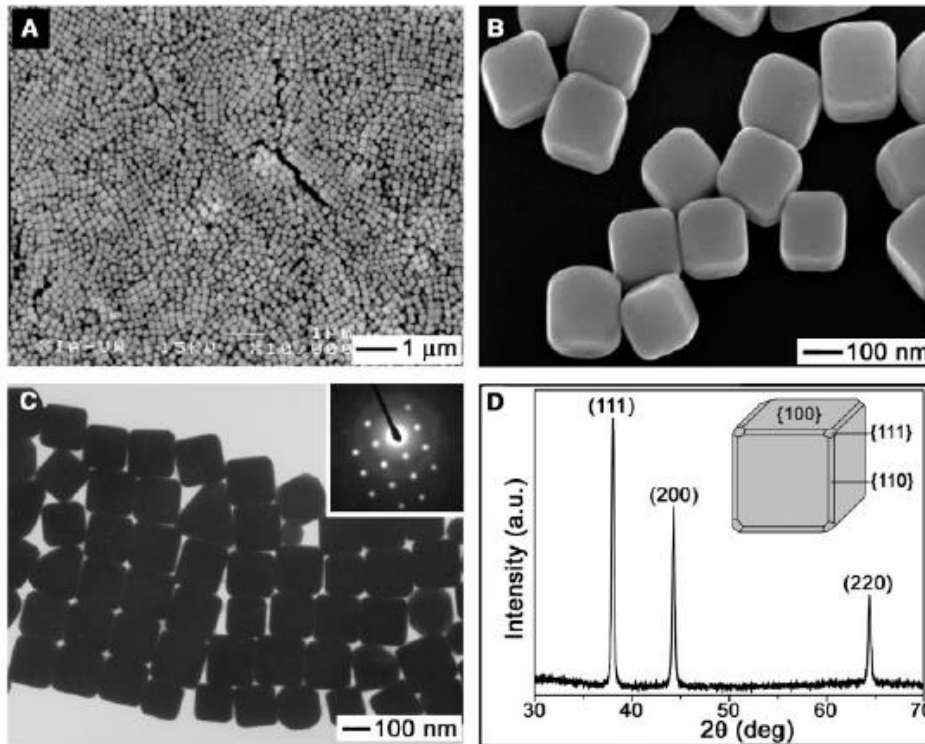
Explanation:

Conversion between photons and plasmons, quantum feature of SPP

Synthesis of Ag and Au nanocubes

Xia YN et al, 2002

Progress work



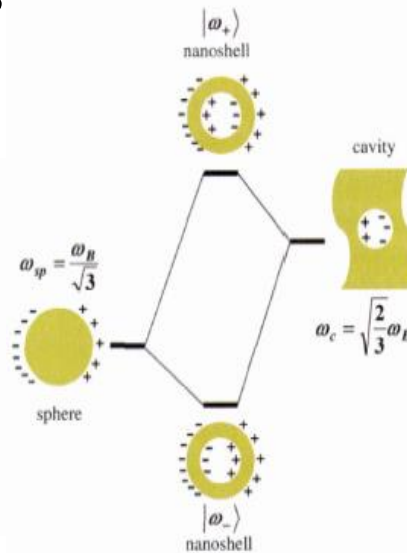
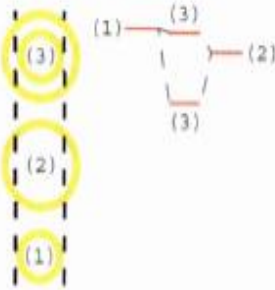
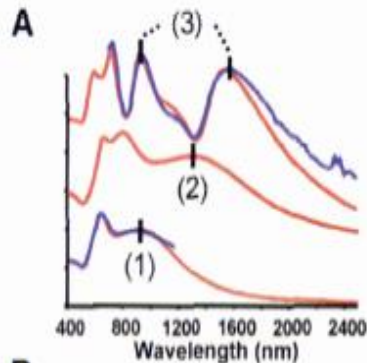
Significance:

Controlling the size, shape, and structure of metal nanoparticles is technologically important to tailor the plasmonic properties.

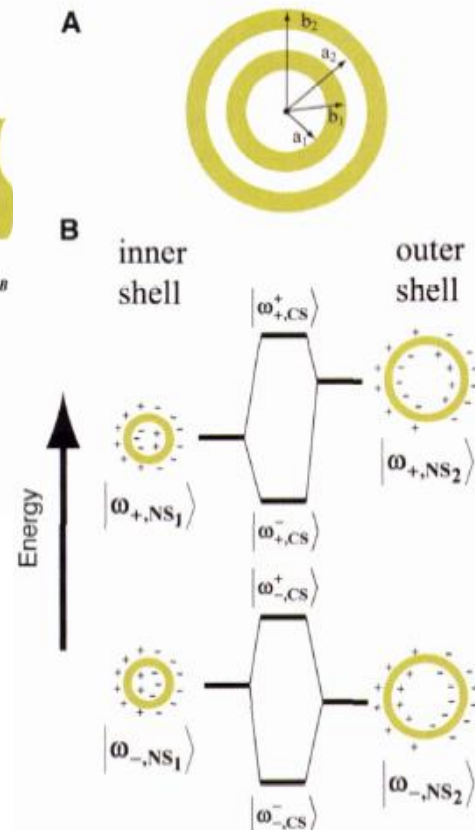
A hybridization model for plasmon response

N J Halas et al, 2003

To solve: surface plasmon resonances in nanoshells



Progress work



A hybridization of sphere and cavity

A hybridization of inner and outer shells

Results:

Several response peaks

[A hybridization model for the plasmon response of complex nanostructures](#)

E Prodan; C Radloff; N J Halas; P Nordlander, Science, 302, 419, 2003.

Surface plasmon subwavelength optics

William L. Barnes, Alain Dereux & Thomas W. Ebbesen, nature, 424, 824 (2003)

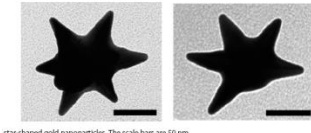
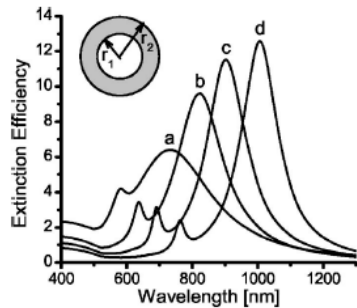
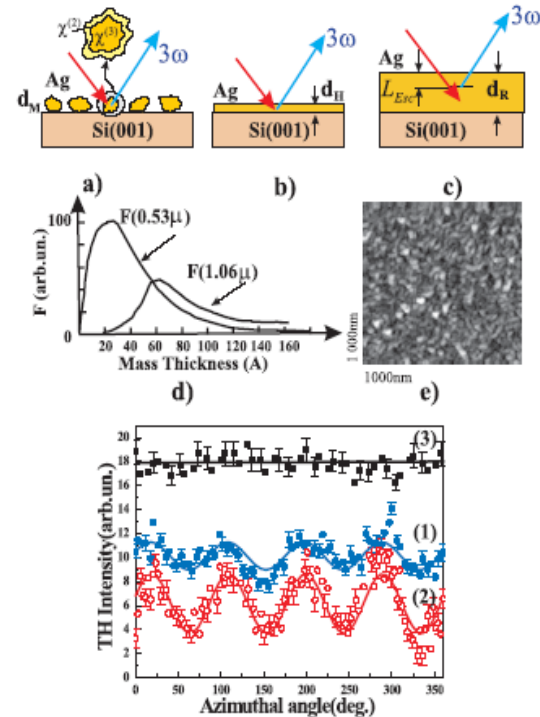
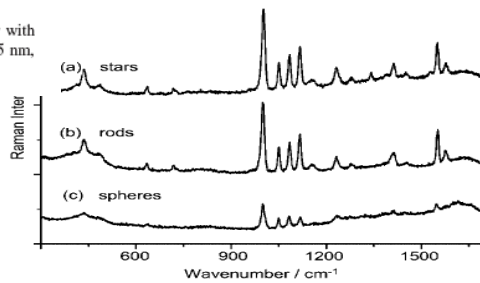


FIG. 1. Plasmon resonances of silica/Au nanoshell structures in water with $r_1=60$ nm and $r_2 =$ (a) 80 nm, (b) 70 nm, (c) 67 nm, and (d) 65 nm, respectively.



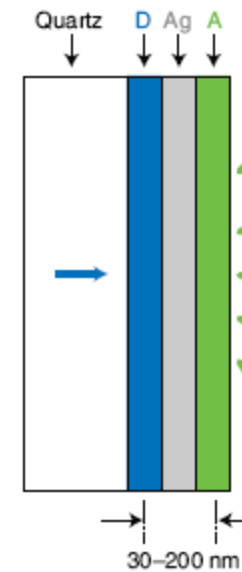
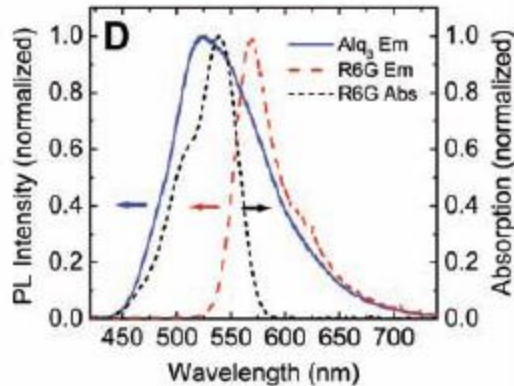
表面等离激元光学是纳米尺度上光子学和电子学的结合，在光子回路，光谱学，生物光子学，太阳能及非线性光学方面都有应用。

Forster Energy Transfer Across a Metal Film

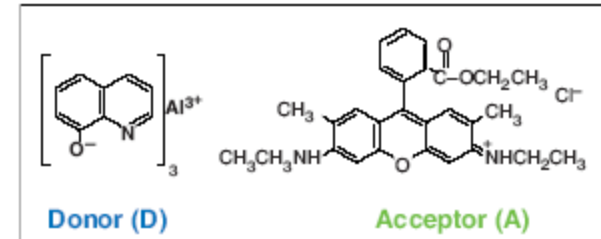
W. L. Barnes et al, 2004

Application work
Molecular plasmonics

Aim to: realize the Forster energy transfer between donor and acceptor across silver film



Significance:
toward the realization of an active plasmonic device by combining thin polymer films with thin silver films



Optical Imaging below the Diffraction Limit

X. Zhang et al, 2005

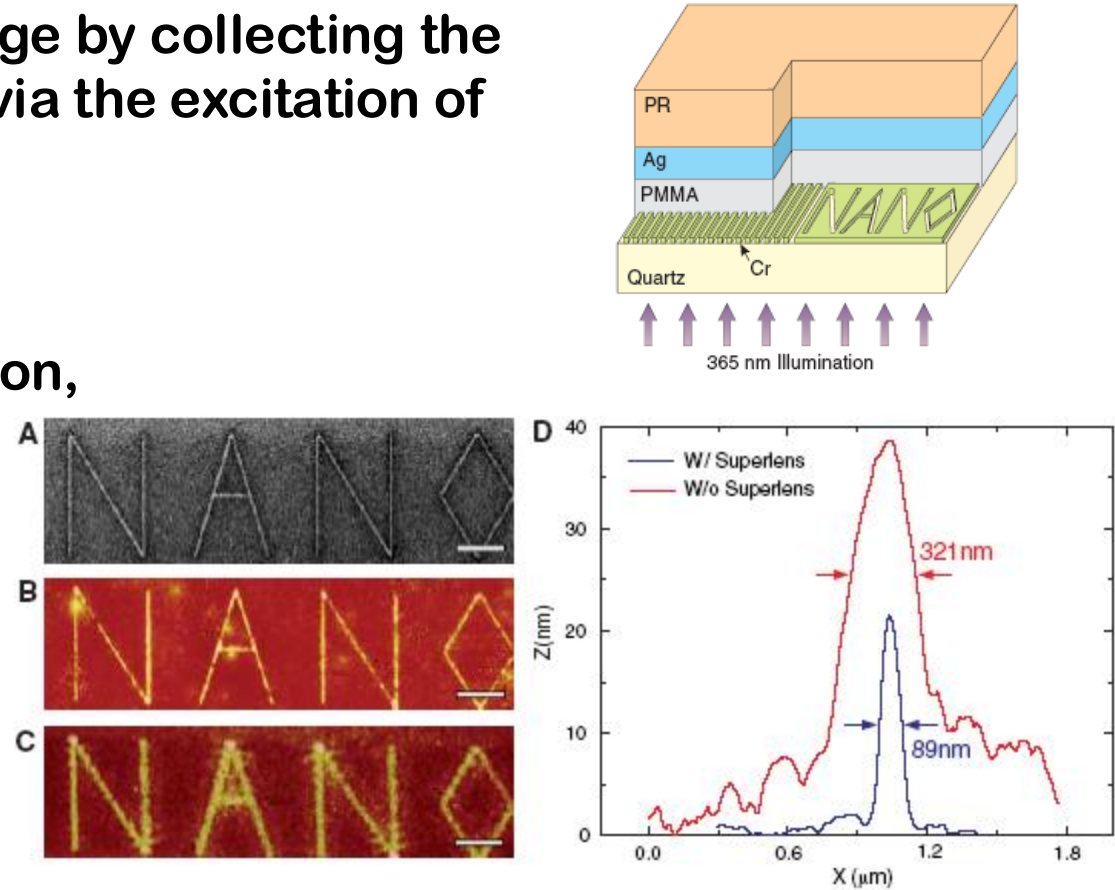
Progress work

Aim to: realize the image by collecting the of evanescent waves via the excitation of surface plasmons

Results:

60-nanometer resolution,
Or 1/6 of wavelength.

Significance:
breakthrough the
diffraction limit



Sub-Diffraction-Limited Optical Imaging with a Silver Superlens

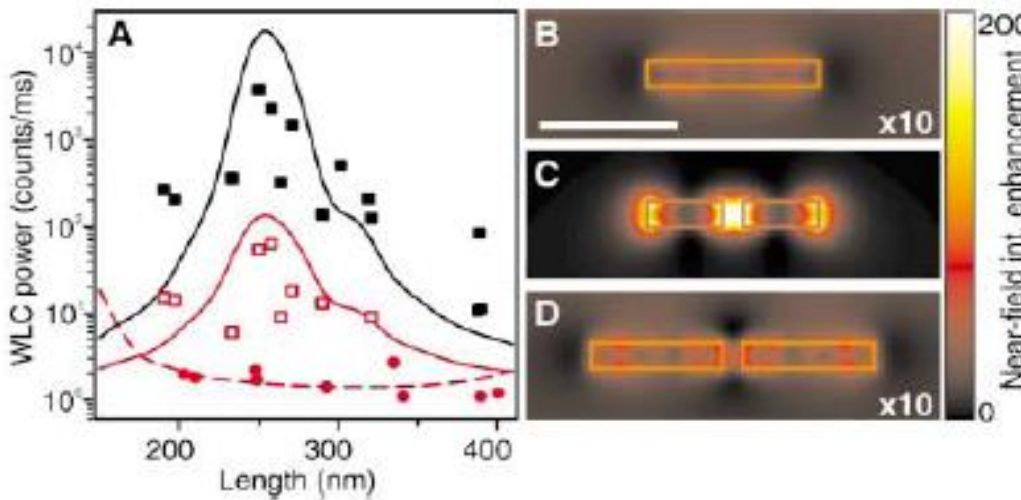
Nicholas Fang, Hyesog Lee, Cheng Sun, Xiang Zhang, Science, 308, 534, 2005.

Resonant Optical Antennas

O.J.F. Martin et al, 2005

Progress work

Aim to: The antenna length at resonance is considerably shorter than one-half the wavelength of the incident light



Results:

Fields localized in the gap and White light emission

Parameters:

Incident light: 830 nm
Size: 255*40*45 nm³
Gap: 30 nm

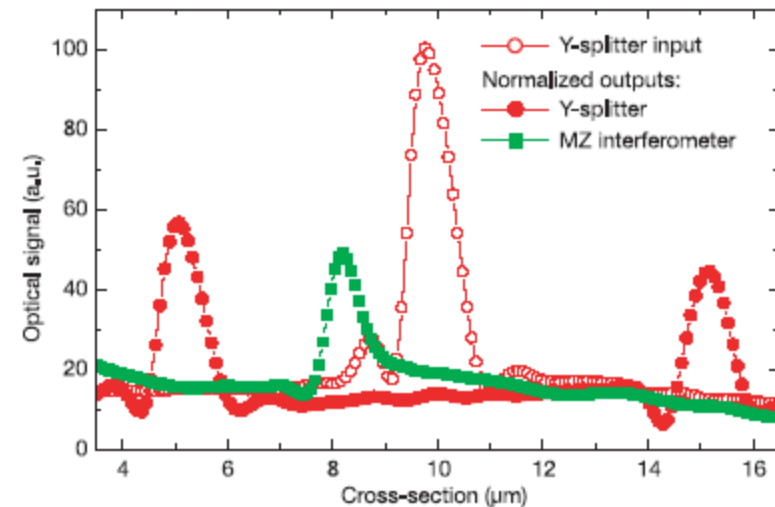
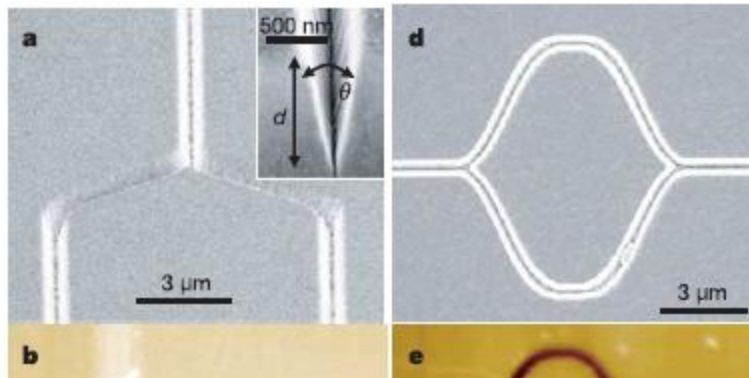
Significance:
Realization of optical nanoantenna

Channel SPP waveguide components including interferometers and ring resonators

T. W. Ebbesen et al, 2006

Application work

challenge to: the miniaturization and high-density integration of optical circuits at telecom. Wavelength



Results:

Grooves in silver, strong light confinement, low propagation loss

Significance:

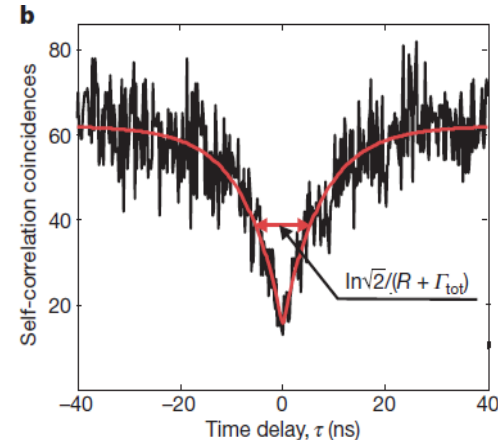
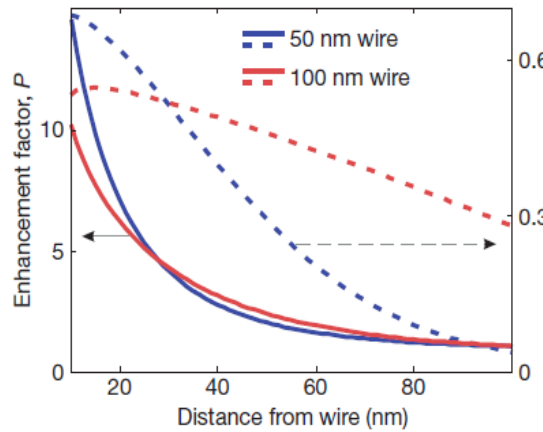
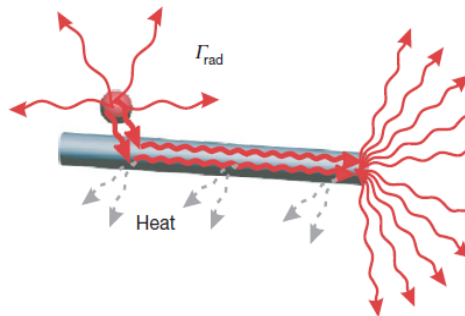
nano devices based Channel SPP

Generation of single optical plasmons in metallic nanowires coupled to quantum dots

M. D. Lukin et al, 2007

Crossing work

Aim to: efficient coupling between quantum dots and SPP, single photon switch and transistor, long range quantum bits.



Results:

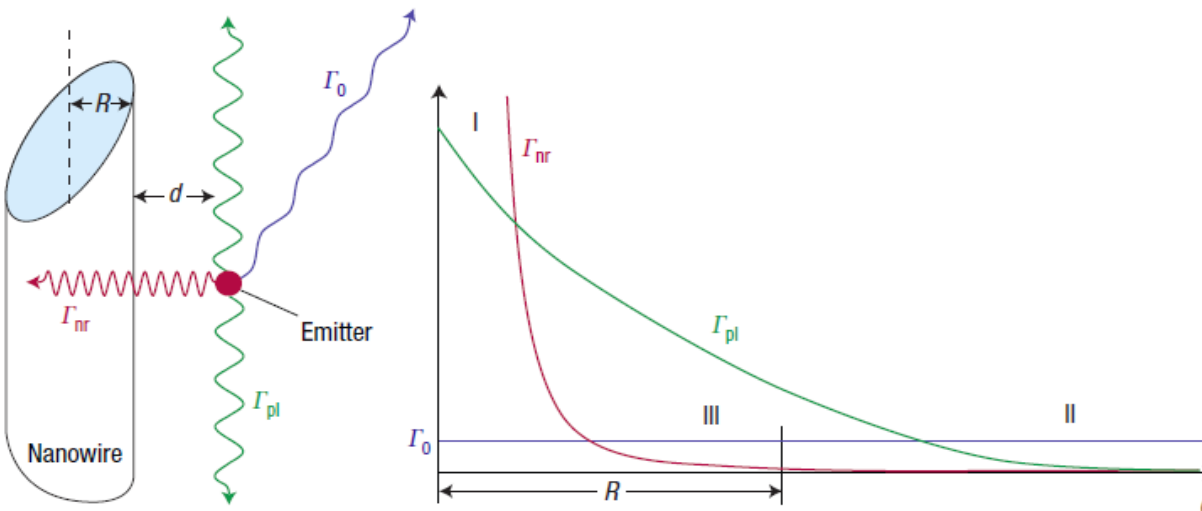
Realizing single quanta of surface plasmon.

Quantum light switch: A single-photon transistor using nanoscale surface plasmons

M. D. Lukin et al, 2007

Crossing work

在未来的计算机中光子能够代替电子吗？光子回路体积小，易于集成，损耗小，传的快，但是光子间没有相互作用，实现量子操控比较困难。量子发射体和表面等离激元强耦合的单光子晶体管，实现了单光子间的强相互作用，可在单光子探测，纠缠，可控相位门，量子的非线性效应方面有应用。

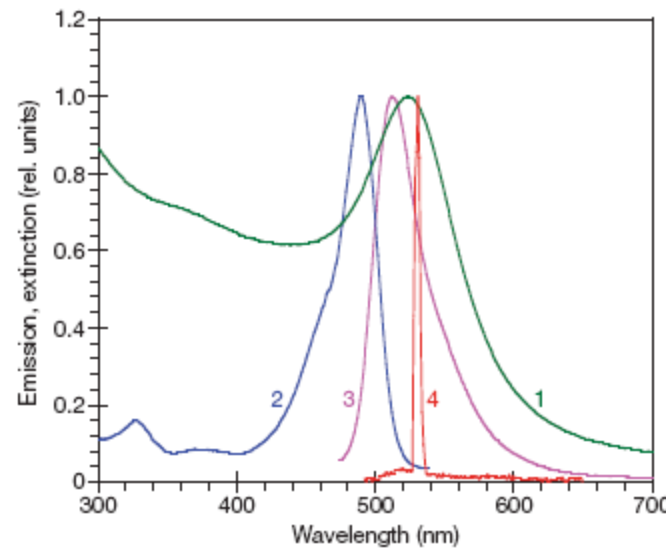
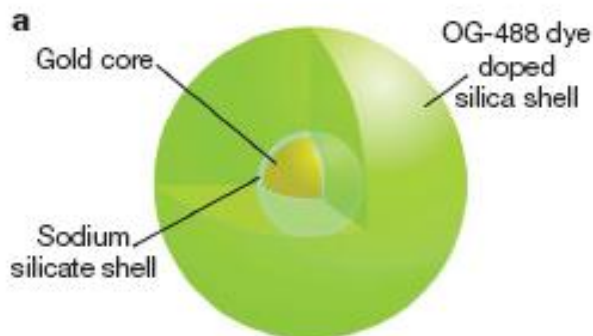


Core-shell nanostructure spaser

M. A. Noginov et al, 2009

Progress work

Aim to: realize a ‘spaser’ generating stimulated emission of surface plasmons in resonating metallic nanostructures adjacent to a gain medium.



Parameters:

gold core : 14 nm

Shell: 44 nm

Wavelength: 525 nm

Significance:

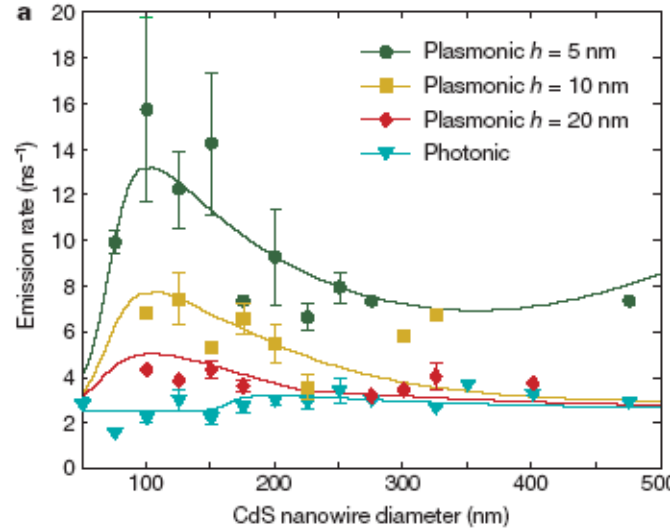
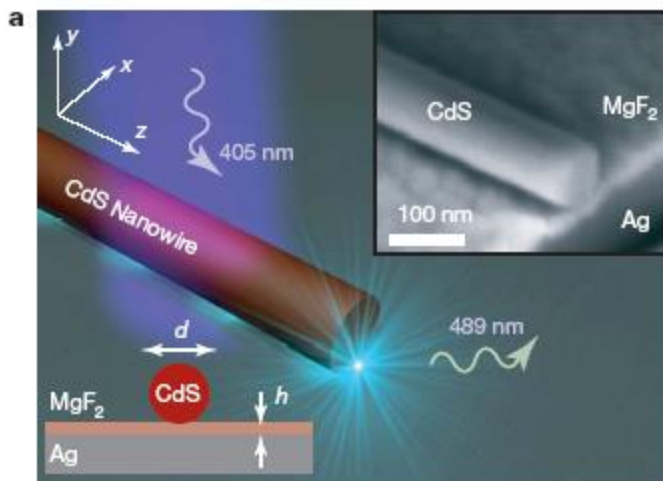
the smallest nanolaser
the first operating at visible wavelengths.

Nano-spaser based on hybrid waveguide

X. Zhang et al, 2009

Progress work

Challenge to: realize ultracompact lasers generating coherent optical fields at a nanoscale, far beyond the diffraction limit



Significance:

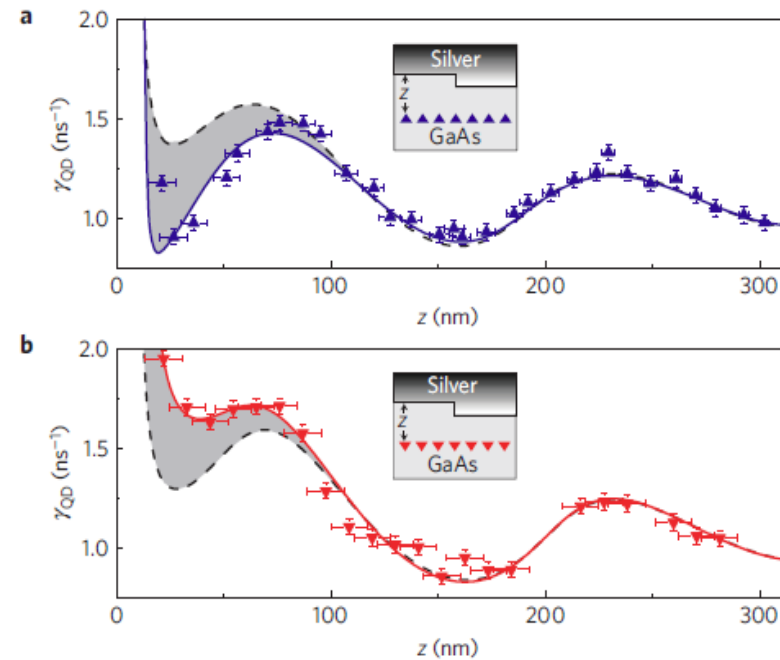
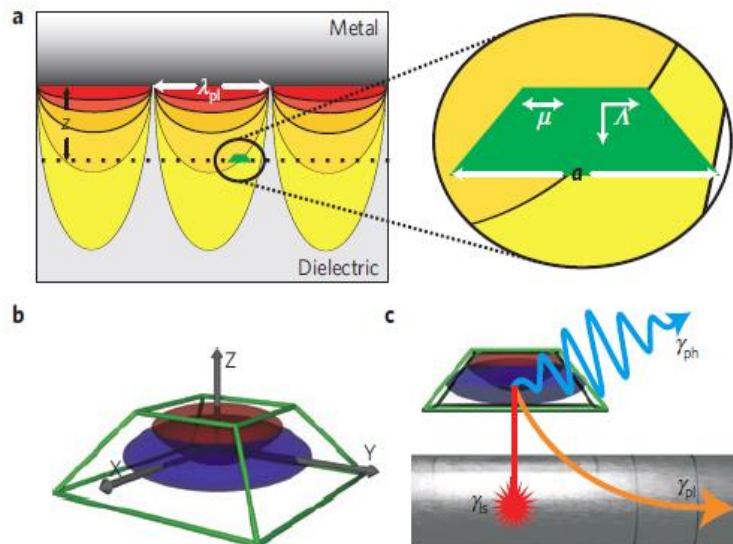
Plasmonic modes have no cutoff, downscaling of the lateral dimensions of both the device and the optical mode is demonstrated.

modified plasmon–matter interaction with mesoscopic quantum emitters

Mads Lykke Andersen, et al. 2010

Progress work

Aim to: experimentally demonstrate various decay channels with considering the size of quantum emitters.

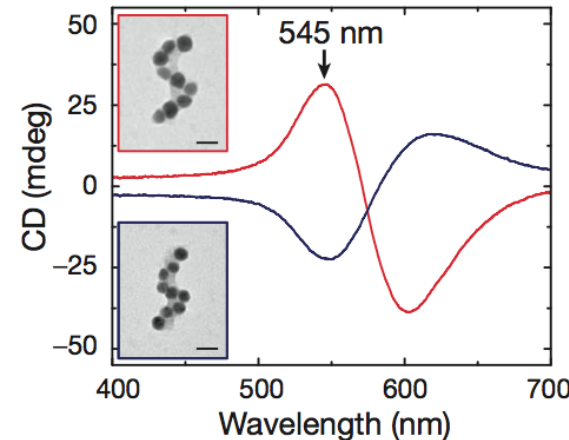
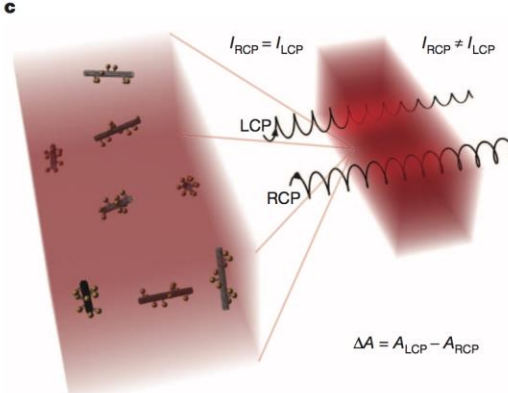
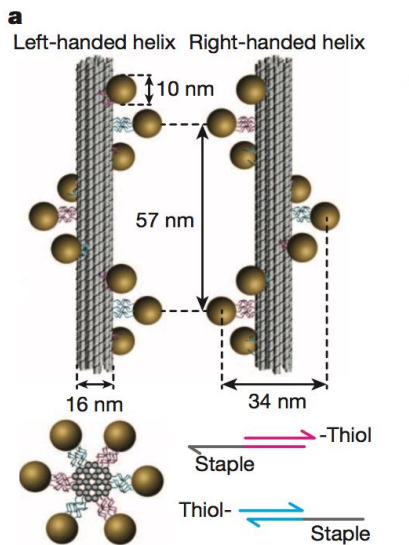


Significance: the effect of the size of nanoscale quantum dot on the coupling between SPP and quantum emitter.

DNA-based self-assembly of chiral plasmonic nanostructures with tailored optical response

Anton Kuzyk and Robert Schreiber et al, 2012 Progress work

Aim to: DNA origami enables the high-yield production of plasmonic structures that contain nanoparticles arranged in nano-metre-scale helices



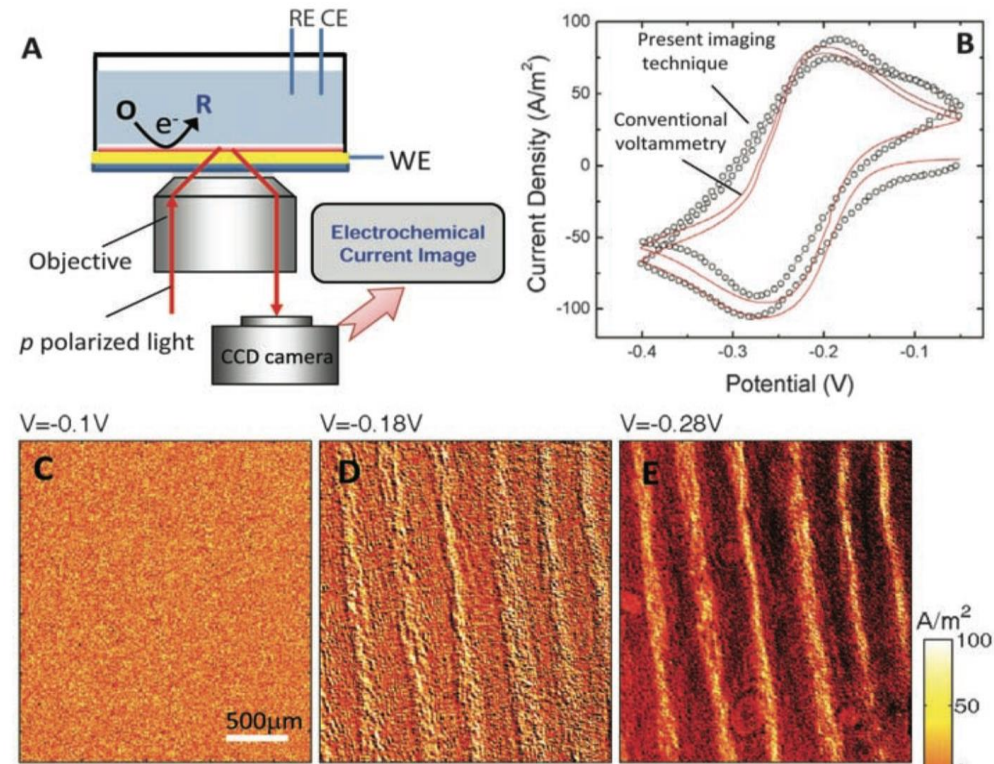
Significance: positioned with an accuracy better than 2 nm; the optical response of our nanoparticle assemblies is rationally designed and tunable in handedness, colour and intensity

Imaging Local Electrochemical Current via Surface Plasmon Resonance

NJ. Tao et al, 2010

Progress work

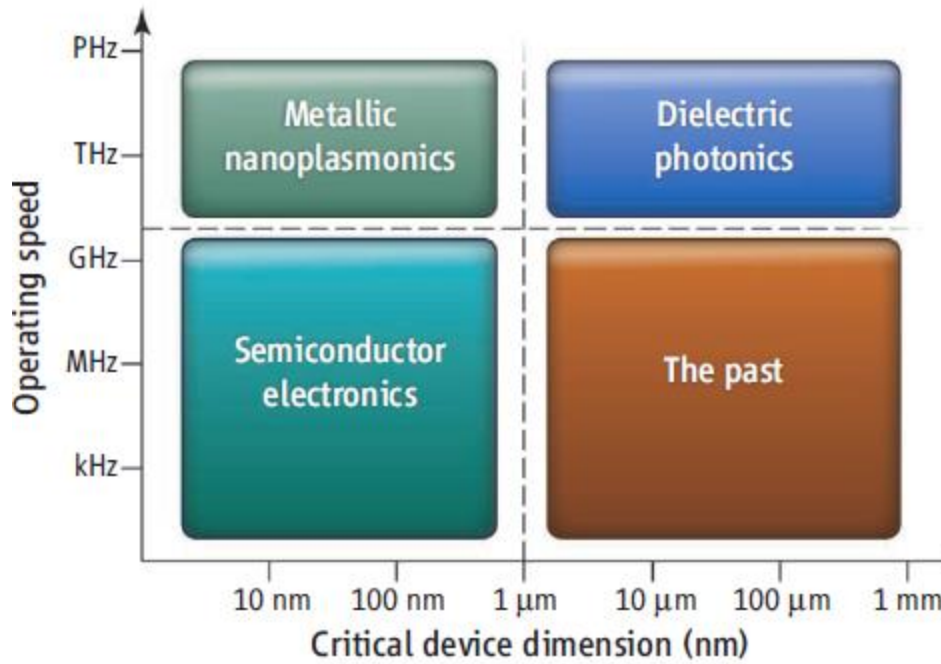
Aim to: developing an electrochemical microscopy technique based on the detection of variations in local electrochemical current from optical signals arising from SPP



Significance: noninvasive, scanning-free, and fast, and it constitutes a powerful tool for studying heterogeneous surface reactions and for analyzing trace chemicals.

APPLIED PHYSICS: The Case for Plasmonics

Mark L. Brongersma, and Vladimir M. Shalaev, 2010



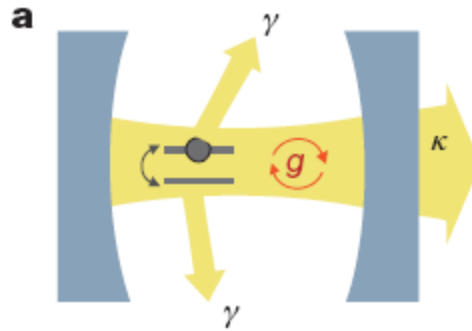
By squeezing light into nanoscale volumes, plasmonic elements allow for fundamental studies of light-matter interactions at length scales that were otherwise inaccessible

hybrid photonic architectures

The assembly of hybrid nanophotonic devices from different fundamental photonic entities—such as single molecules, nanocrystals, semiconductor quantum dots, nanowires and metal nanoparticles—can yield functionalities that exceed those of the individual subunits.

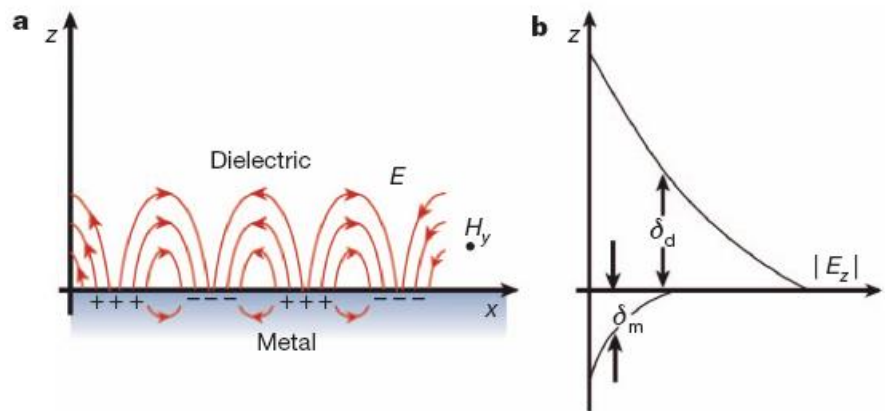
BOX 1

Cavity QED



BOX 2

Plasmonic enhancement



Functionality on the nanoscale

Light guiding and sorting

Enhanced emission and absorption

Nonlinear elements and switches

Nanophotonic–plasmonic hybrid devices

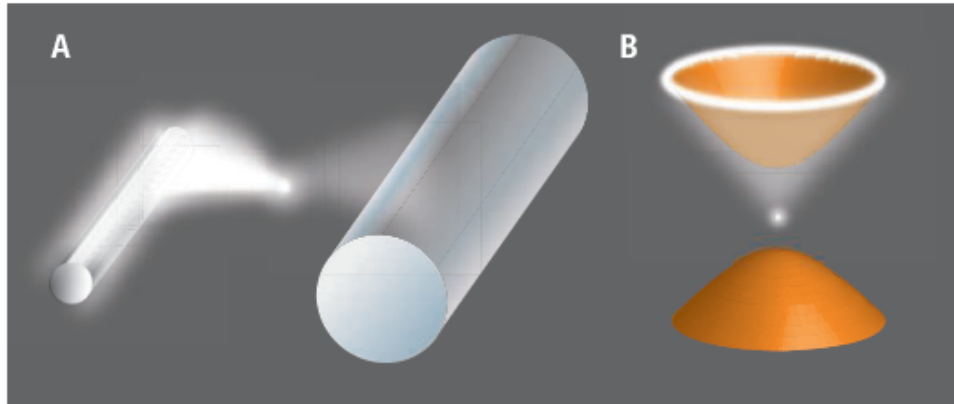
Plasmonically enhanced single-photon sources

Nanowire photonic elements

Future prospects

plasmons. Also, nonlinear interactions facilitating logical operations are feasible using CQED or plasmonic effects. There is great potential

Plasmonics Goes Quantum



Make it quantum. Building blocks of an integrated nanoscale quantum information system. (A) The nanowire supports a single plasmonic oscillation conceptually similar to a single-mode optical fiber. However, the nanoscale mode volumes of the plasmon lead to strong coupling with the quantum emitter. (B) An unorthodox approach of enhancing light-matter interaction is by tailoring the dielectric constant of a medium so that it is dielectric in one direction and metallic in another. The resulting hyperboidal dispersion relation supports infinitely many electromagnetic states for channeling light into a single-photon resonance cone.

A combined plasmonics and metamaterials approach may allow light-matter interaction to be controlled at the single-photon level.

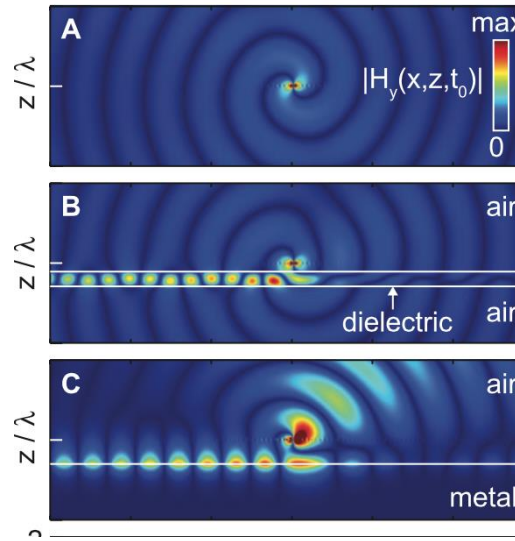
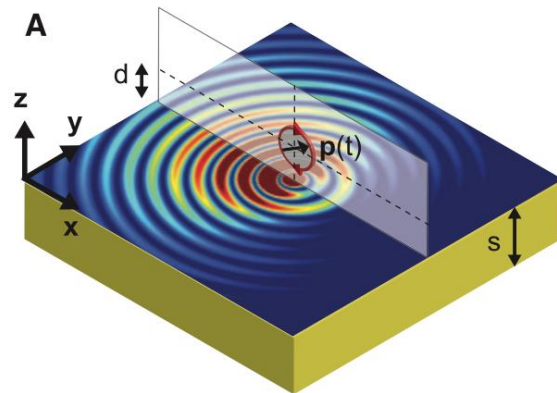
single plasmon →
antibunching statistics
nanoscale-mode volume →
strong coupling
entangling+squeezing →
quantum information
quantum plasmonics →
Spaser
Cavity QED
QI system

Unidirectional Chiral Propogating SPP

Anatoly V. Zayats et al, 2013

Progress work

Aim to: the near-field interference of a circularly polarized dipole results in the unidirectional excitation of guided electromagnetic modes in the near field, with no preferred far-field radiation direction



Significance: opens exciting possibilities for directional switching, polarization sorting, and processing of polarization-encoded information, including polarization-entangled optical qubits.

Quantum spin Hall effect of light (2015, science)

[Near-Field Interference for the Unidirectional Excitation of Electromagnetic Guided Modes](#)

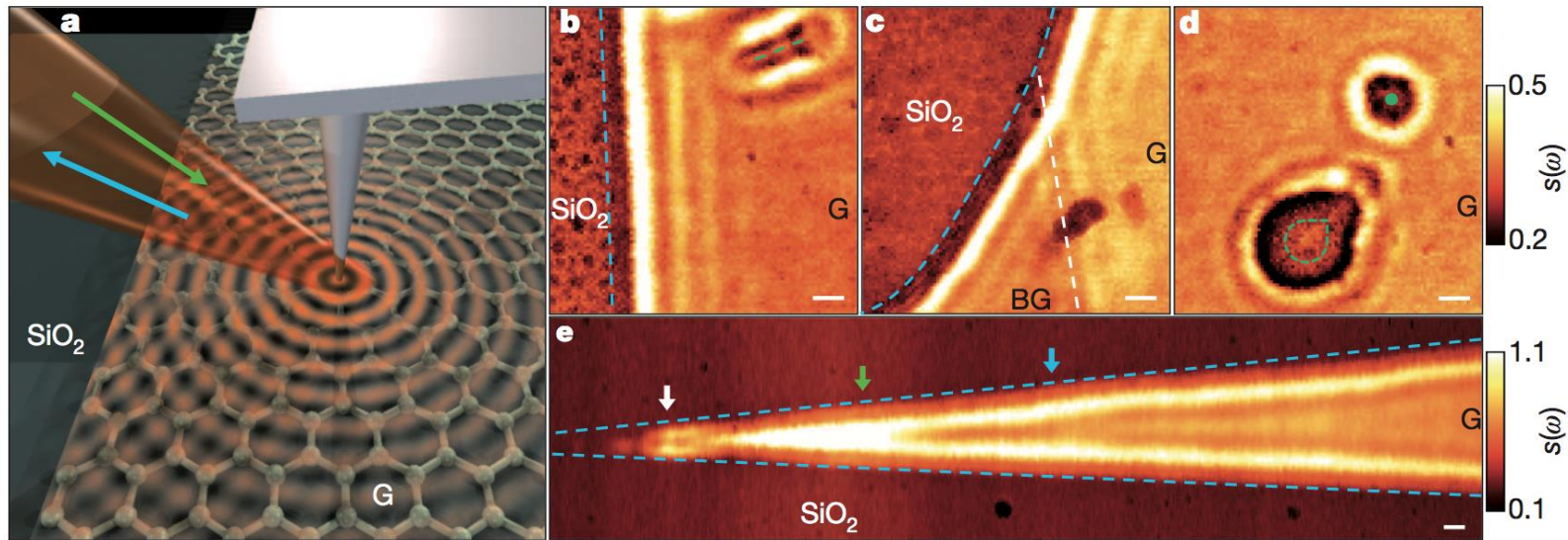
Anatoly V. Zayats et al, Science|Vol 340|328| 2013

Gate-tuning of graphene plasmons revealed by infrared nano-imaging

Z. Fei et al, 2012

Progress work

Aim to: graphene/SiO₂/Si back-gated structures support propagating surface plasmons.



Significance: Intrinsic plasmonic losses in graphene is less; plasmon tuning is realized; first generation of plasmonic devices; an ideal medium for active infrared plasmonics.

[Gate-tuning of graphene plasmons revealed by infrared nano-imaging](#)

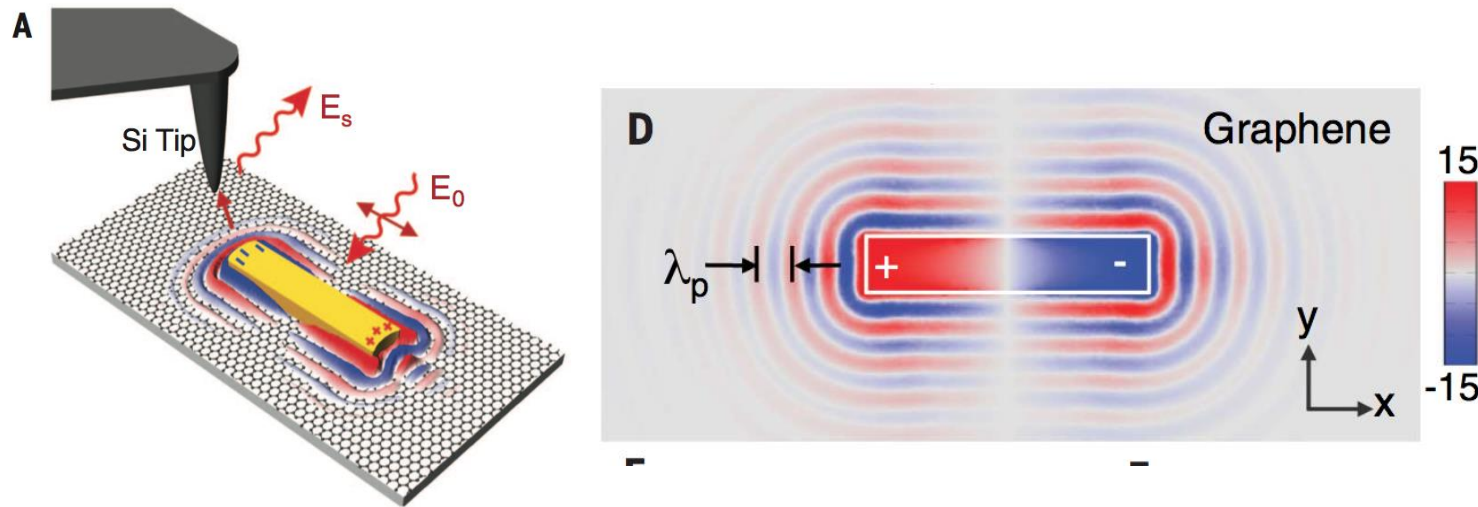
Z. Fei et al, NATURE|Vol 487|82| 2012

Controlling graphene plasmons with resonant metal antennas

R. Hillenbrand et al, 2014

Progress work

Aim to: infrared graphene plasmons with metal antennas and observed a two-dimensional conductivity pattern of a bilayer



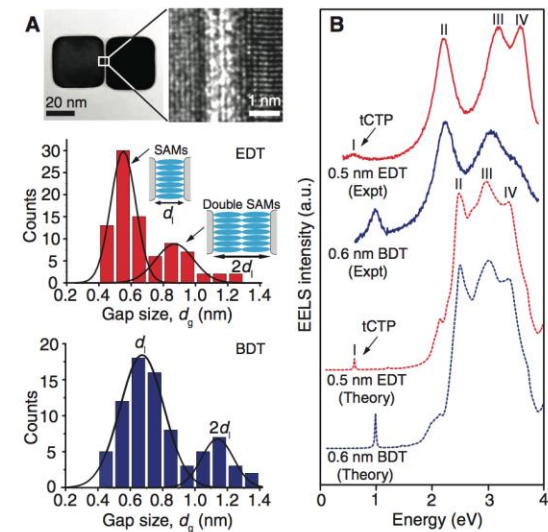
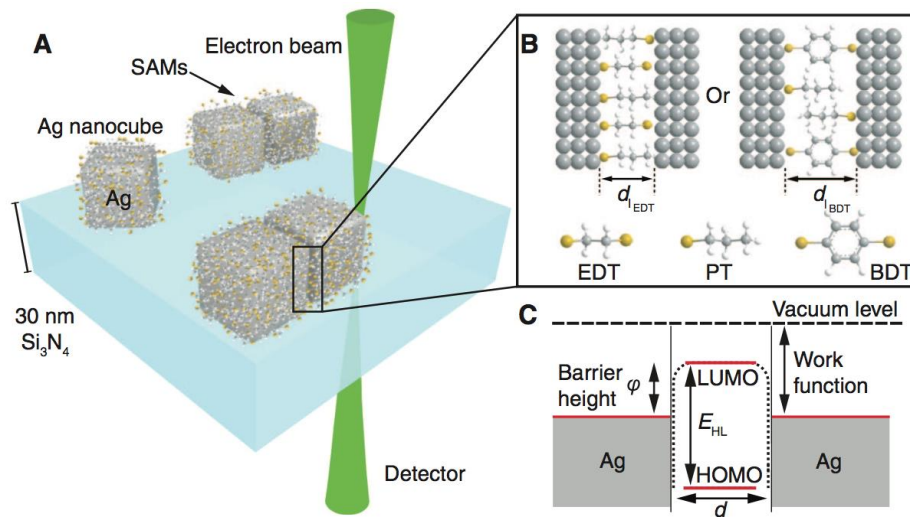
Significance: a versatile platform based on optical antennas; launching and control of propagating graphene plasmons; an essential step for the graphene plasmonic circuits
Mid-infrared plasmonic biosensing with graphene (Science 2015)

Quantum Tunnelling between Plasmon nanostructures

Christian A. Nijhuis et al, 2013

Progress work

Aim to: direct observation of quantum plasmon resonances in the range 0.4 to 1.3 nm across molecular tunnel junctions made of two plasmonic resonators bridged by self-assembled monolayers (SAMs)



Significance: Our results show that tunneling can reconcile molecular electronics with plasmonics, opening up a whole new interdisciplinary field of exploration.

Other important affairs

Review articles: 1

Surface plasmon resonance sensors: review

Jiri Homola, Sinclair S. Yee, Gunter Gauglitz, Sensors and Actuators B 54 (1999) 3–15

Surface plasmon subwavelength optics

T. W. Ebbesen et al, NATURE | VOL 424 | 824| 2003

Photonic structures in biology

J.R. Sambles et al, NATURE | VOL 424 | 852| 2003

Review articles: 2

**Plasmonics: Merging Photonics and Electronics
at Nanoscale Dimensions**

Ekmel Ozbay, SCIENCE VOL 311, 189, 2006

Nano-optics from sensing to waveguiding

N.J. Halas, nature photonics | VOL 1 | 641 | 2007

Progresses: 1

Local detection of electromagnetic energy transport below the diffraction limit in metal nanoparticle plasmon waveguides

S. A. Maier et al, nature materials | VOL 2 | 229 | 2003

Experimental Verification of Designer Surface Plasmons

Alastair P. Hibbins, Benjamin R. Evans, J. Roy Sambles, SCIENCE, 308, 670, 2005

Nanofabricated media with negative permeability at visible frequencies

A. N. Grigorenko and A. K. Geim et al, NATURE | Vol 438 | 335 | 2005

Progresses: 2

Magnifying Superlens in the Visible Frequency Range (using metamaterial)

Igor I. Smolyaninov, Yu-Ju Hung, Christopher C. Davis, science, 315, 1699, 2007

Transmission resonances through aperiodic arrays of subwavelength apertures

Tatsunosuke Matsui, NATURE| Vol 446|517| 2007

Ultrasmooth Patterned Metals for Plasmonics and Metamaterials

Prashant Nagpal et al, SCIENCE, 325, 594, 2009

Wave–particle duality of single surface plasmon polaritons

Roman Kolesov et al, NATURE PHYSICS, VOL 5, 470, 2009

Progresses: 3

Efficient hot-electron transfer by a plasmon-induced interfacial charge-transfer transition 作者: Wu, K.; Chen, J.; McBride, J. R.; 等.

SCIENCE 卷: 349 期: 6248 页: 632-635 出版年: AUG 7 2015

Fundamental limits to graphene plasmonics

作者: Ni, G. X.; McLeod, A. S.; Sun, Z.; 等.

NATURE 卷: 557 期: 7706 页: 530--+ 出版年: MAY 24 2018

Determining plasmonic hot-carrier energy distributions via single-molecule transport measurements

作者: Reddy, Harsha; Wang, Kun; Kudyshev, Zhaxylyk; 等.

SCIENCE 卷: 369 期: 6502 页: 423--+ 出版年: JUL 24 2020

Applications: 1

Controlling anisotropic nanoparticle growth through plasmon excitation

Rongchao Jin et al, NATURE | VOL 425 | 487 | 2003

Negative Refraction at Visible Frequencies

Henri J. Lezec, Jennifer A. Dionne, Harry A. Atwater, science,316,430,2007

Slow guided surface plasmons at telecom frequencies

M. SANDTKE AND L. KUIPERS, nature photonics,1,2007

Measurement of the Distribution of Site Enhancements in Surface-Enhanced Raman Scattering

Ying Fang et al, SCIENCE,321,388,2008

Applications: 2

High-Q surface-plasmon-polariton whispering-gallery microcavity

Bumki Min et al, NATURE| Vol 457|455| 2009

Nanoplasmonic Probes of Catalytic Reactions

Elin M. Larsson et al, SCIENCE VOL 326,1091, 2009

Applications: 3

Mid-infrared plasmonic biosensing with graphene

作者: Rodrigo, Daniel; Limaj, Odetta; Janner, Davide; 等.

SCIENCE 卷: 349 期: 6244 页: 165-168 出版年: JUL 10 2015

Femtosecond laser reshaping yields gold nanorods with ultranarrow surface plasmon resonances

作者: Gonzalez-Rubio, Guillermo; Diaz-Nunez, Pablo; Rivera, Antonio; 等.

SCIENCE 卷: 358 期: 6363 页: 640-644 出版年: NOV 3 2017

Real-space and real-time observation of a plasmon-induced chemical reaction of a single molecule

作者: Kazuma, Emiko; Jung, Jaehoon; Ueba, Hiromu; 等.

SCIENCE 卷: 360 期: 6388 页: 521-525 出版年: MAY 4 2018

Amino-acid- and peptide-directed synthesis of chiral plasmonic gold nanoparticles

作者: Lee, Hye-Eun; Ahn, Hyo-Yong; Mun, Jungho; 等.

NATURE 卷: 556 期: 7701 页: 360-+ 出版年: APR 19 2018

Applications: 4

Low-loss plasmon-assisted electro-optic modulator

作者: Haffner, Christian; Chelladurai, Daniel; Fedoryshyn, Yuriy; 等.
NATURE 卷: 556 期: 7702 页: 483-+ 出版年: APR 26 2018

Stable, high-performance sodium-based plasmonic devices in the near infrared

作者: Wang, Yang; Yu, Jianyu; Mao, Yi-Fei; 等.
NATURE 卷: 581 期: 7809 页: 401-+ 出版年: MAY 28 2020

Plasmonic enhancement of stability and brightness in organic light-emitting devices

作者: Fusella, Michael A.; Saramak, Renata; Bushati, Rezlind; 等.
NATURE 卷: 585 期: 7825 页: 379-+ 出版年: SEP 17 2020

2.1节结束语：

第一章讲清楚SPP的基本概念后，本节以 Nature 和 Science 上进展、应用和综述文章为主要线索，总结了 plasmonics 发展过程中的重要事件，试图对 plasmonics 有一个全局的了解。Plasmonics 是微纳光学 的重要组成部分，目前在应用领域和交叉学科方面有重要发展。



第二章 表面等离激元的发展、前沿及应用

2.1 表面等离激元发展简史（1-43）

2.2 表面等离激元的应用

2.2.1 表面等离激元（SPP）波导（46-64）

2.2.2 表面等离激元共振（SPR）及应用（66-95）

2.2.3 周期性结构中SPP性质（97-111）

2.2.1 表面等离激元 (SPP) 波导

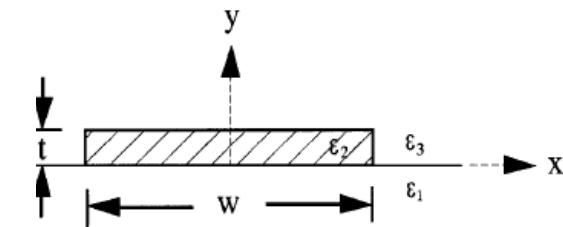
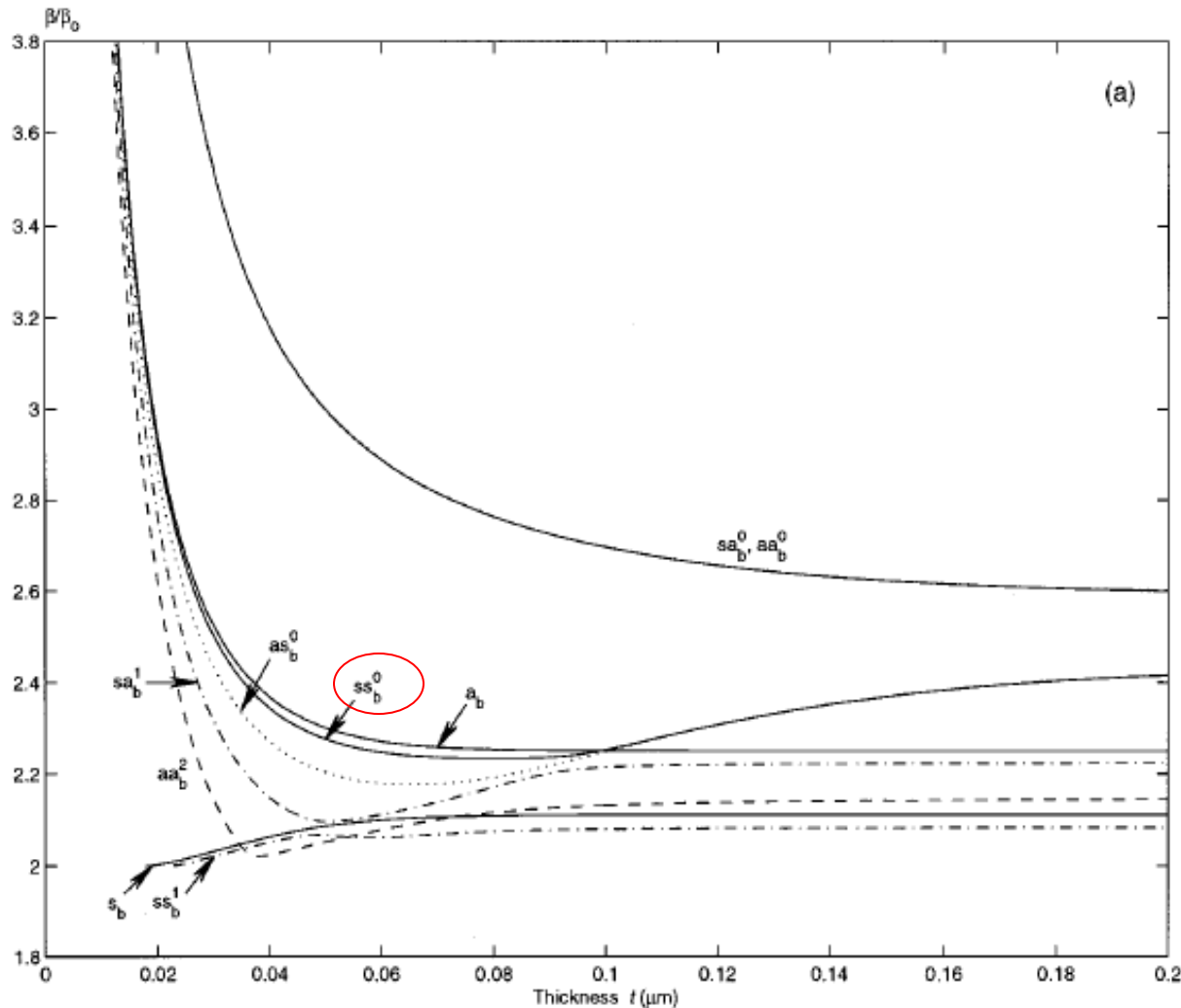
类型：平面波导、槽形波导、柱形波导、球链波导、
弯形波导、金属介质混合型波导（杂化波导）

特点：结构的尺度在亚波长范围内、
电场束缚在金属表面、传播长度有限
(倏逝波、有损耗)

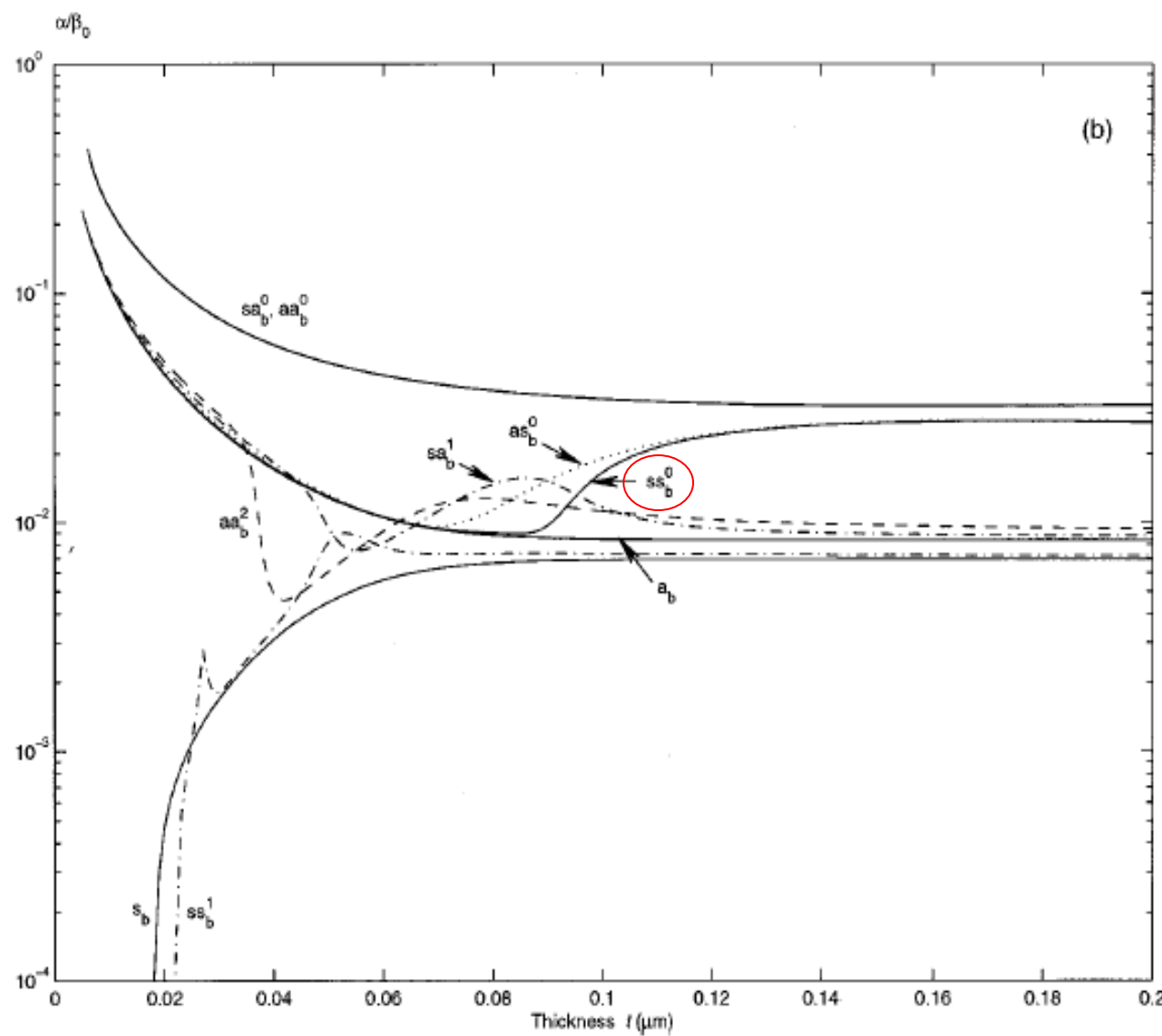
用途：分束器、干涉仪等纳米的光子器件

意义：实现器件的小型化、信息传输速度快、
各种光子器件的基础

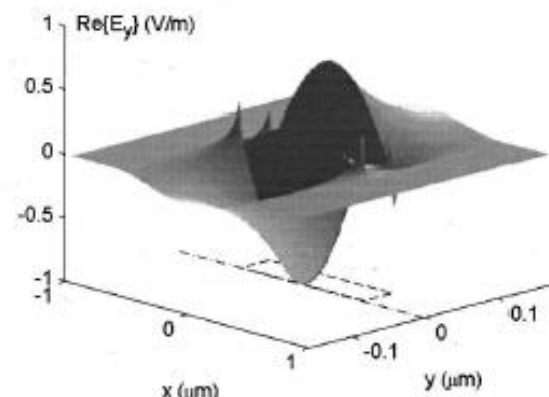
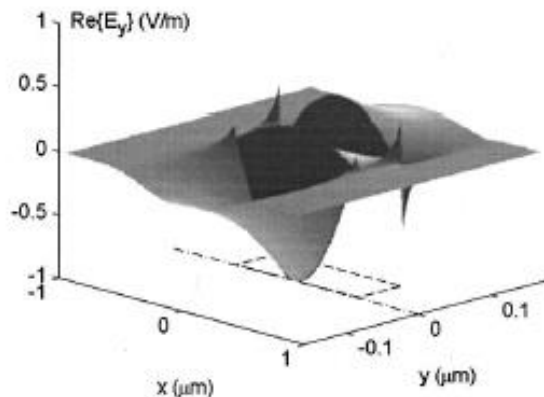
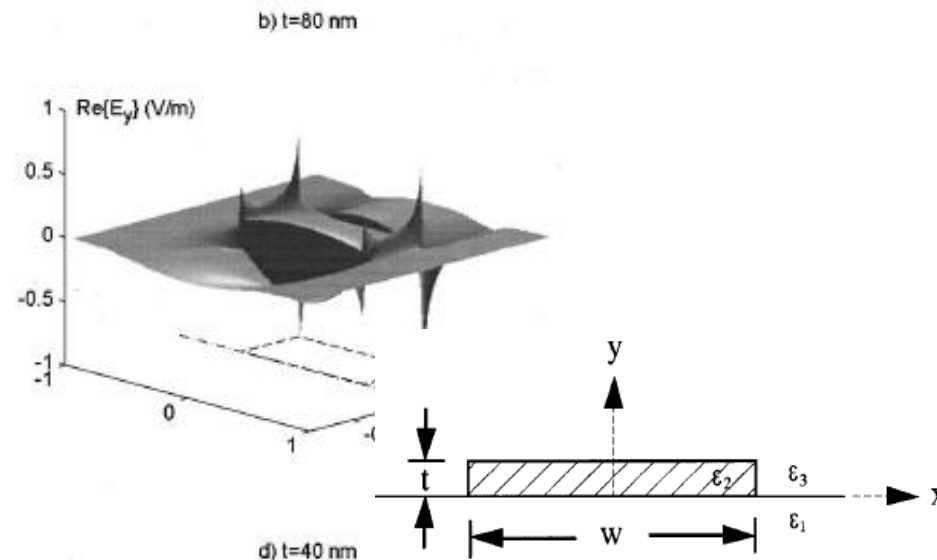
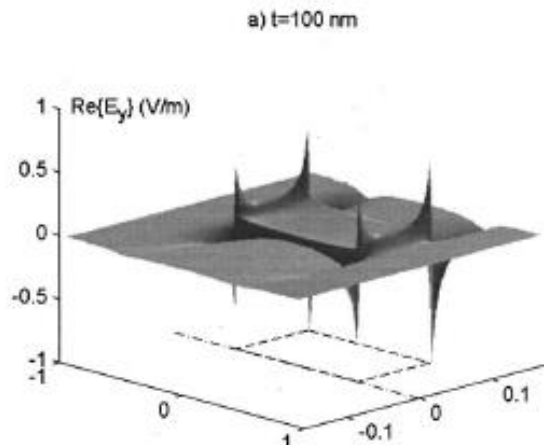
纳米金属条形SPP波导



传播常数的实部
关于x和y对称和反
对称共有4支SP模
式。



传播常数的虚部



SS_b^0 在宽度是1um厚度变化时的 E_y 电磁场分布
厚度薄的时候倏逝波特征明显

槽形SPP波导

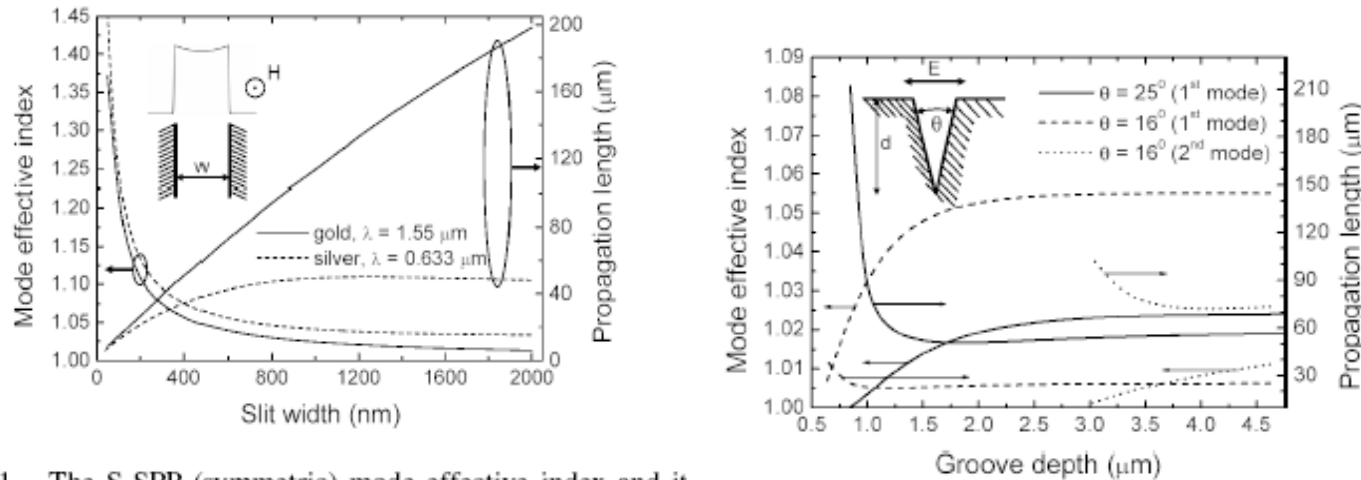
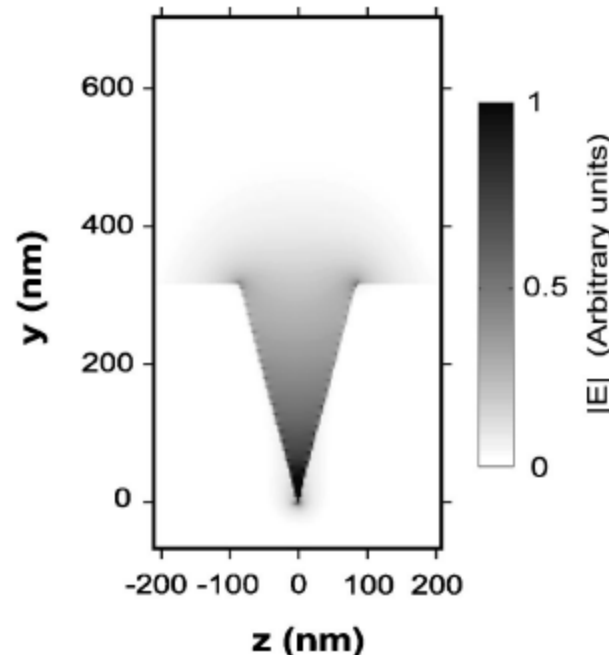
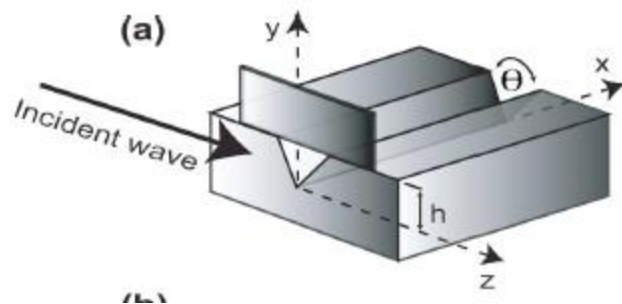


FIG. 1. The S-SPP (symmetric) mode effective index and it

想法：与MIM型波导的比较的角度去理解，
以期找到局域性好传播又长的模式。

槽形SPP波导中电场



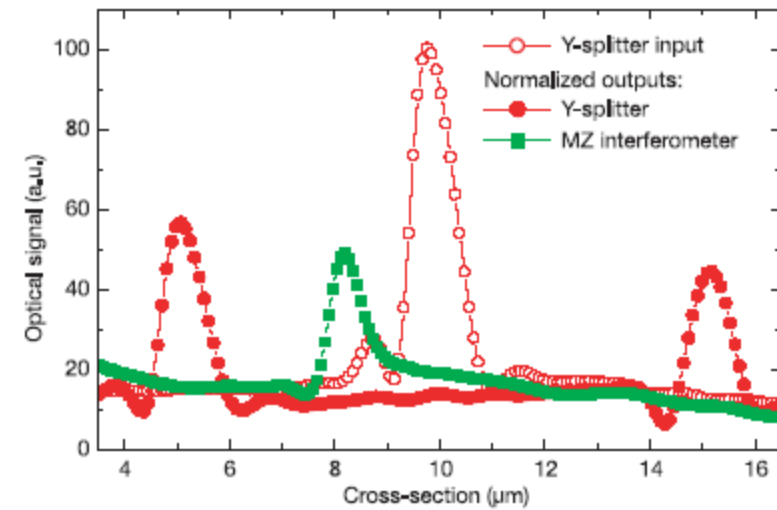
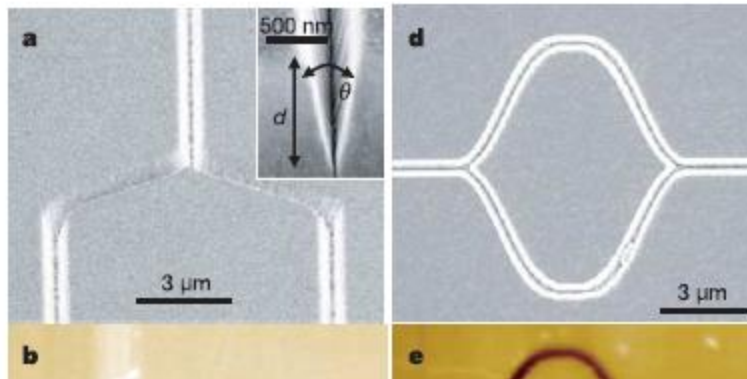
可以看到：在以金属为基底的槽形波导中，模式的能量集中在槽中，利于导波。

[Single-mode subwavelength waveguide with channel plasmon-polaritons in triangular grooves on a metal surface,](#) D. K. Gramotnev and D. F. P. Pilea, Appl. Phys. Lett., Vol. 85, 6323 (2004).

Channel SPP waveguide components including interferometers and ring resonators

T. W. Ebbesen et al, 2006 (2.1节中提过)

challenge to: the miniaturization and high-density integration of optical circuits at telecom. Wavelength



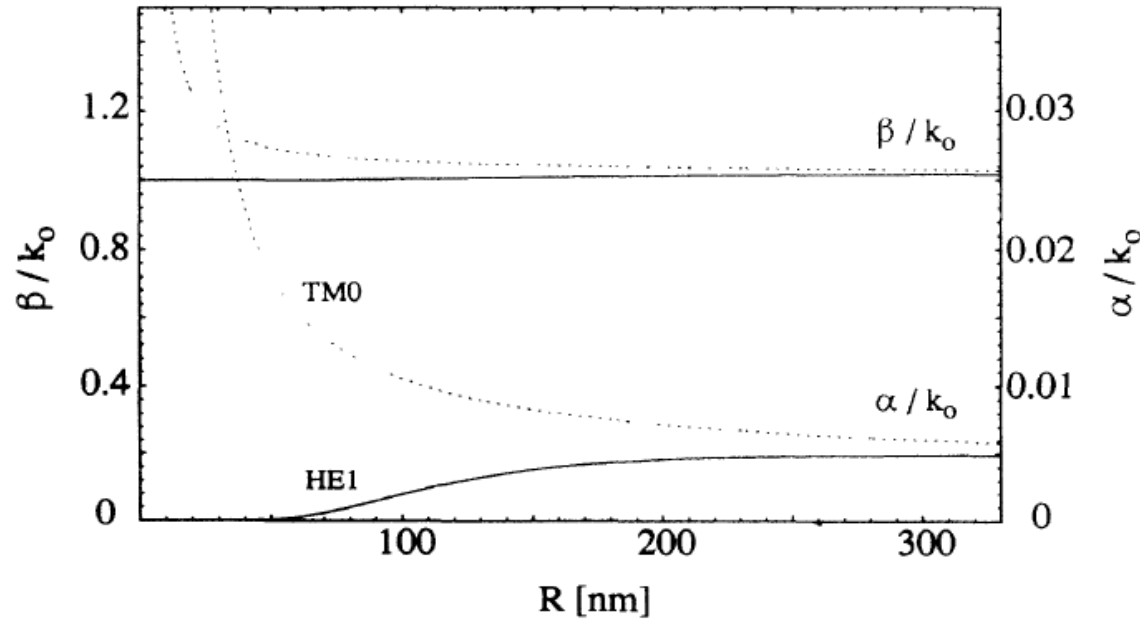
Results:
Grooves in silver, strong light confinement, low propagation loss

Significance:
nano devices based Channel SPP

柱形SPP波导（一维，柱对称、解析解）

金属纳米线

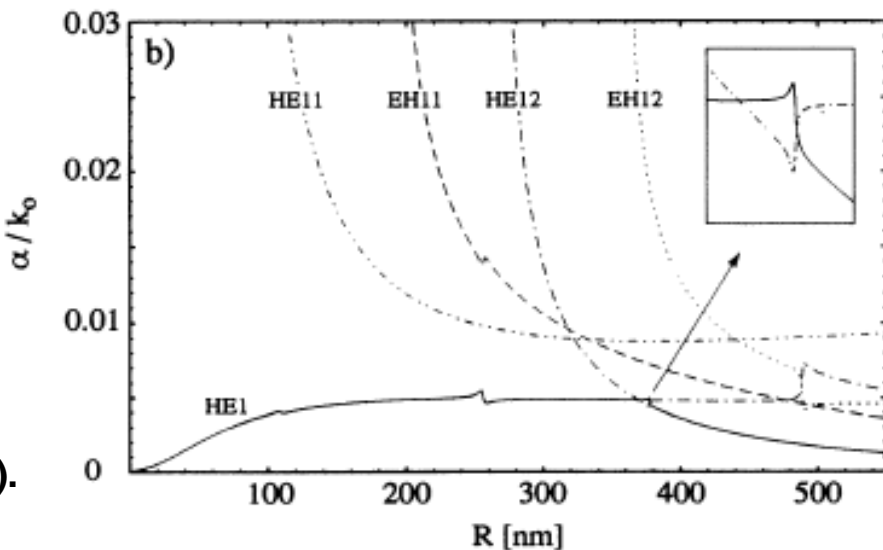
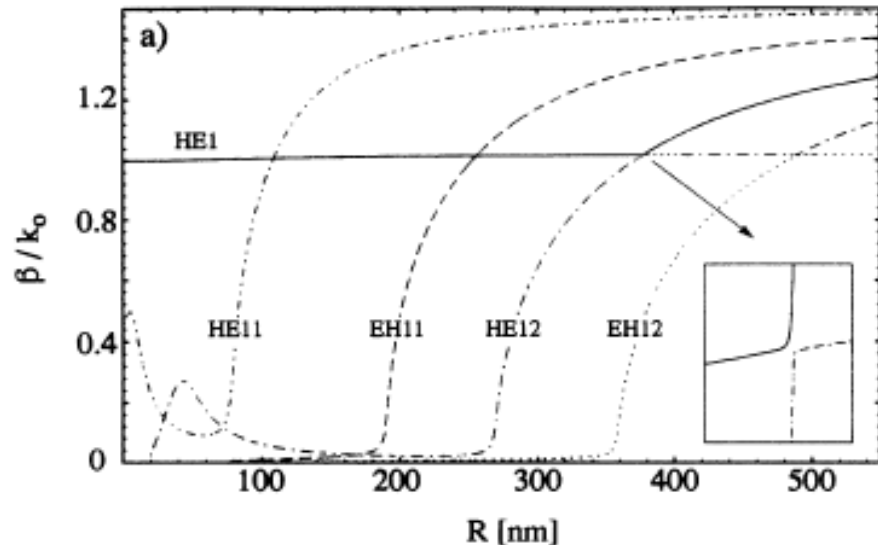
- 对每个n，存在表面模式 TM_0 , HE_n 。



铝纳米线，波长488nm

金属纳米管

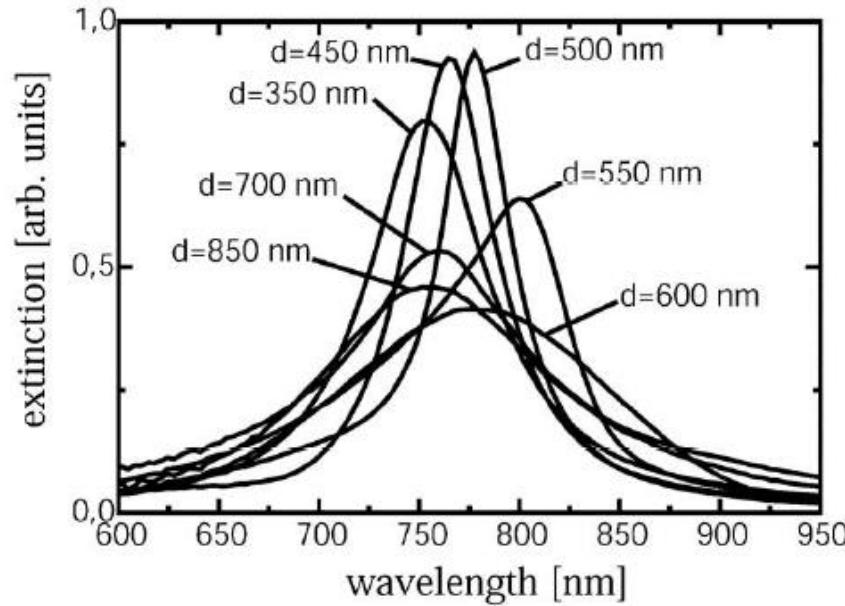
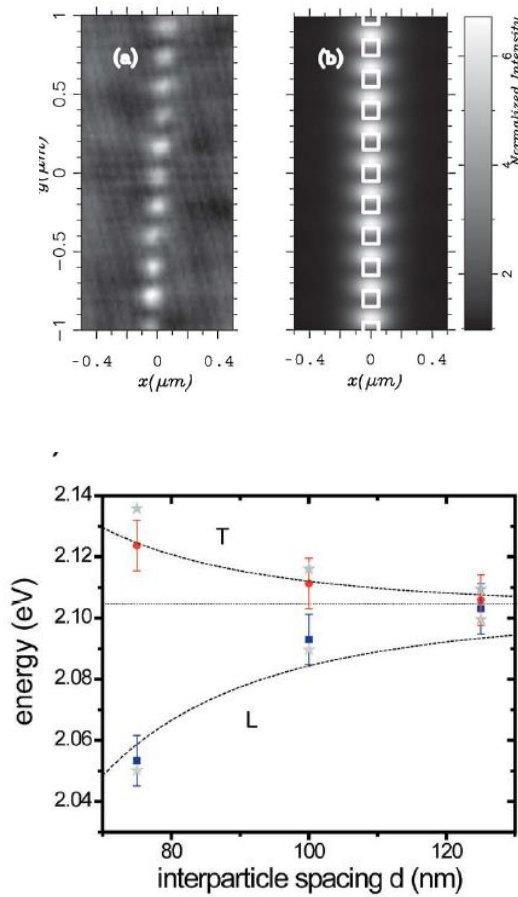
- HE₁表面模式
- 众多波导模式 HE_{1n}, 在管内径减小截止。
- 表面模式和波导模式之间存在模式转换现象。



L. Novotny et al, Phys. Rev. E 50, 4094 (1994).

球链SPP波导

原理：通过纳米金属颗粒间的近场耦合实现光的传递



可以看到：由于小球上电场偏振的不同而出现T模式和L模式；小球间距离的不同导致消光峰的位置不同。

聚焦后用SPP波导传输

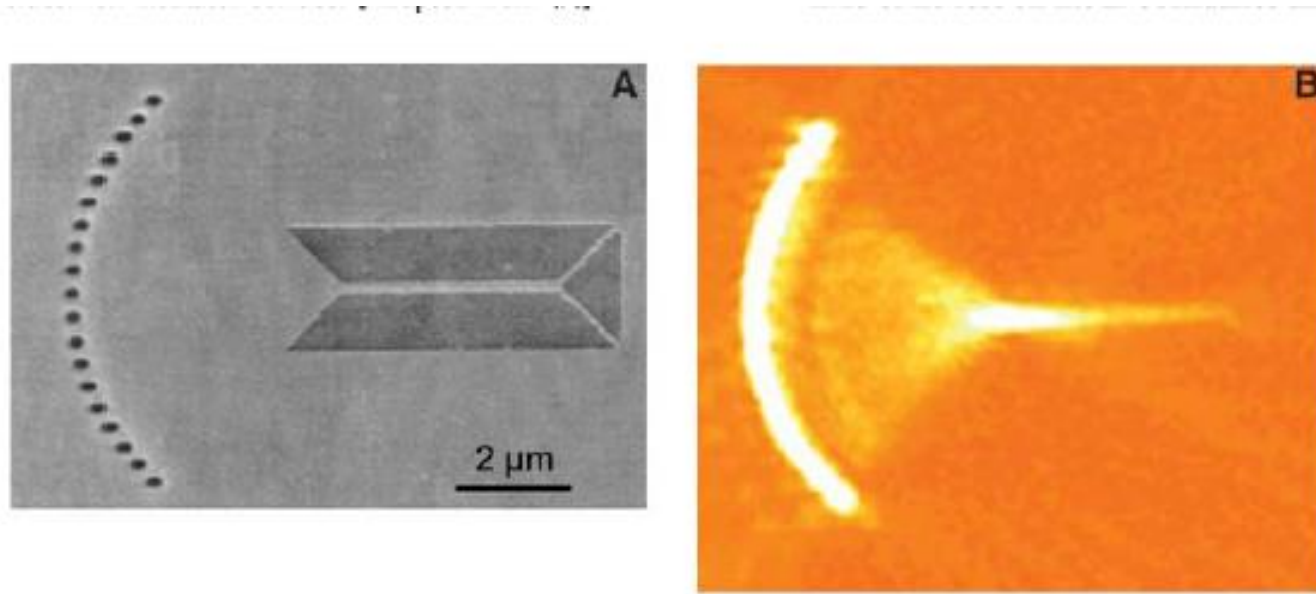
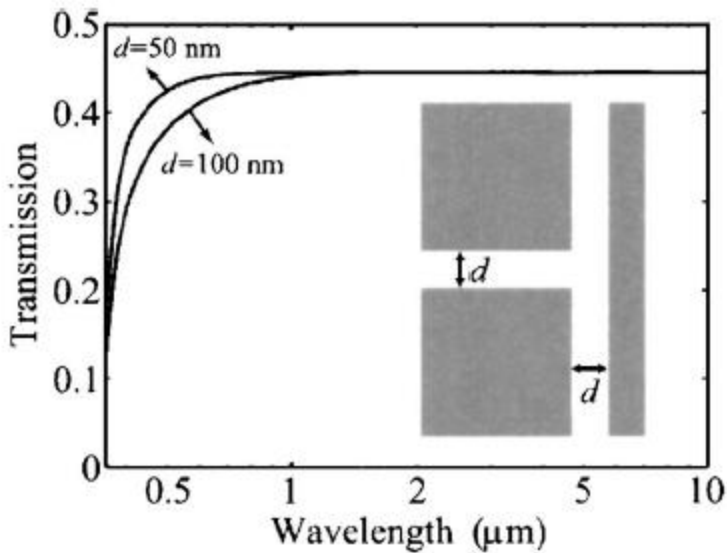
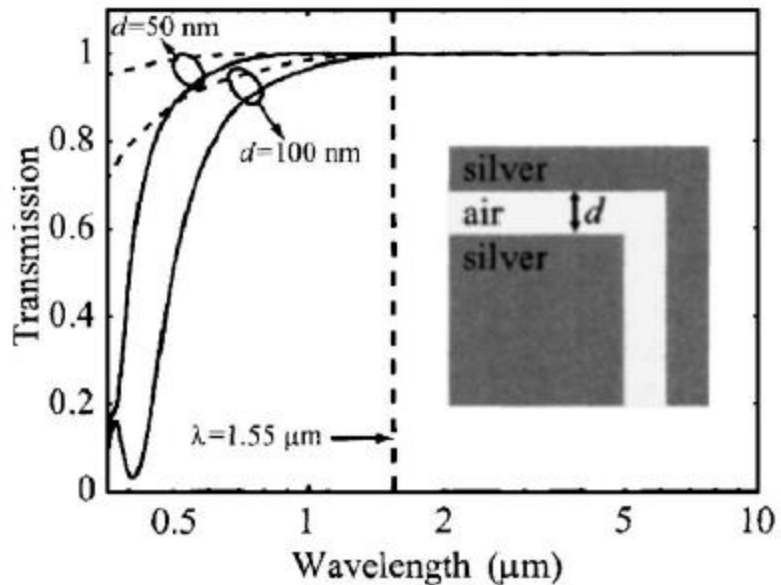


Fig. 2. (A) SEM image of a nanodot focusing array coupled to a 250-nm-wide Ag strip guide. **(B)** NSOM image of the SP intensity showing subwavelength focusing. [Adapted from (15)]

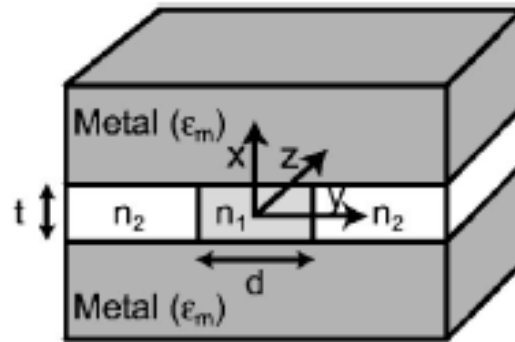
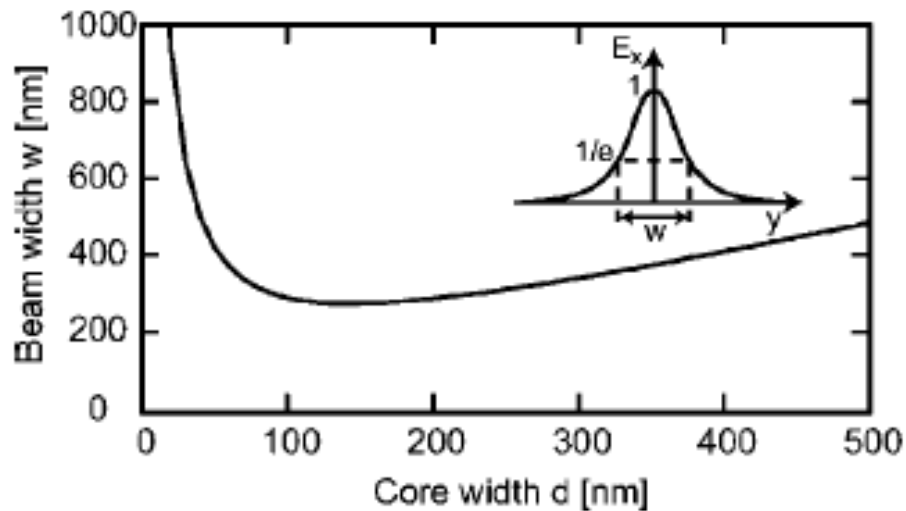
原理：如上图所示，光场通过半圆排列的纳米小洞后聚焦，聚焦后的能量通过SPP波导传递。

弯形SPP波导



结果：如上图所示，SPP通过弯形波导和T型分束器后，透射率很高。

金属介质混合型波导



632nm, Au

$n_1=1.45, n_2=1.0$

$t=100\text{nm}$

结果：

将传播的SP进一步局域在宽度为d的介质条中。

金属介质混合型波导

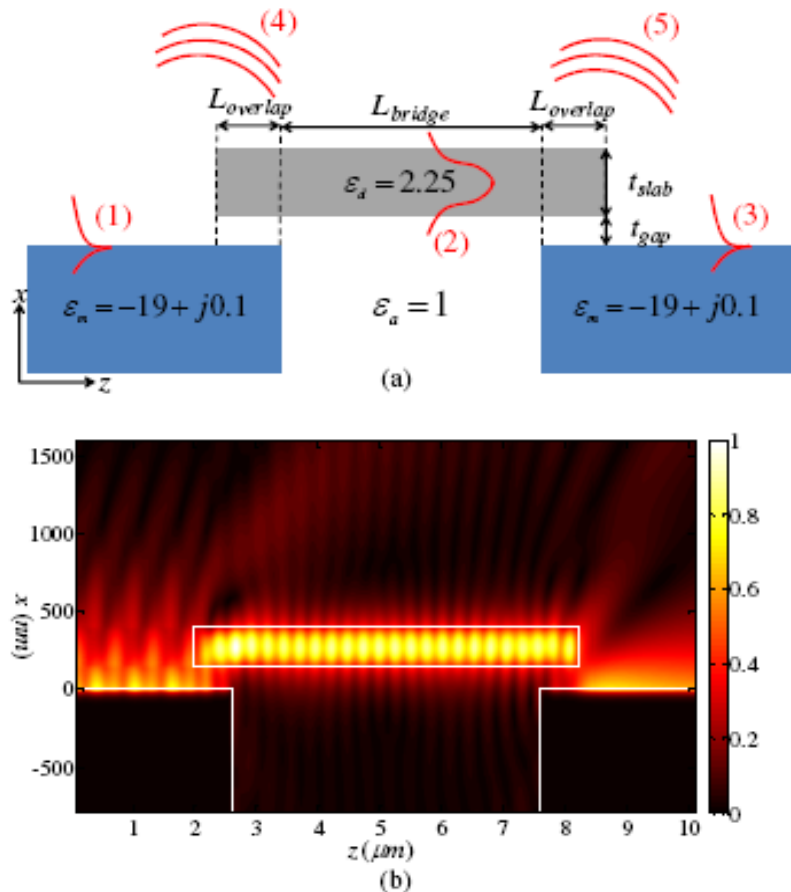


Fig. 1. (a) Schematic diagram of a floating dielectric slab interconnection between two air-based single metal-dielectric interface SPP waveguides. Each red drawing with number indicates corresponding eigenmode or scattered wave in given geometry. (b) (Media 1) The amplitude distribution of the magnetic field (H_y) of the floating dielectric slab interconnection; with $t_{gap}=150\text{ nm}$, $t_{slab}=250\text{ nm}$, $L_{overlap}=600\text{ nm}$, and $L_{bridge}=5\text{ }\mu\text{m}$, respectively.

结果：

通过近场耦合，将传播的**SP**的能量局域在介质条上。

杂化SPP波导

Sub-wavelength confinement and long-range propagation

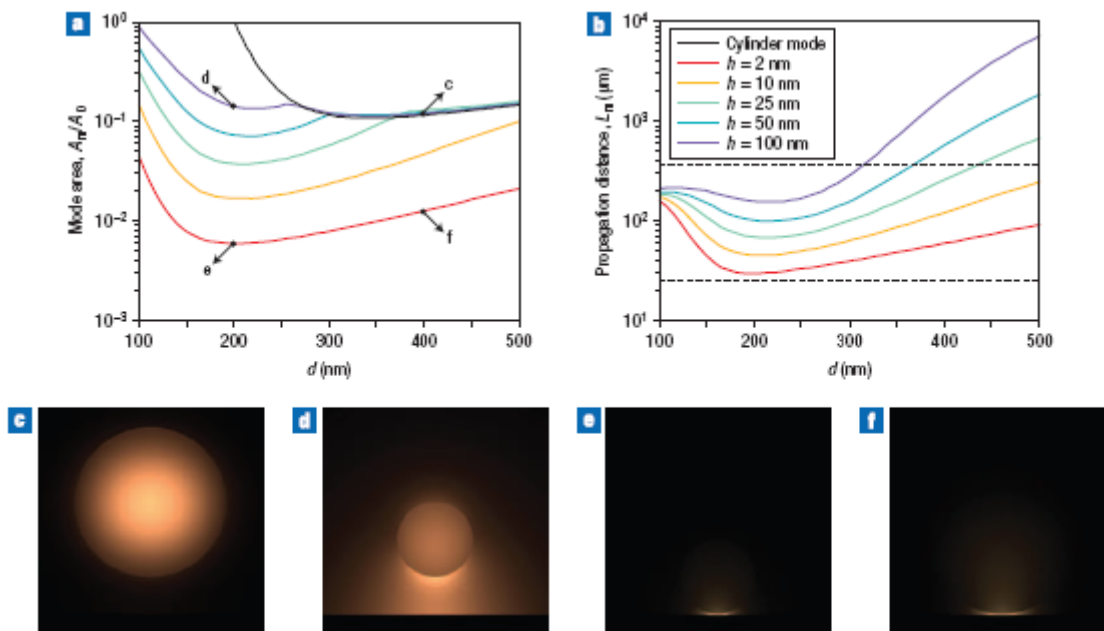
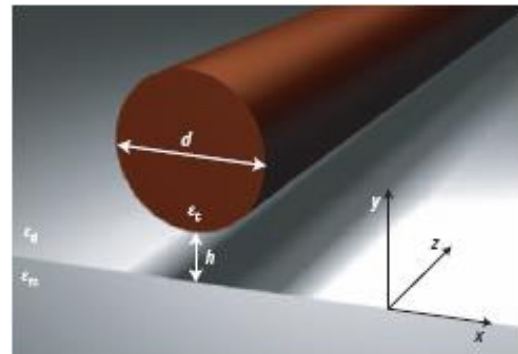
Hybrid waveguide:
dielectric cylindrical nanowire

$\epsilon_c = 12.25$, d

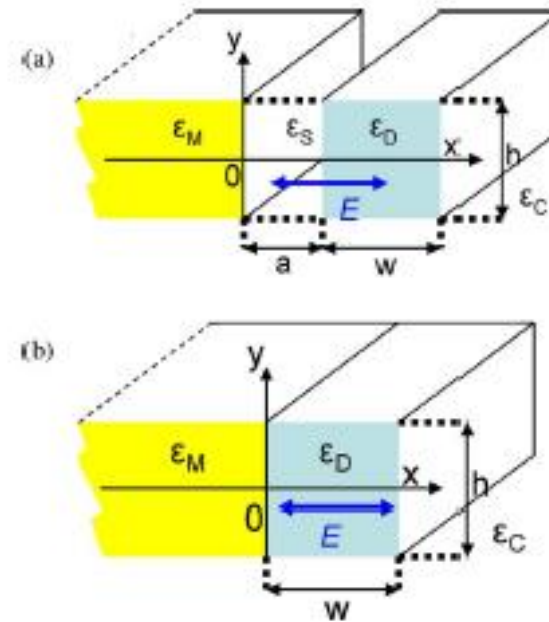
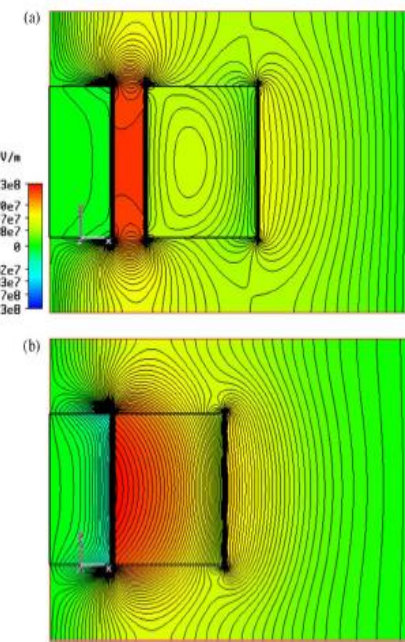
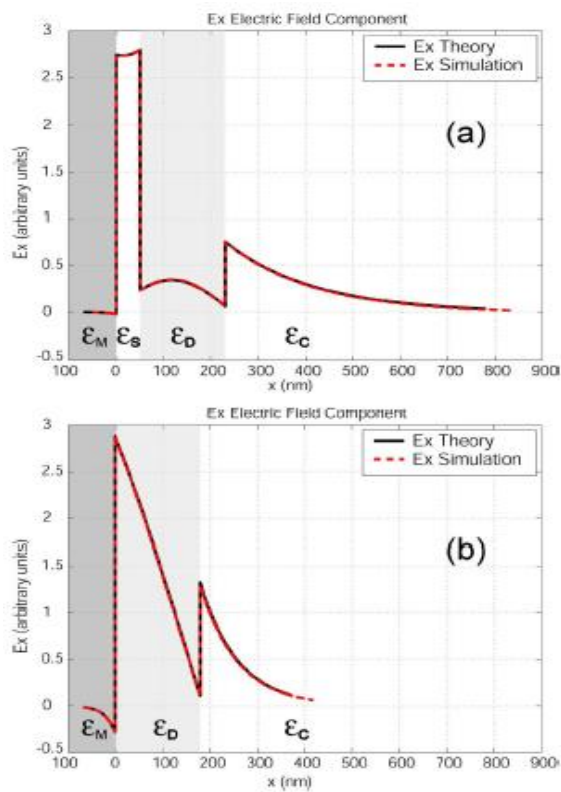
dielectric gap $n_c = 2.25$, h
metallic half-space Ag

Results:
tightly confined field
in the vicinity of the
gap, low-loss light
transport

Explanation:
Hybridization of the fundamental mode of a dielectric cylinder
with the SPP of a dielectric-metal interface.



杂化SPP波导



参数：

$$\epsilon_S = \epsilon_C = 1, \epsilon_D = 11.9, \epsilon_M = -115.8 + j10.33$$

$$h = 200 \text{ nm}, a = 50 \text{ nm}, w = 180$$

$$1550 \text{ nm.}$$

结论：
电磁场被局域在gap中或
高介电常数材料中

其它类型SPP波导

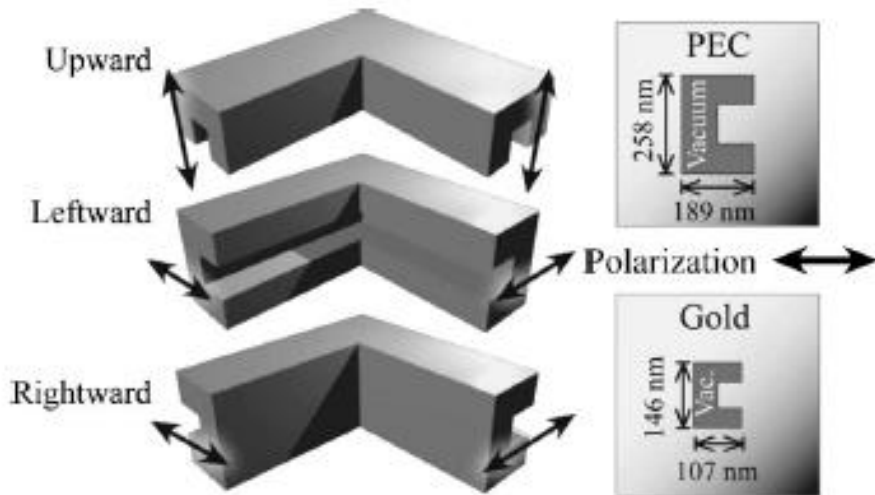


Fig. 1. Waveguide simulation schematic showing the possible orientations for a 90° bend in a C-aperture waveguide, as well as the cross-sectional dimensions of the simulated structures.

C型波导

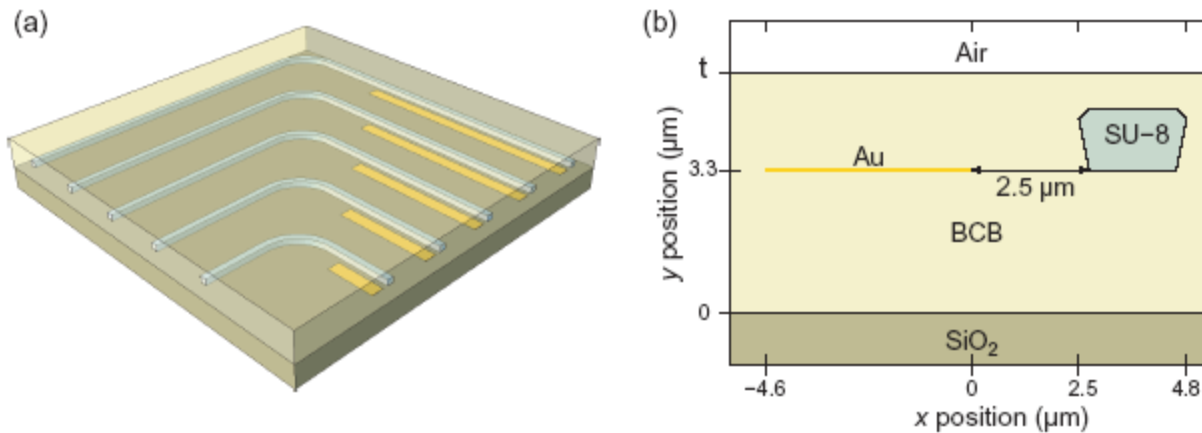
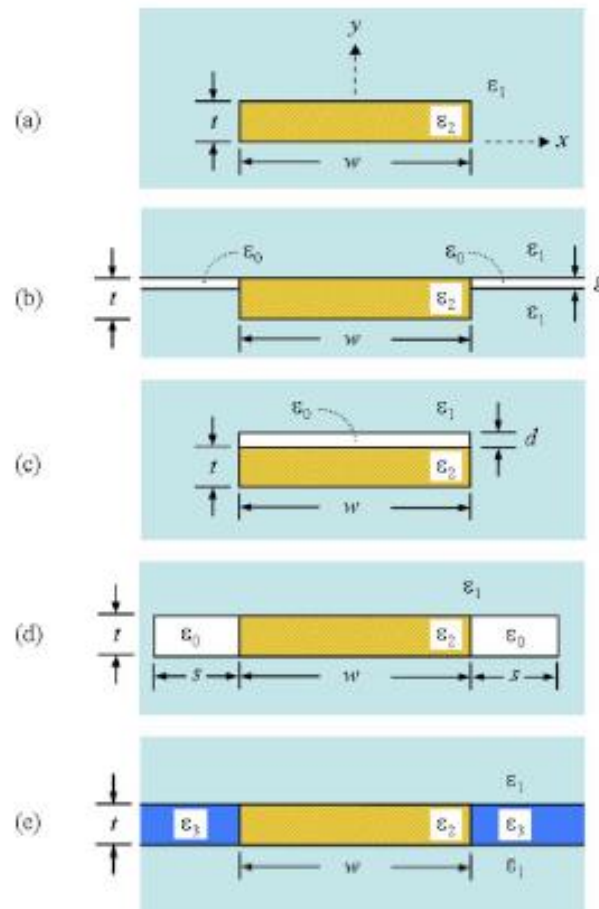
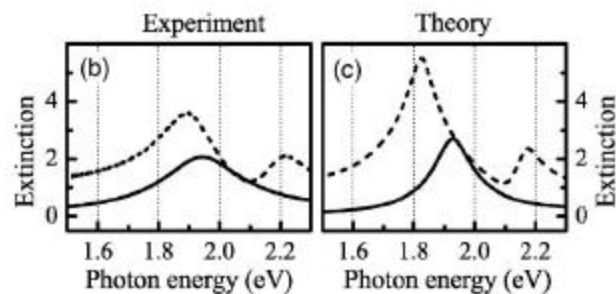
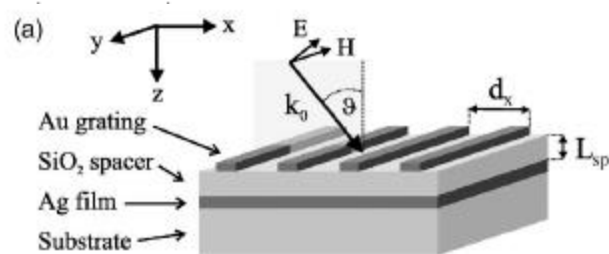
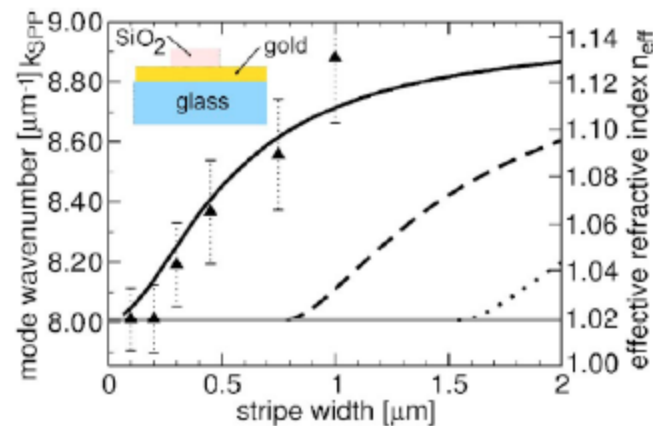


Figure 1. (a) Overview of the structures consisting of a series of SU-8 waveguides coupled to Au stripes. The radius of curvature of the SU-8 waveguides is 1 mm. (b) Cross-sectional view of a coupler. Except for the thickness t of the BCB layer, the coupler dimensions are kept constant throughout this study and the couplers are always positioned 3.3 μm above the SiO_2 substrate. The Au stripe has a width of 4.6 μm , a thickness of 36 nm, and is separated from the SU-8 waveguide by a gap of 2.5 μm . The average width and thickness of the SU-8 waveguide are 2 μm and 1.5 μm . At $\lambda = 1.55 \mu\text{m}$, the permittivity of Au is $-132 + 12.65i$ [22] and the refractive indices of SiO_2 , BCB and SU-8 are, respectively, 1.444 [20], 1.535 [21] and $1.57 + 8e - 5i$. Note that we have added an imaginary part to the refractive index of SU-8 so as to fit the losses of our real waveguides. These losses were determined with cut-back measurements.

弯型混合波导

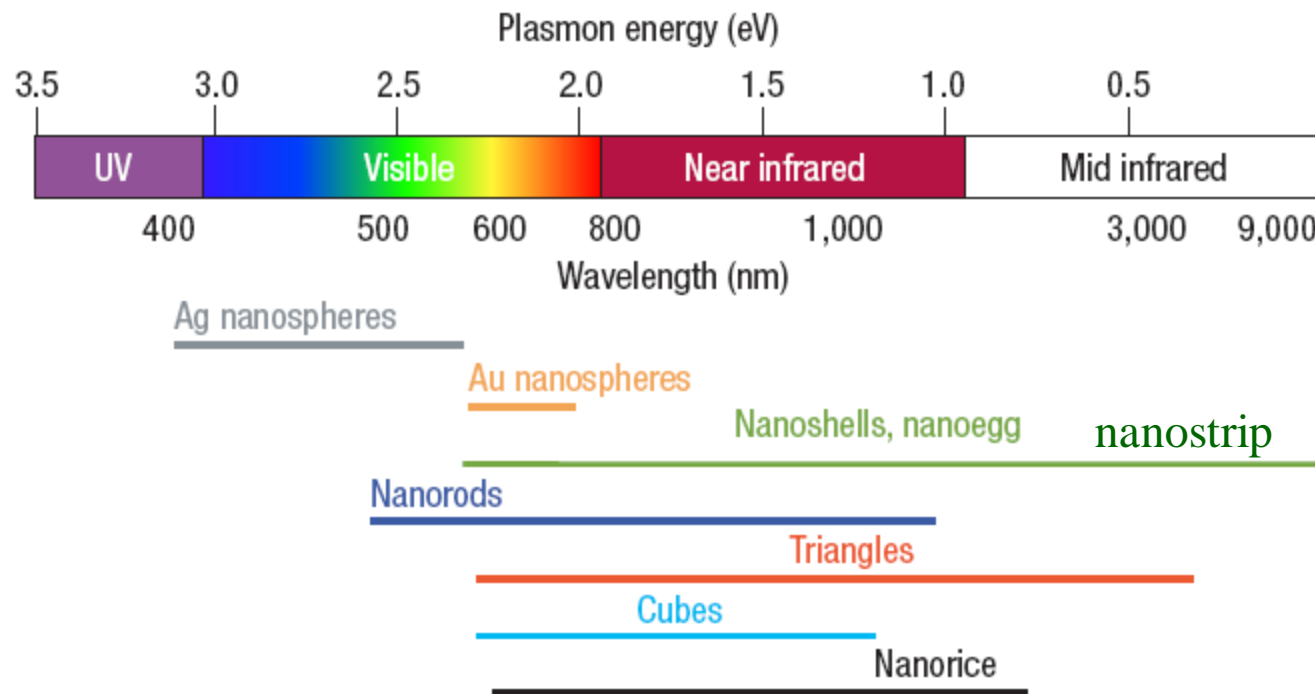
其它类型SPP波导（仅给出示意图）





2.2.2 表面等离激元共振 (SPR) 及应用

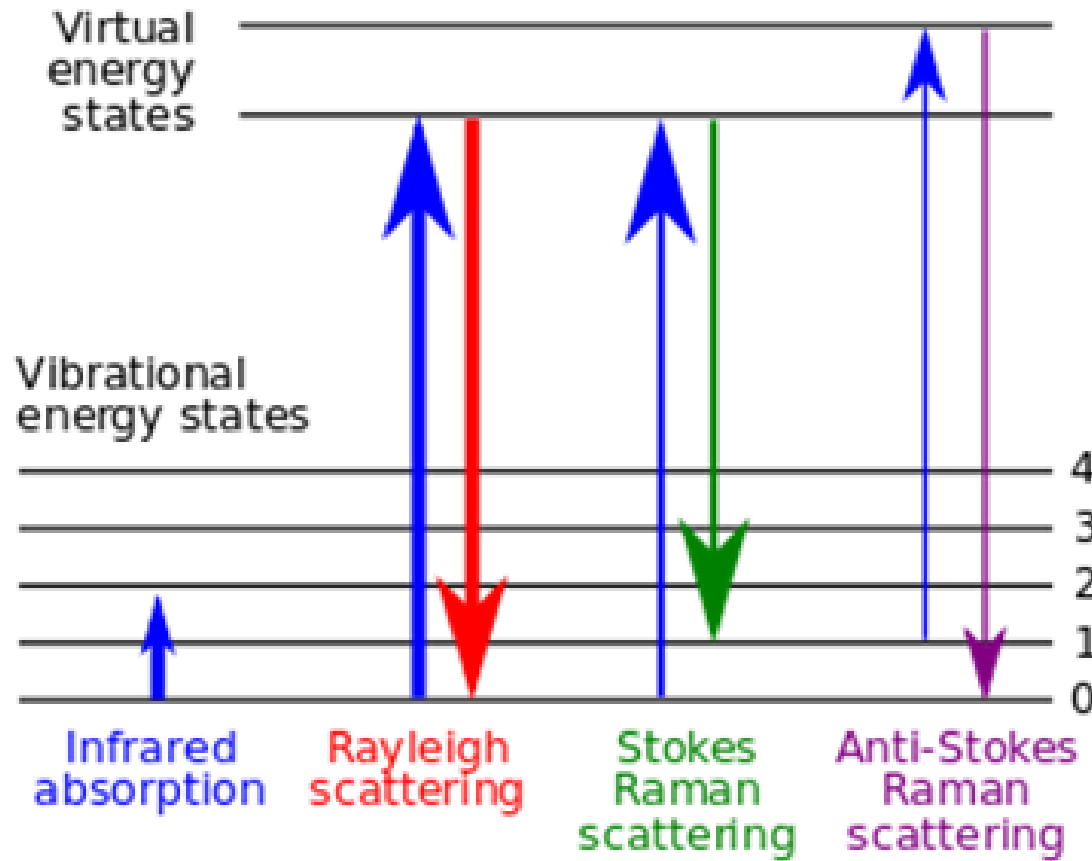
各种形状金属颗粒SPR的共振范围



结论：通过调节纳米金属颗粒的形状，SPR可发生在可见光、红外和中红外波段。

实际上：在通讯、太赫兹和微波波段，SPR的研究也很广泛。

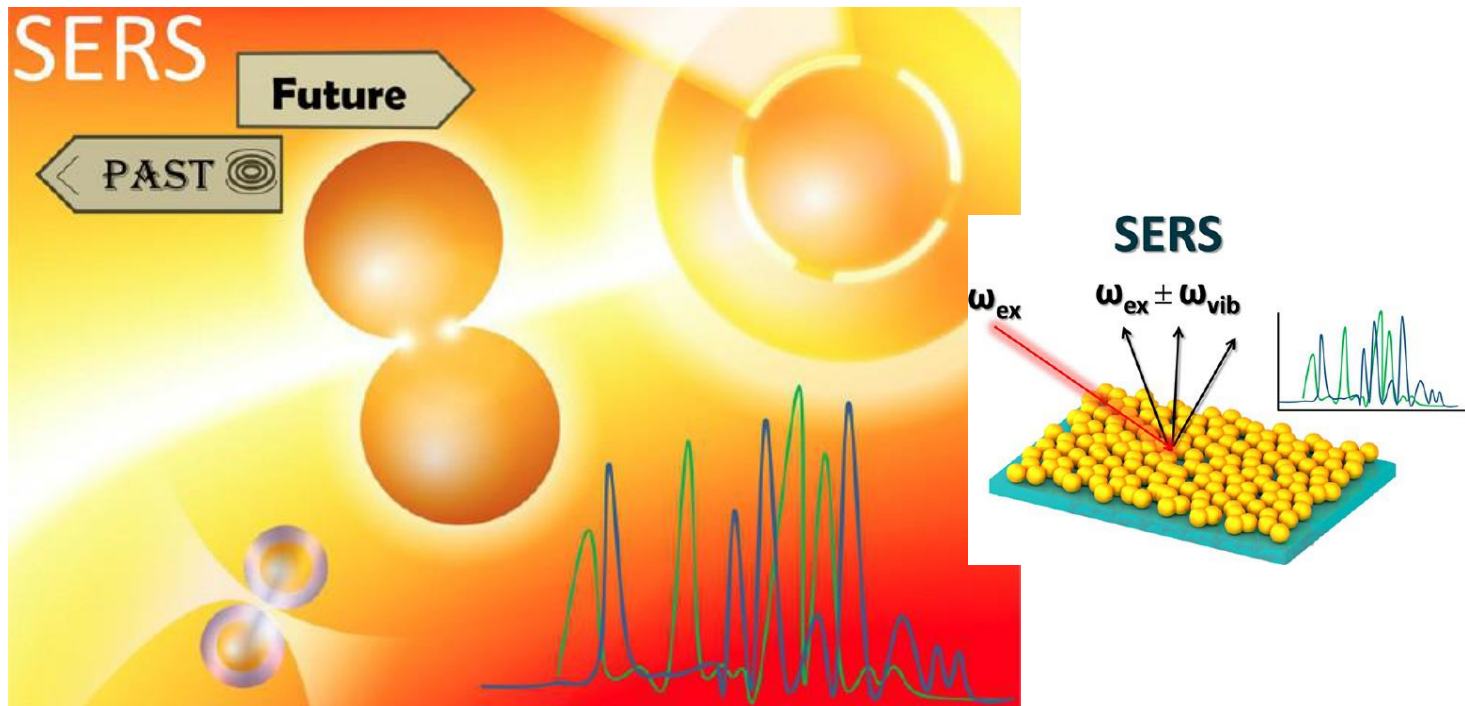
拉曼散射



来自吕国伟老师的PPT

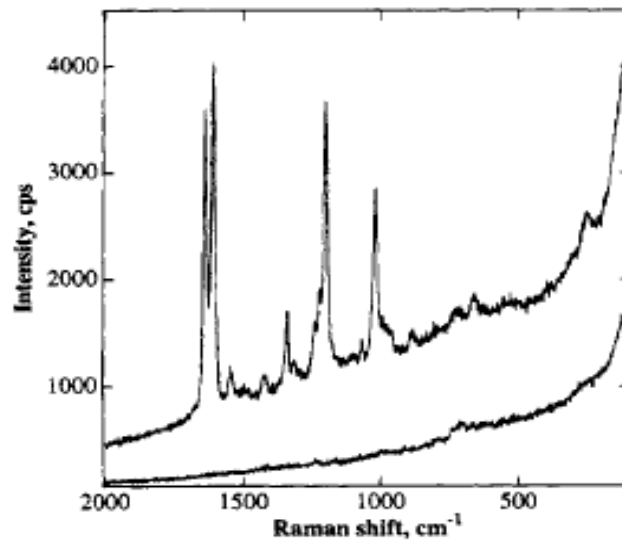
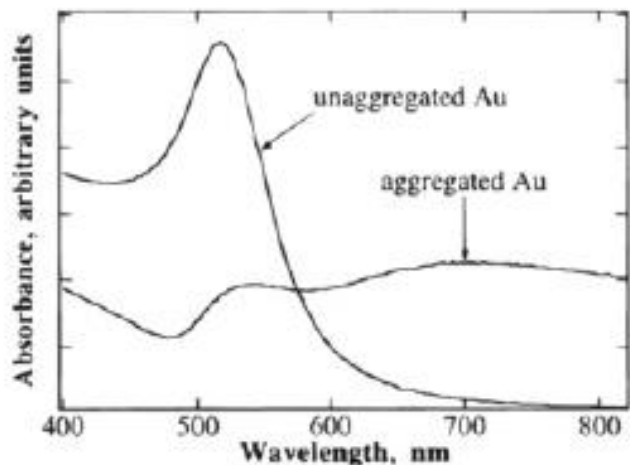
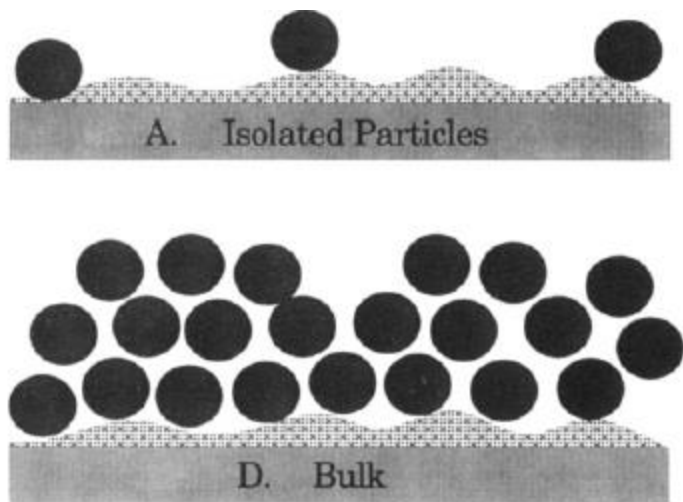
SERS/TERS

Surface/Tip Enhanced Raman Scattering



来自吕国伟老师的PPT

金小球的SPR及SERS



结果：13nm的金小球，在 isolated情况下，共振在520nm，在聚集时，共振在700nm。以及在647nm共振时的SERS。

银纳米岛的SPR及SERS

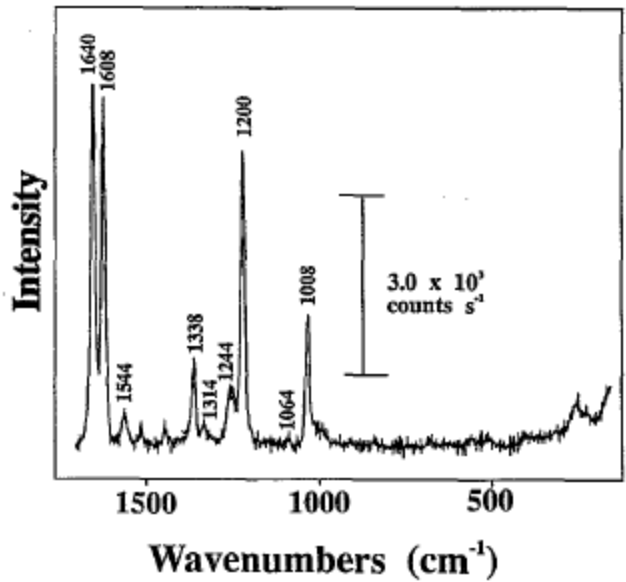
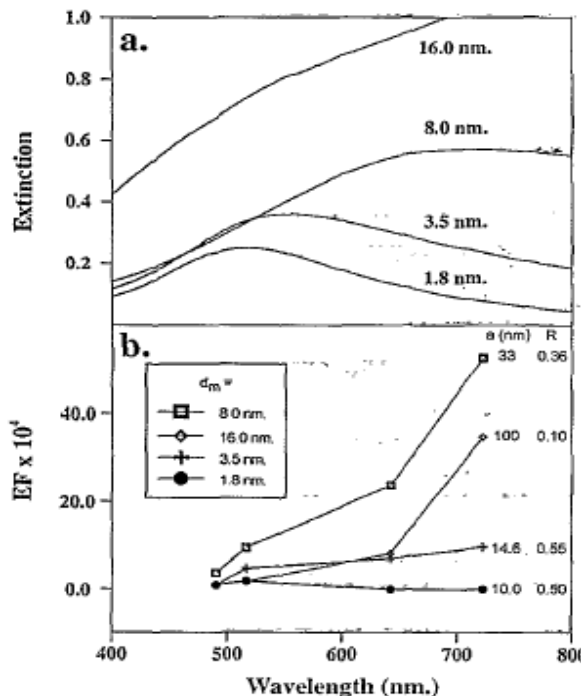
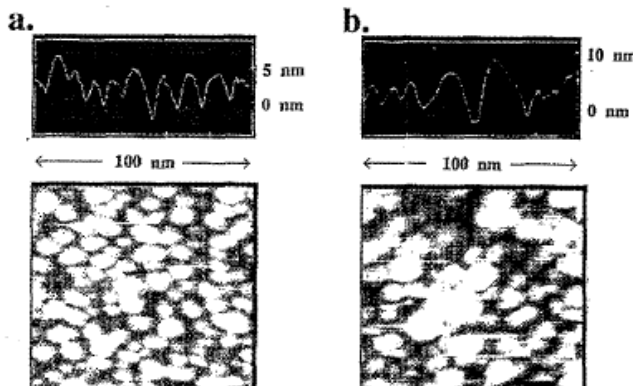


FIG. 10. SERS spectrum of 1.0 monolayer of BPE spin coated on a Ag island film, $d_m=8$ nm. 10 mW of $\lambda_{ex}=722$ nm.

结果：随着纳米小球尺寸的增加，共振红移，场增益系数增加，以及在722nm共振时的SERS。



银纳米三角形结构的制备及通讯波段SPR

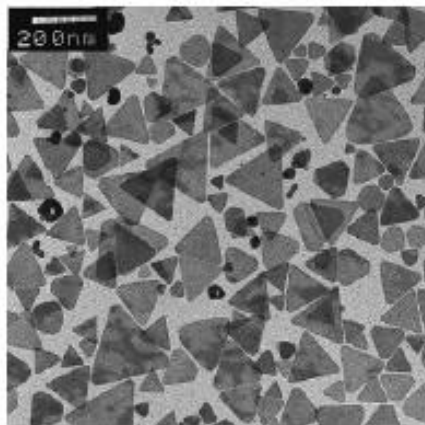
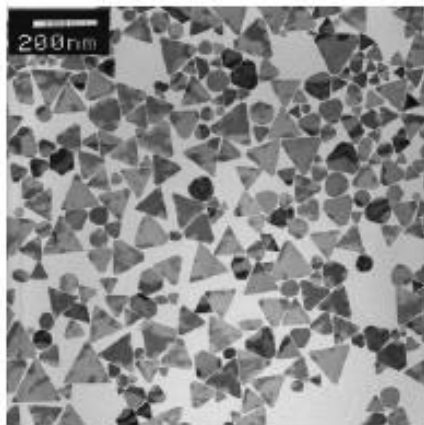
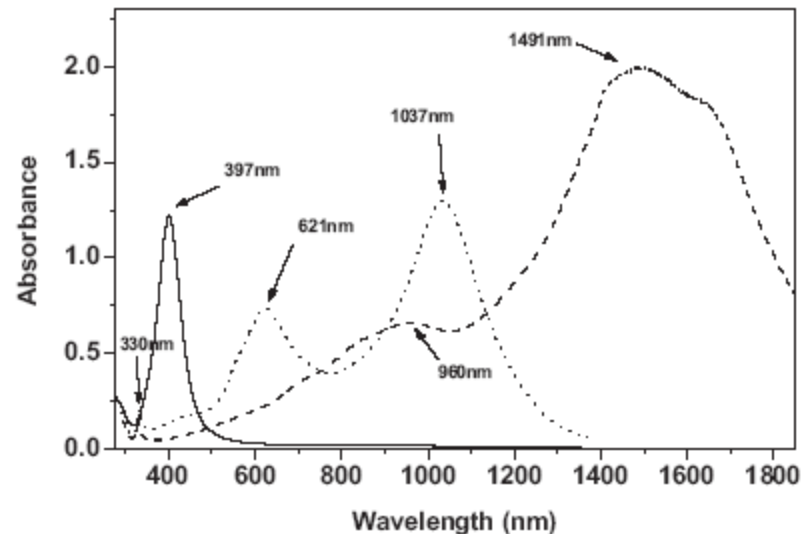


Figure 3. Representative TEM images of Ag nanoprisms prepared by illumination of Ag seeds with green (left) and red (red2, right) LEDs.



结果：除了光波段，我们看到了在1000到1500纳米间的SPR

银纳米三角形结构的SPR及近场分布

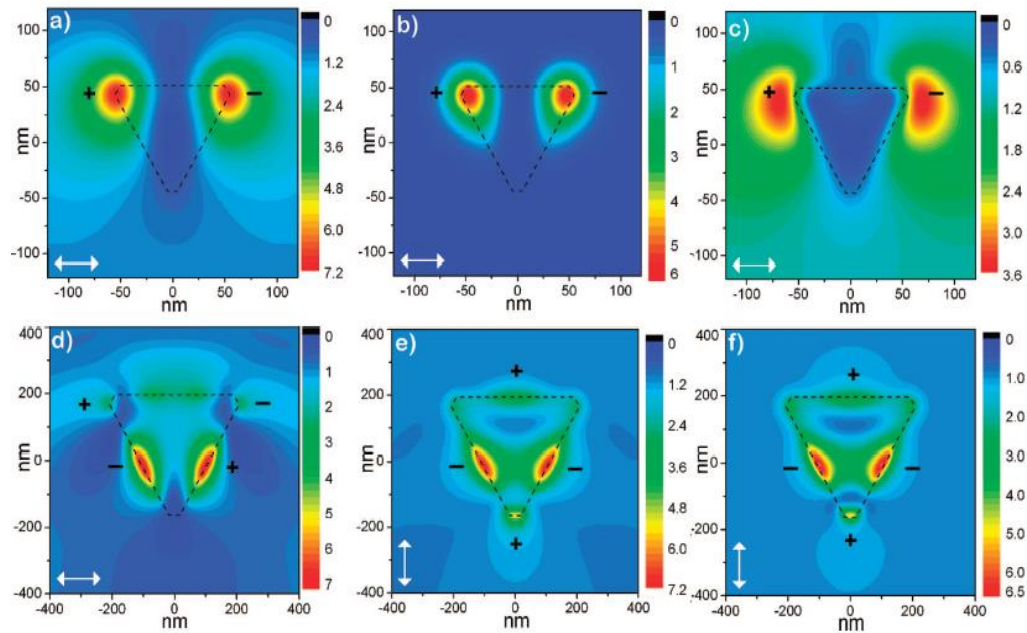
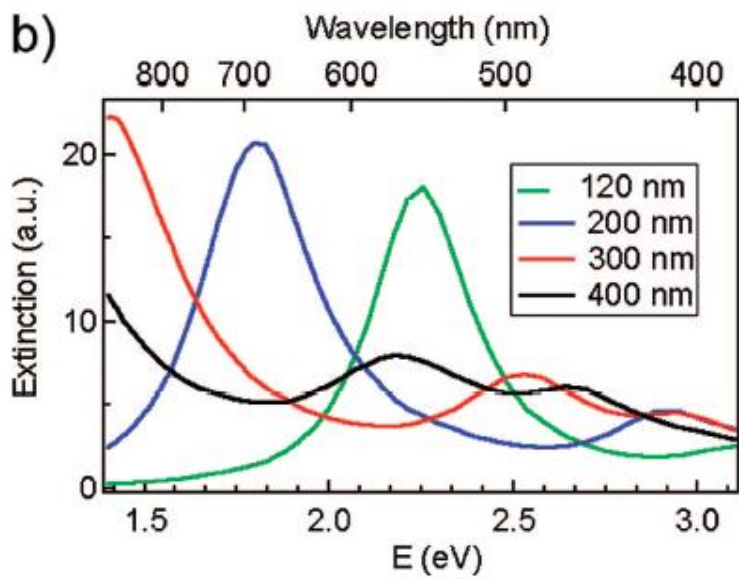
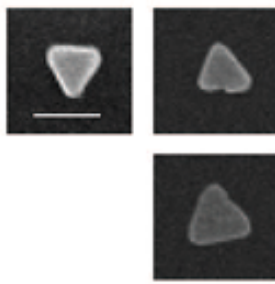
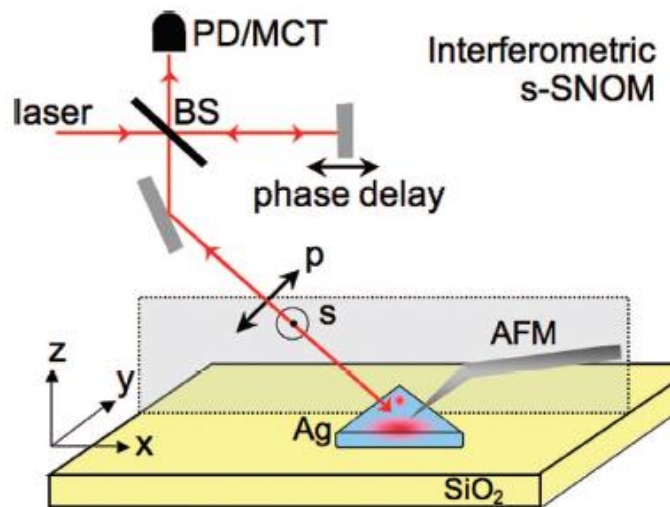


Figure 6. Calculated optical near-field distribution of the Ag nanoprism for 633 nm excitation. Top row: dipolar mode for nanoprism with

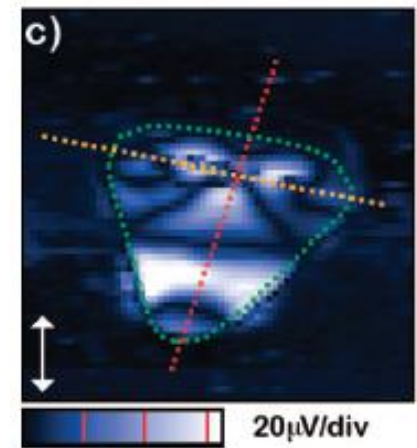
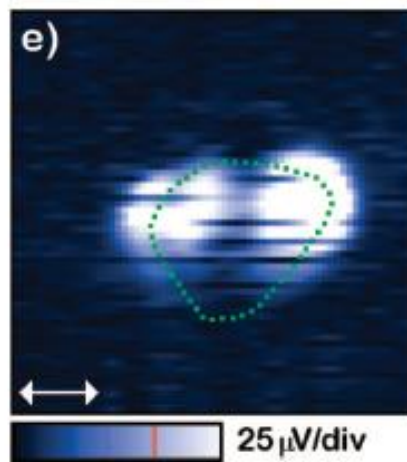
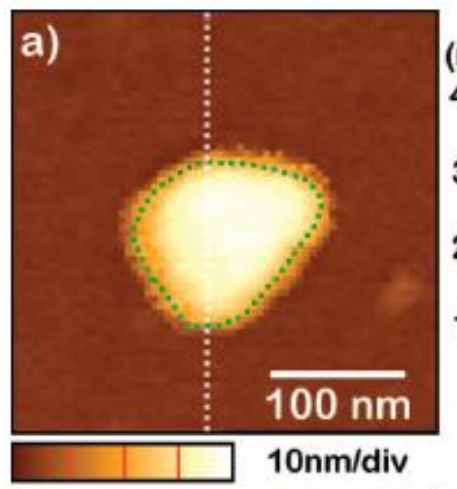


结果：随纳米三角形结构尺度的增加，共振红移；上图给出电偶极和电四极共振时的电场分布和电荷分布。

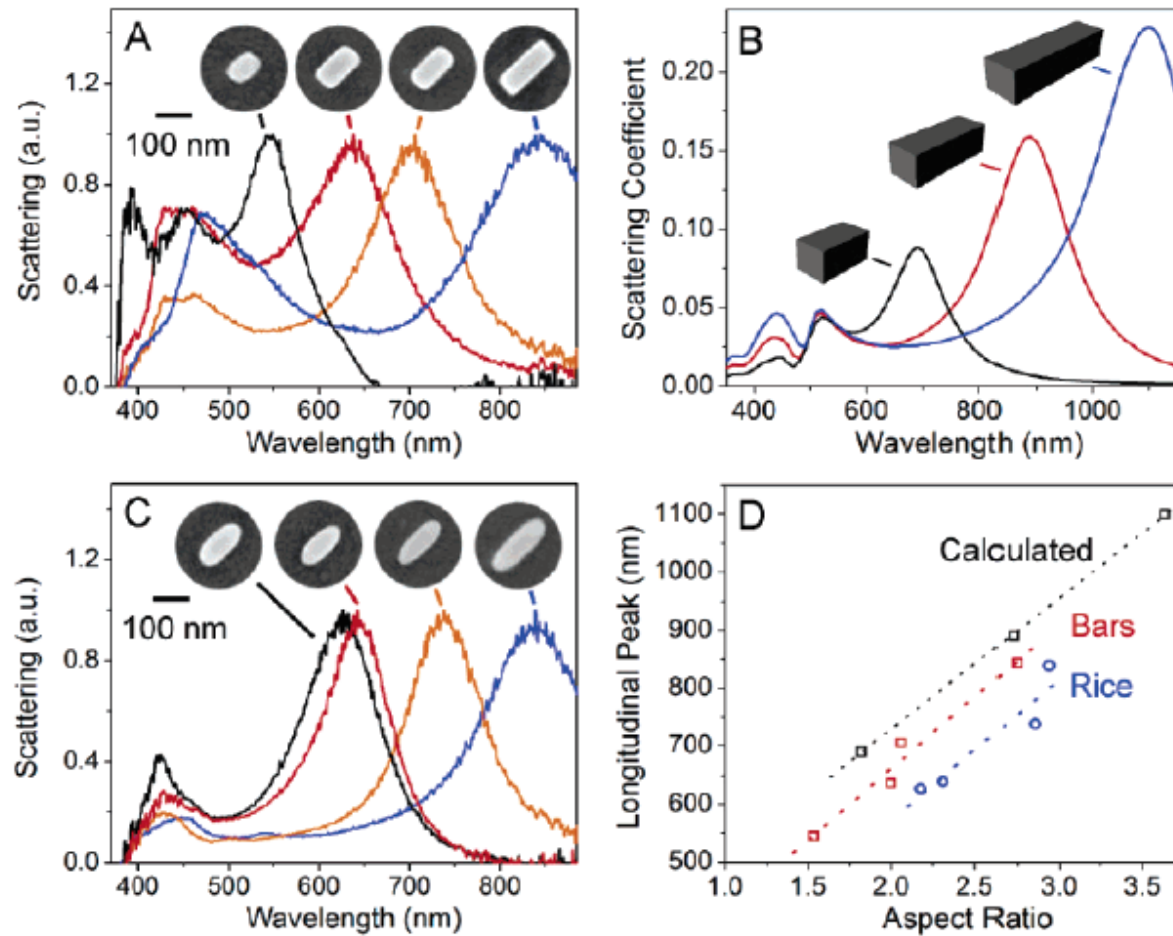
SNOM近场分布



结果：用**SNOM**探测到的共振时的近场分布，**AFM**探测到纳米三角形结构，结果与理论计算相符。

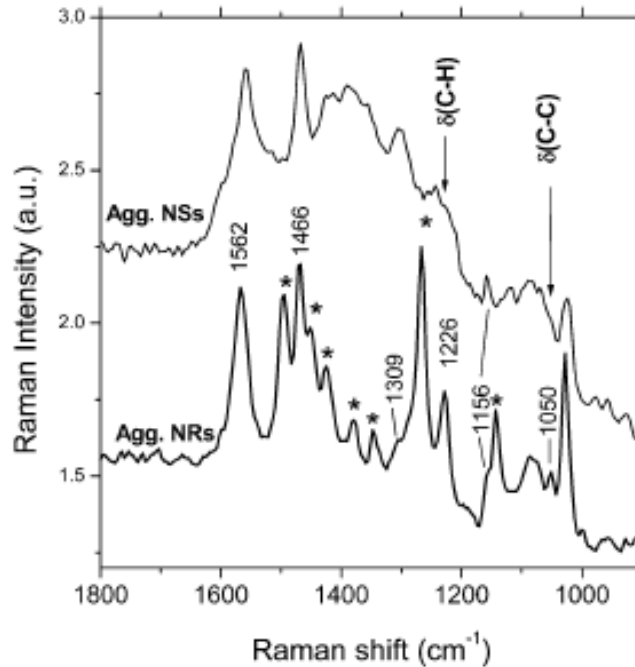
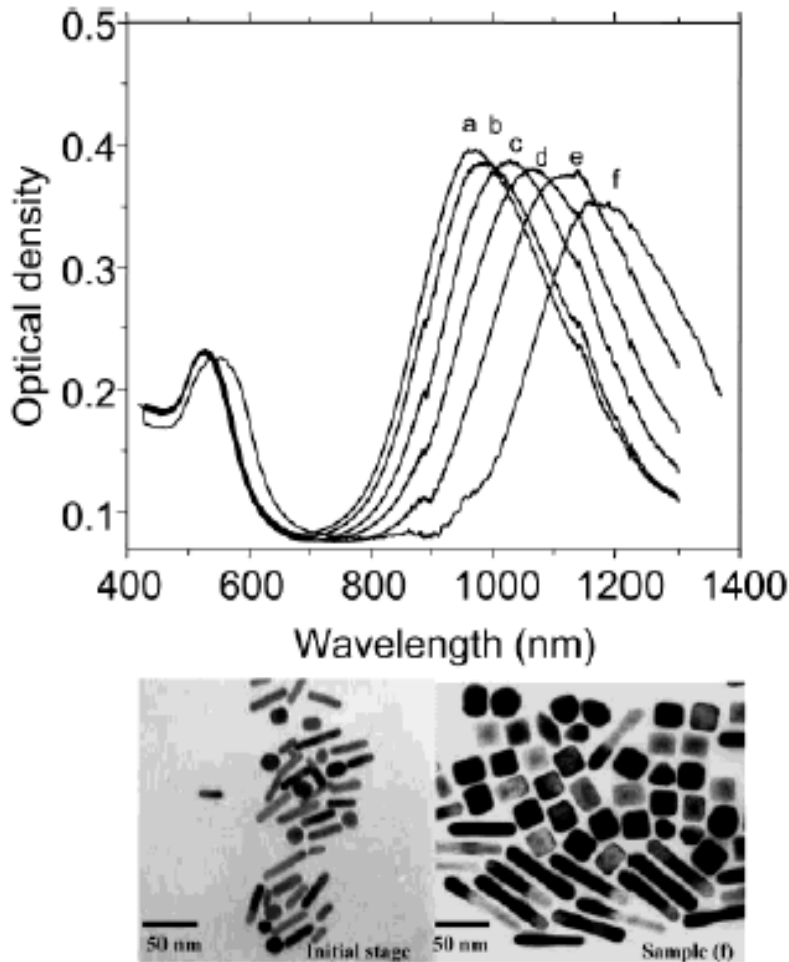


银 Nanobars 和 Nanorices 的 SPR



结果：制备出的银纳米颗粒尺度在百纳米内，共振在光波段，用散射谱表征SPR。理论计算用DDA。

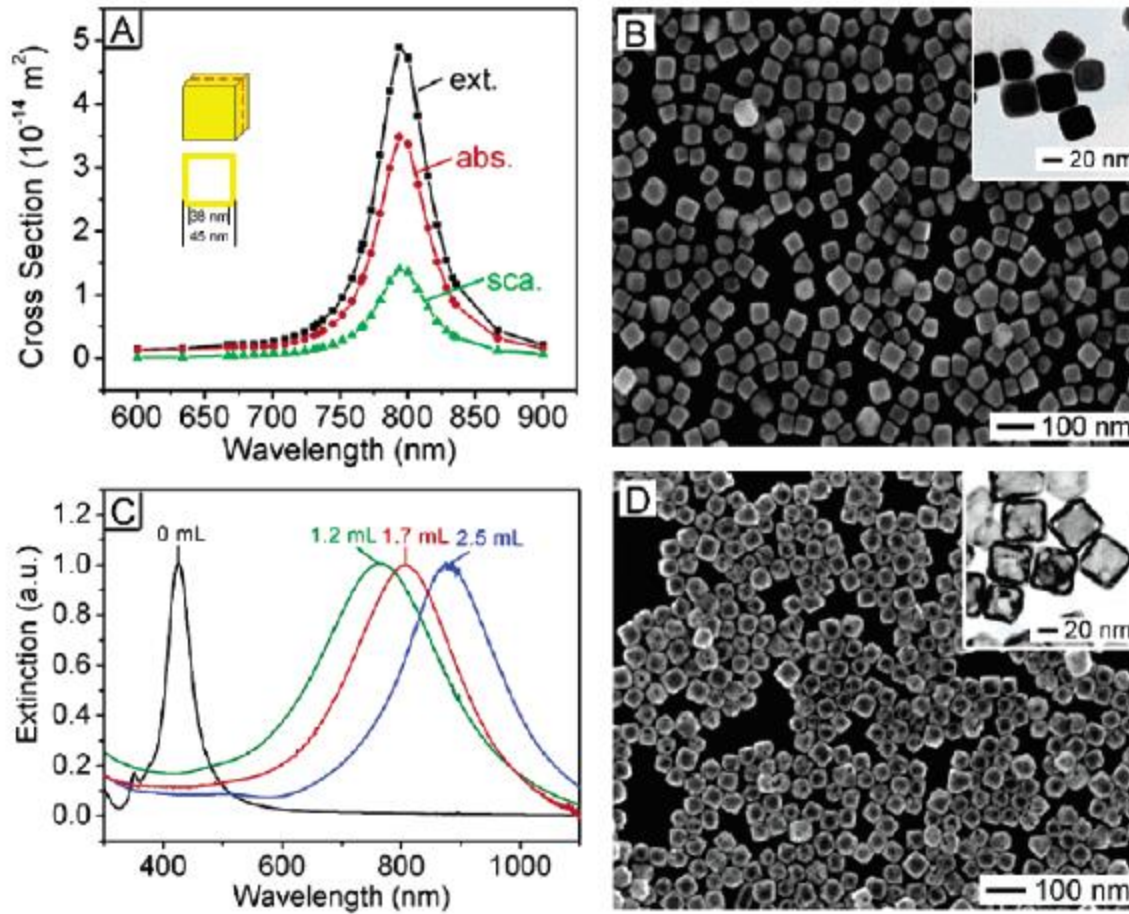
金Nanorods 的SPR及SERS



结果：制备出的金纳米颗粒尺度在百纳米的尺度，共振波长在光到近红外，可增强SERS。

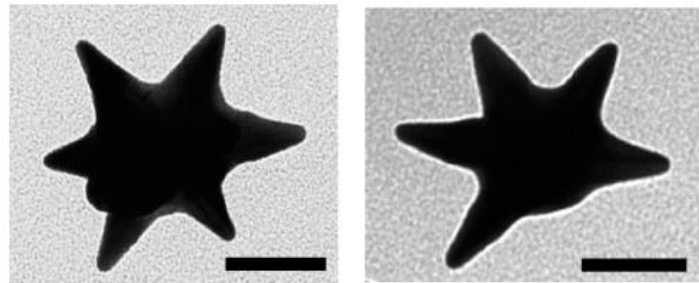
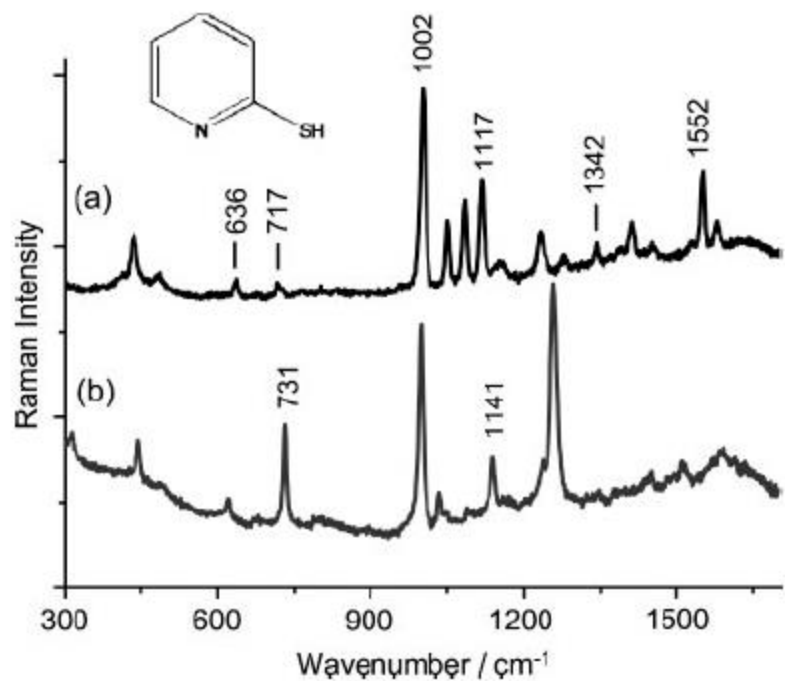
- [Preparation and Growth Mechanism of Gold Nanorods \(NRs\) Using Seed-Mediated Growth Method](#)
Babak Nikoobakht and Mostafa A. El-Sayed, Chem. Mater. 2003, 15, 1957-1962
[Surface-Enhanced Raman Scattering Studies on Aggregated Gold Nanorod](#),
Babak Nikoobakht and Mostafa A. El-Sayed, J. Phys. Chem. A 2003, 107, 3372-3378

纳米金笼的SPR

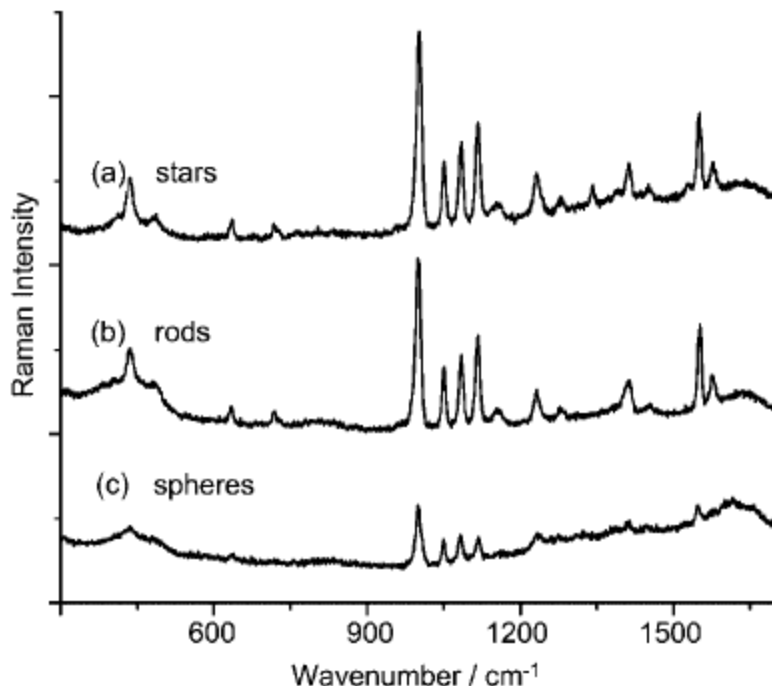


结果：制备出的纳米金笼尺度在百纳米内，共振波长在光波段，可用于癌症细胞的靶向治疗或免疫等。

金Nanostar的SPR及SERS

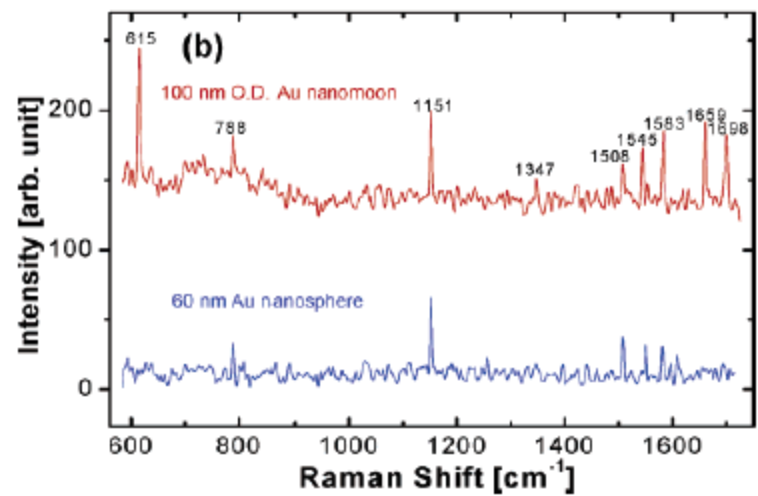
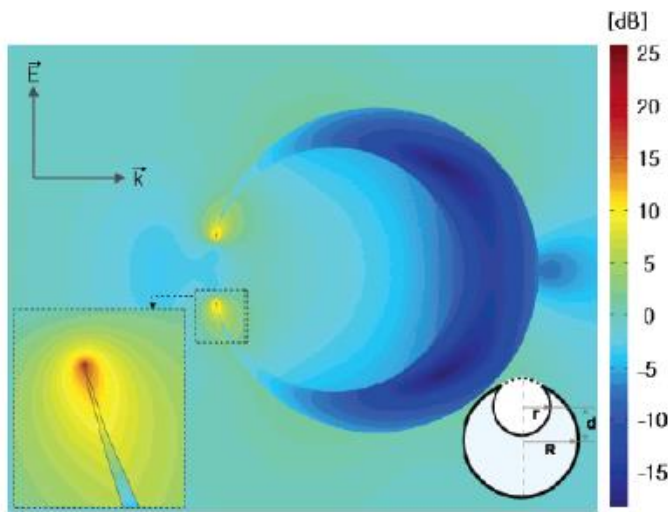
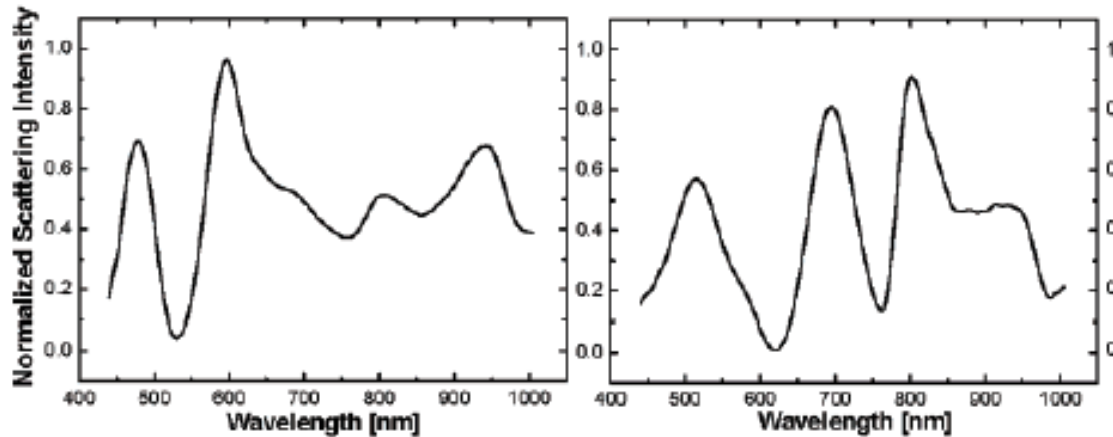
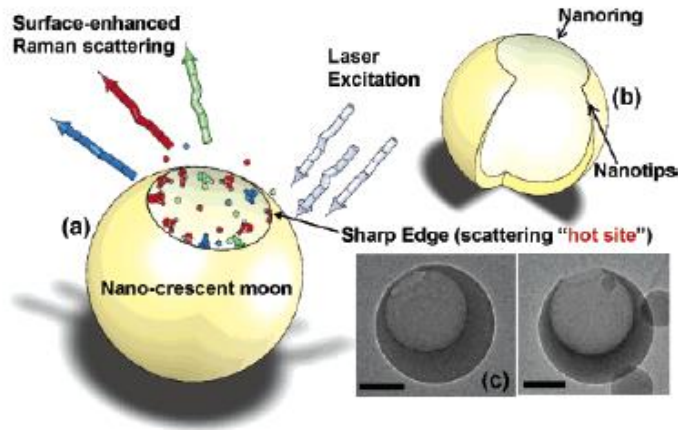


star-shaped gold nanoparticles. The scale bars are 50 nm.



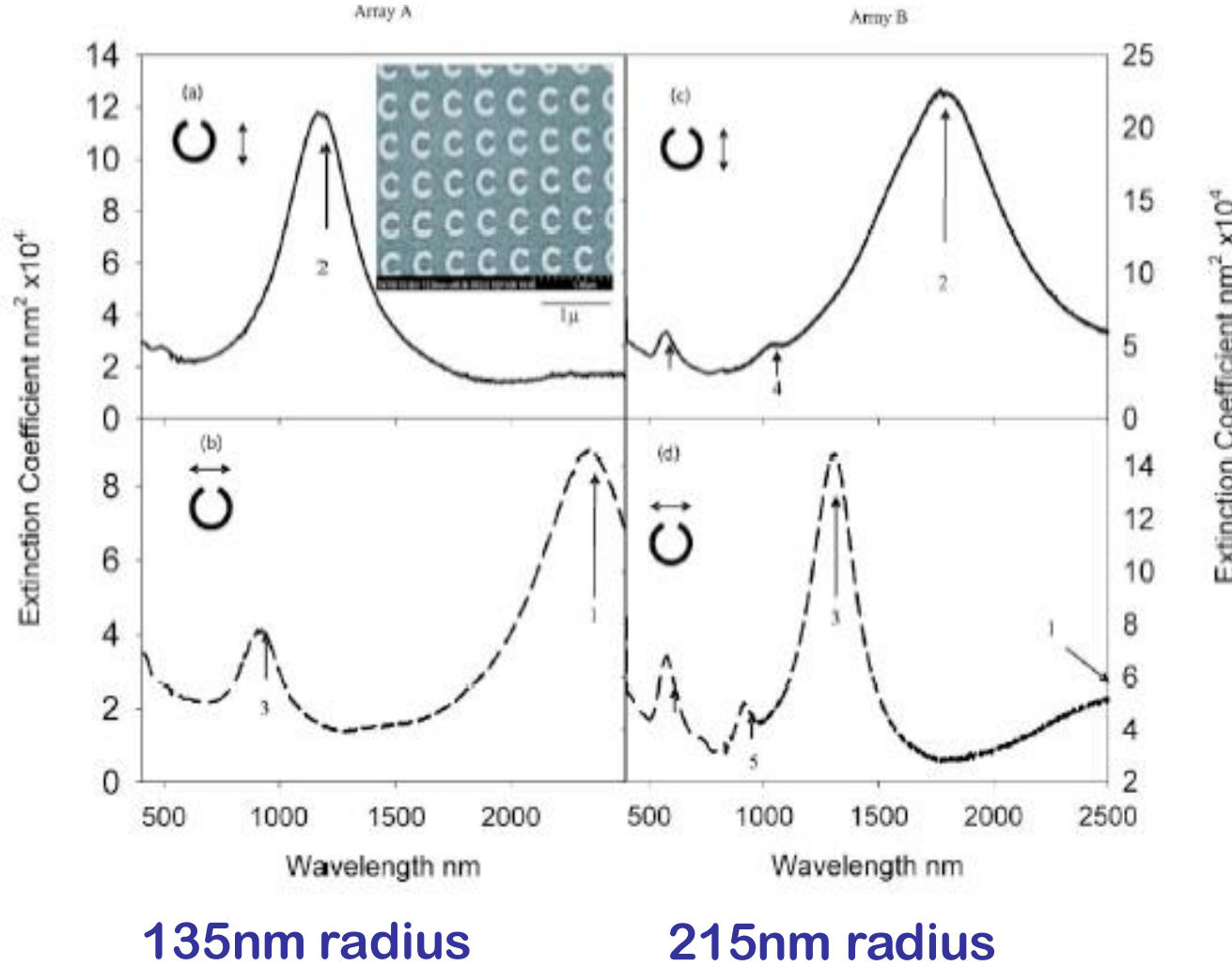
结果：制备出的纳米金星在增强表面拉曼散射方面的应用。一方面，出现更多拉曼峰，另一方面，强度增加。

金Nanocrescent的SPR及SERS



结果：制备出的纳米金月形，出现多重共振，电场局域在尖角，在增强表面拉曼散射方面的应用。

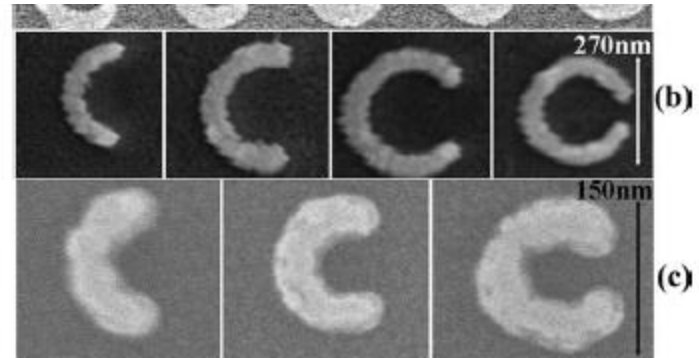
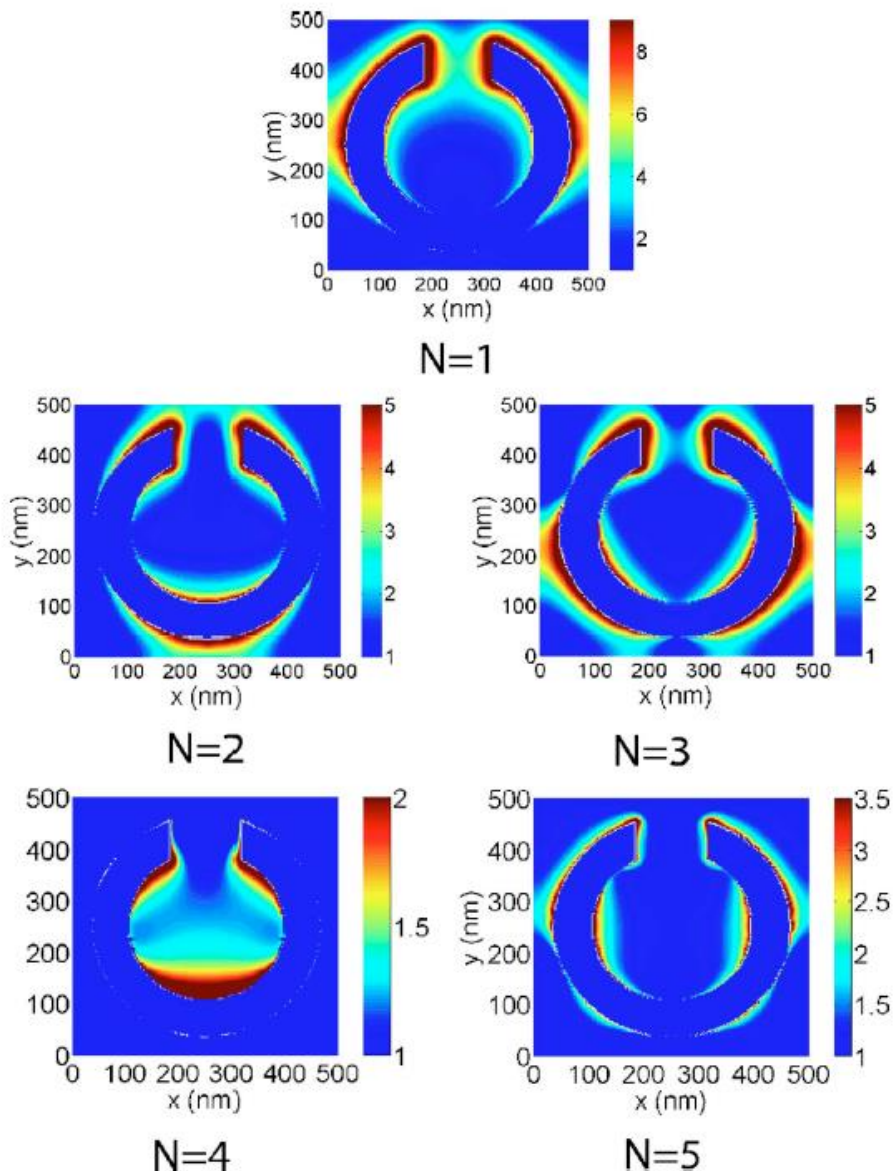
金Nanoring的多重SPR



结果：制备出的纳米C形，出现多重共振，1,2,3,4,5.

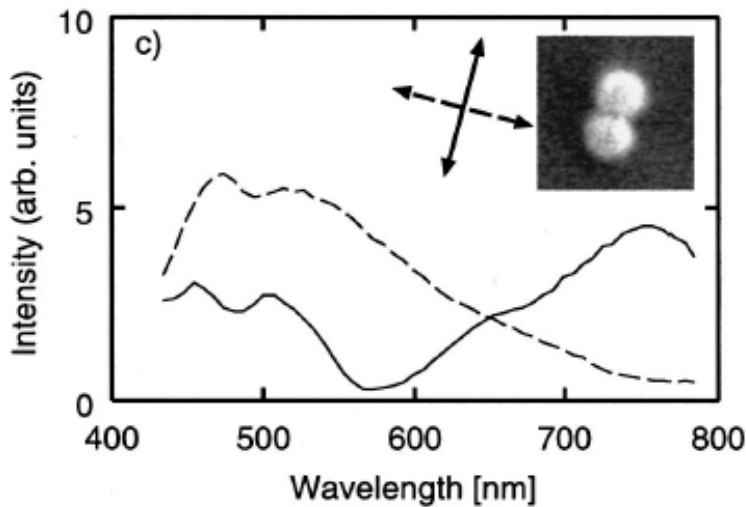
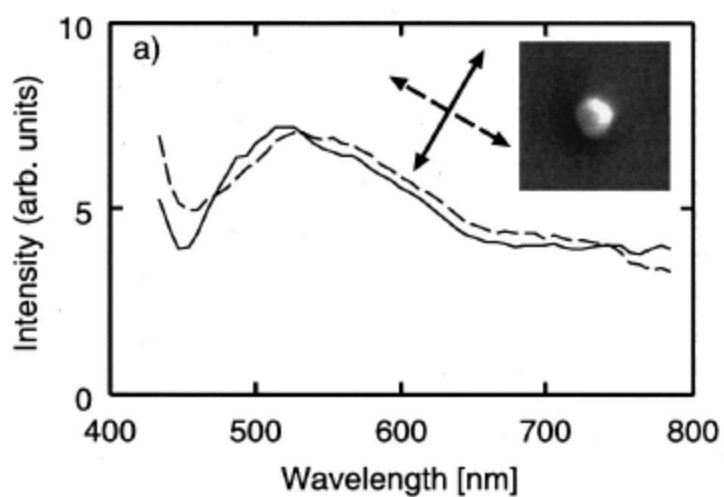
Multiple plasmon resonances from gold nanostructures,

A. K. Sheridan et al, APPLIED PHYSICS LETTERS 90, 143105 (2007).



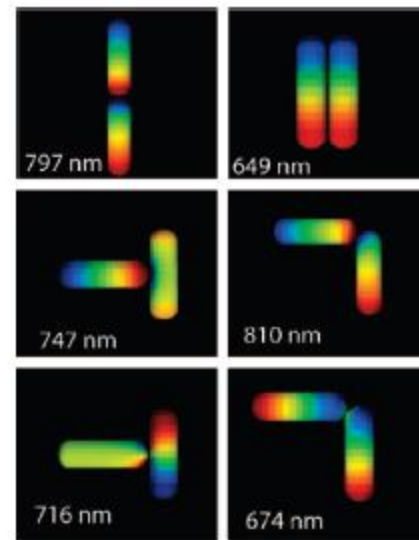
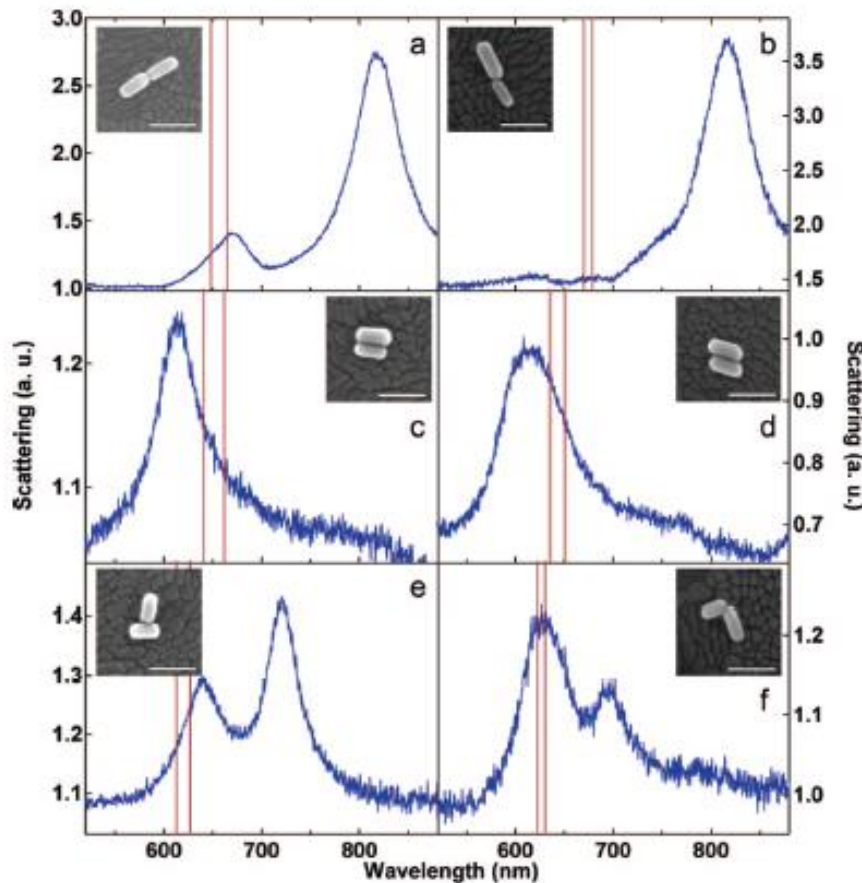
以上模式的电场分布。

银纳米金属颗粒间的SPR相互作用



结果：100nm直径的银球共振在520nm左右，两个银球放在一起时，加平行中心线的光场，共振红移到760nm，加垂直光场时，共振蓝移到470nm。

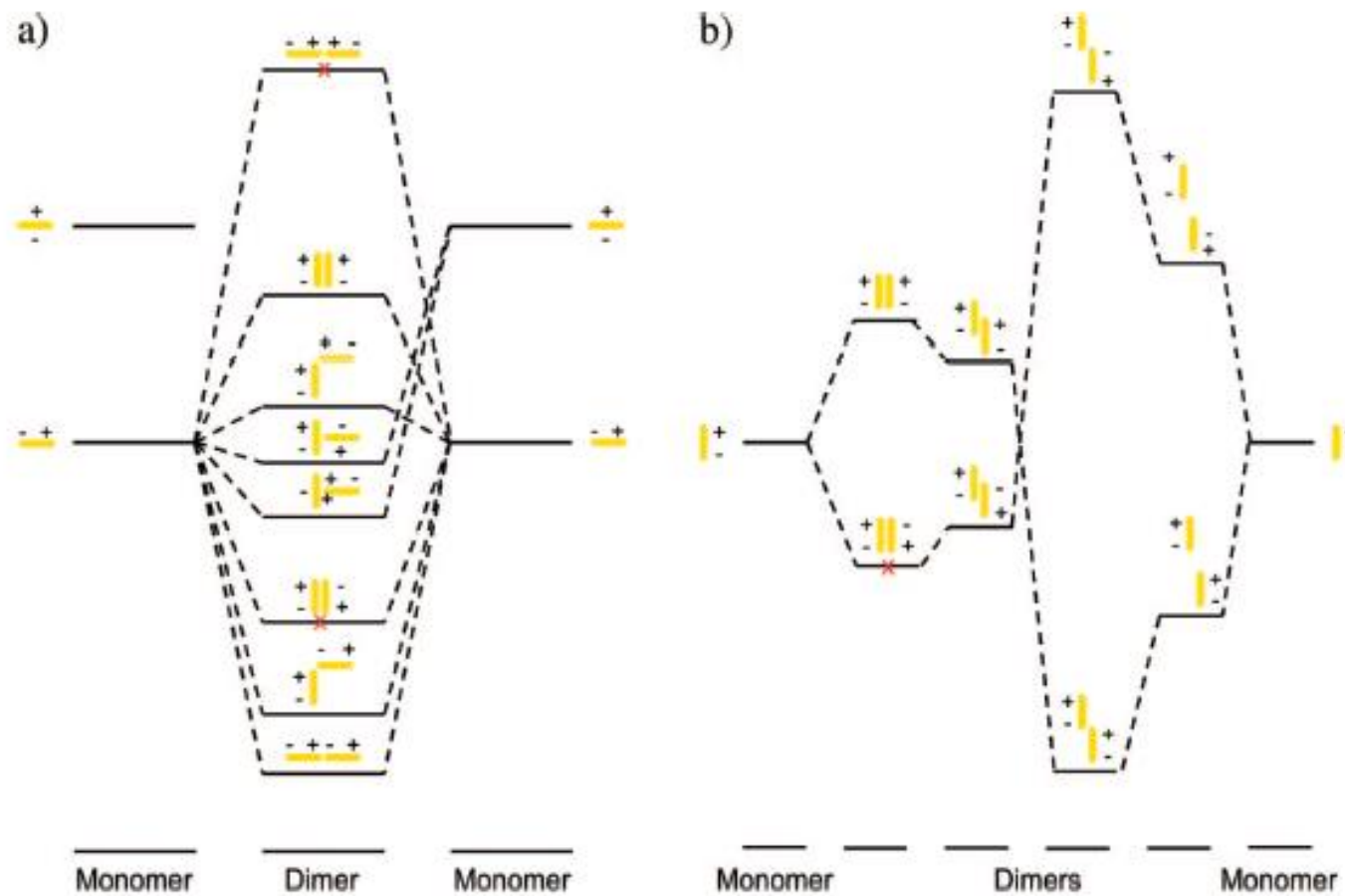
百纳米金棒间的SPR耦合



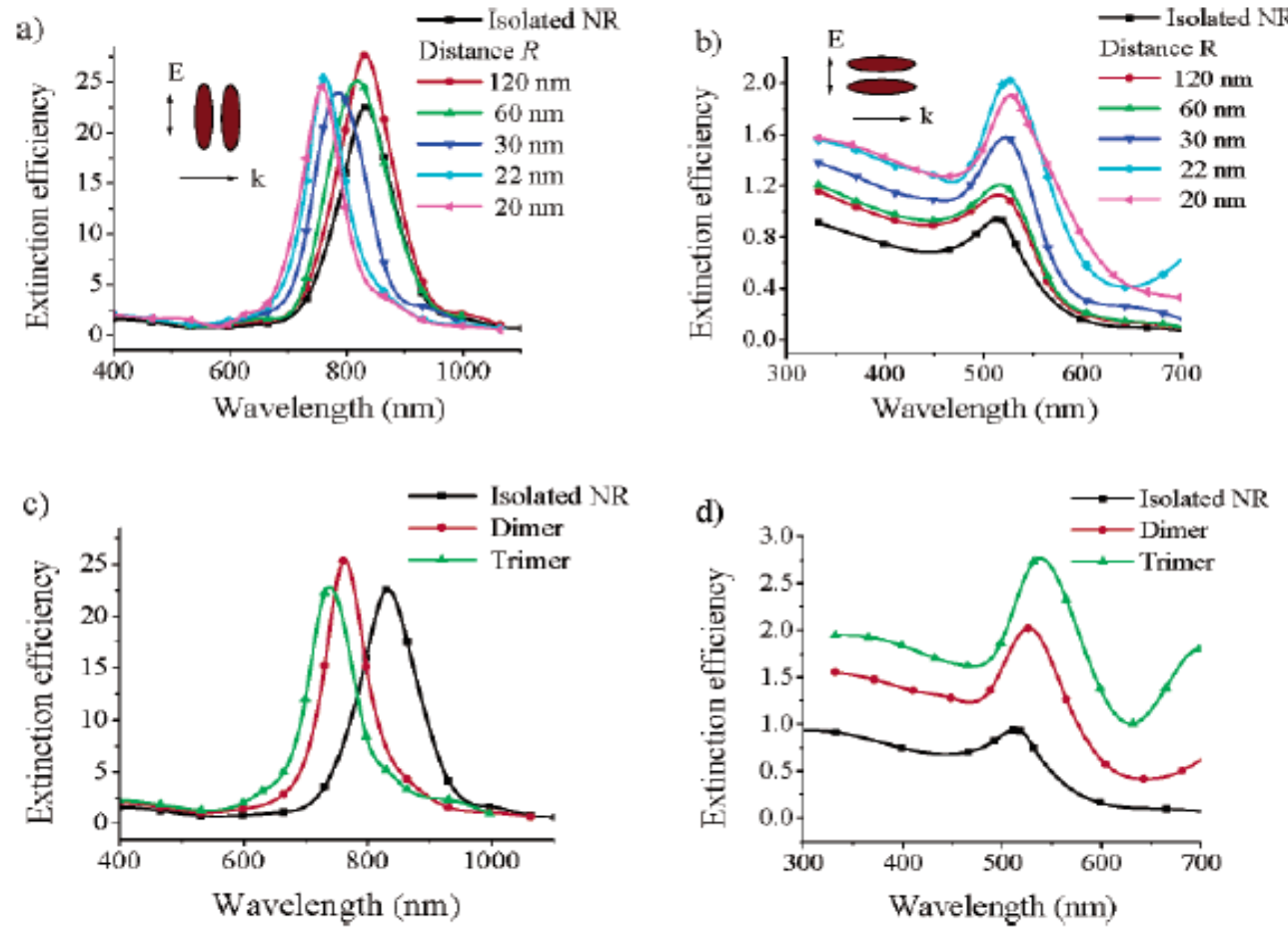
结果：金的结果与银类似，平行排列时SPR红移，垂直时蓝移，相互垂直是发生分裂。

[Plasmon Coupling of Gold Nanorods at Short Distances and in Different Geometries](#)
Alison M. Funston et al, NANO LETTERS (2009) Vol. 9, No. 4, 1651-1658

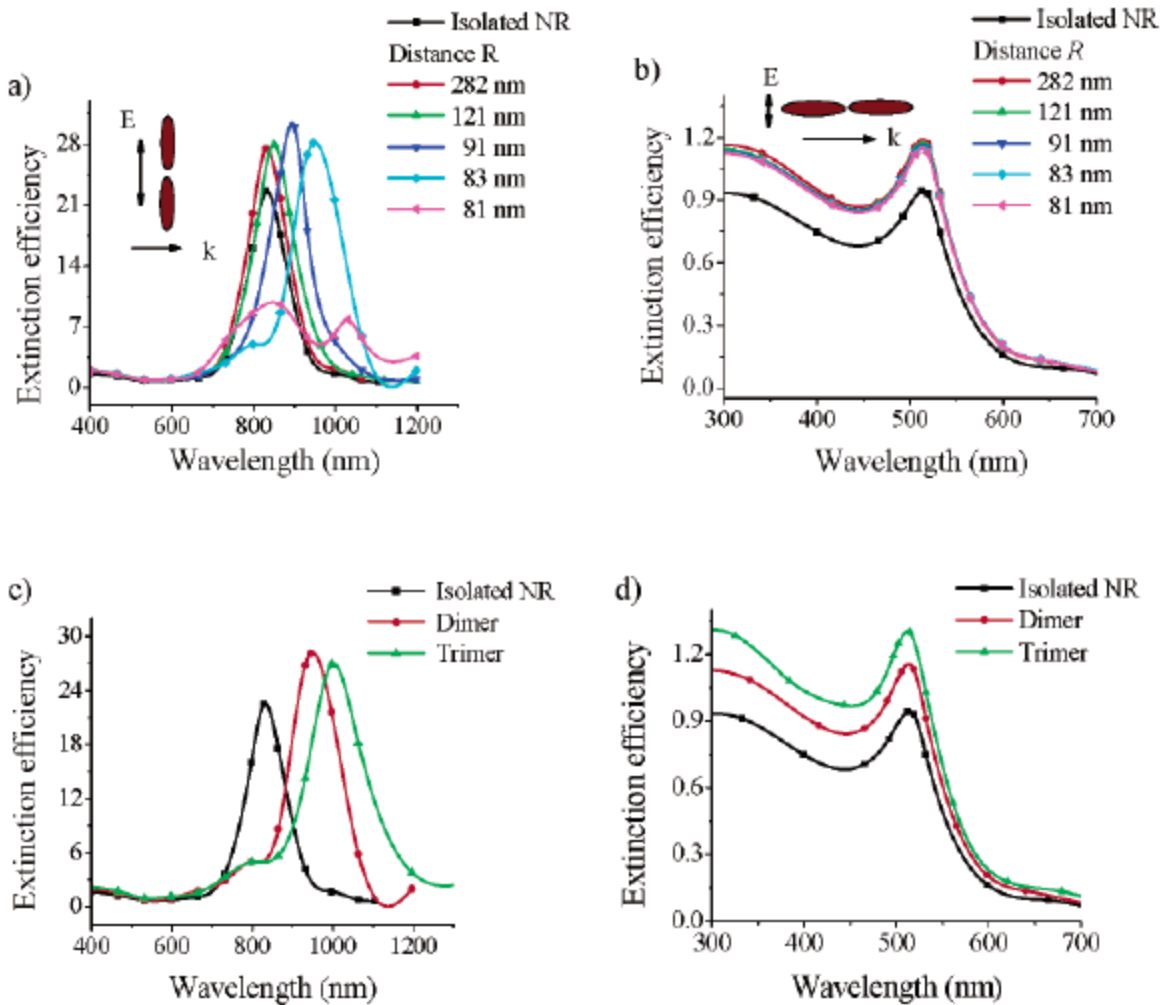
SPR的“能级”分裂图



百纳米量级金棒SPR耦合与金棒间距离的关系

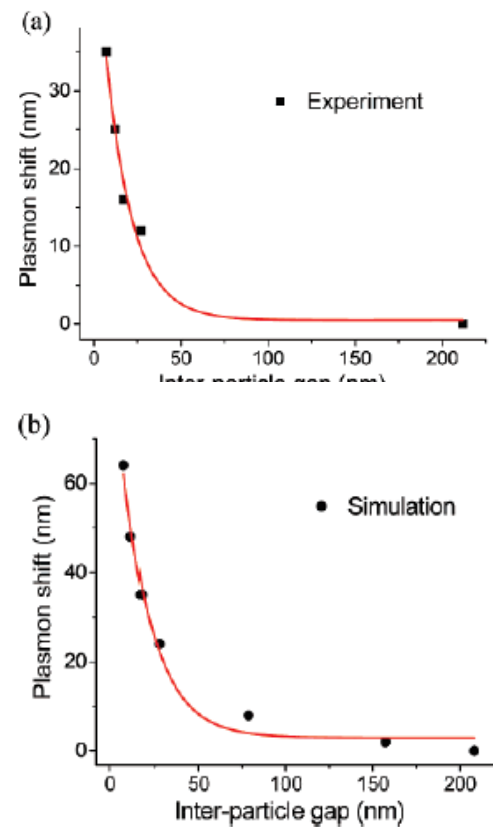
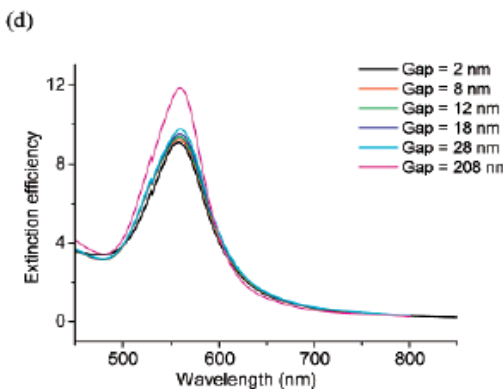
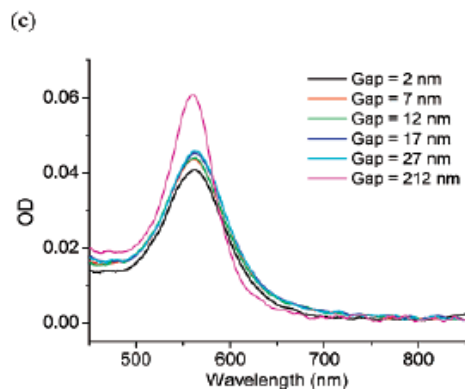
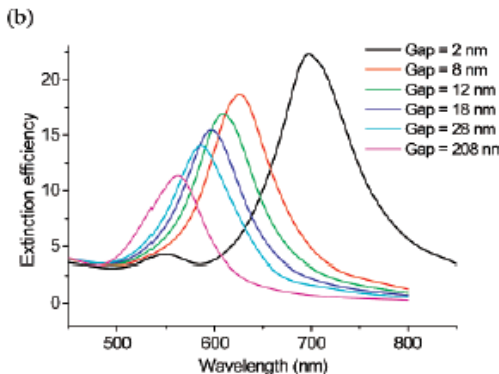
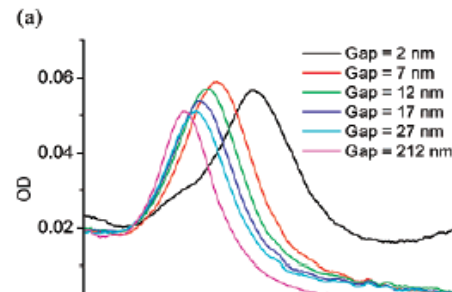


结果：在光场偏振垂直于纳米棒间的中心连线时，当棒间距离越近，蓝移得越远；当增加棒的个数时，蓝移得越远。



结果：在光场偏振平行于纳米棒间的中心连线时，当棒间距离越近，红移得越远；当增加棒的个数时，红移得越远。

纳米金属颗粒间SPR耦合的标度律



结果：从两个样品的吸收和消光峰以及理论和实验上共振峰移动规律，可以得到标度律

$$\frac{\Delta\lambda}{\lambda_0} \approx 0.18 \exp\left(\frac{-(s/D)}{0.23}\right)$$

[On the Universal Scaling Behavior of the Distance Decay of Plasmon Coupling in Metal nanoparticle Pairs: A Plasmon Ruler Equation](#)

Prashant K. Jain et al, NANO LETTERS (2007) Vol. 7, No. 7, 2080-2088

用纳米金球壳结构的SPR收集太阳能

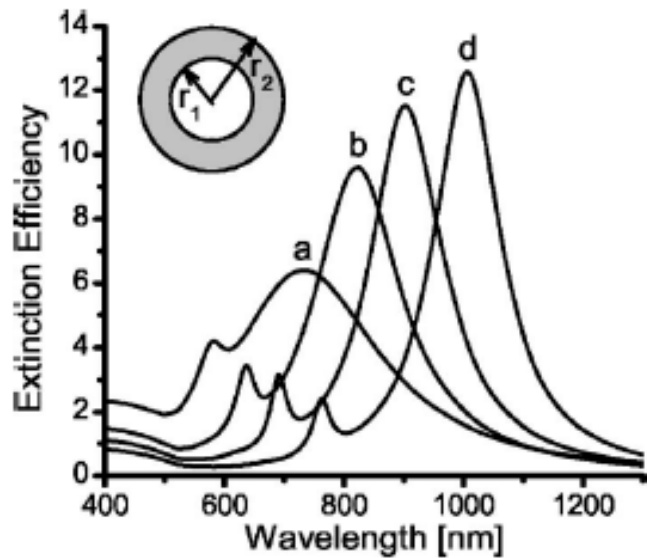
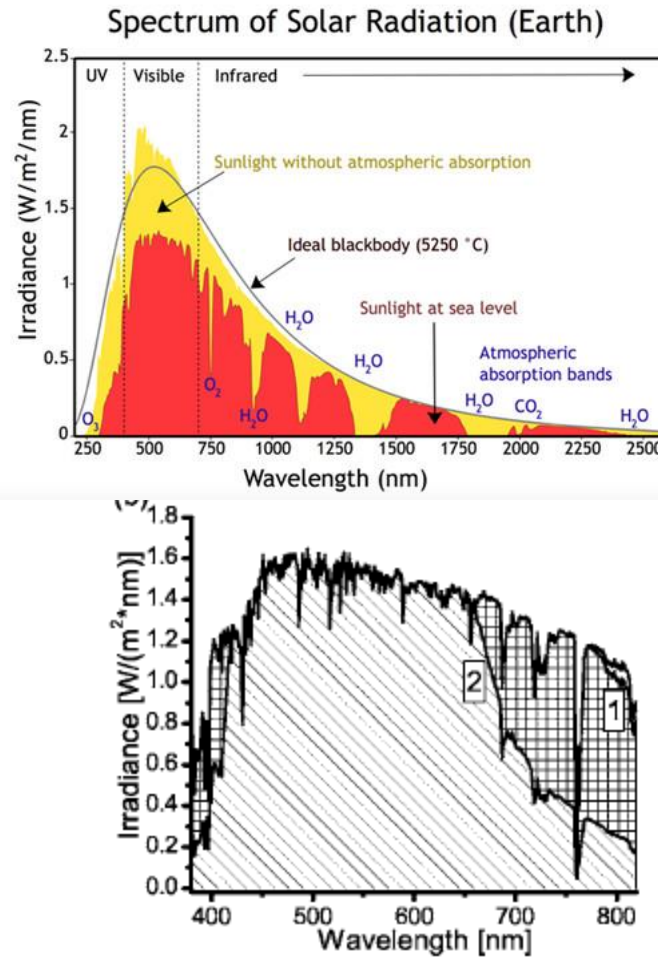
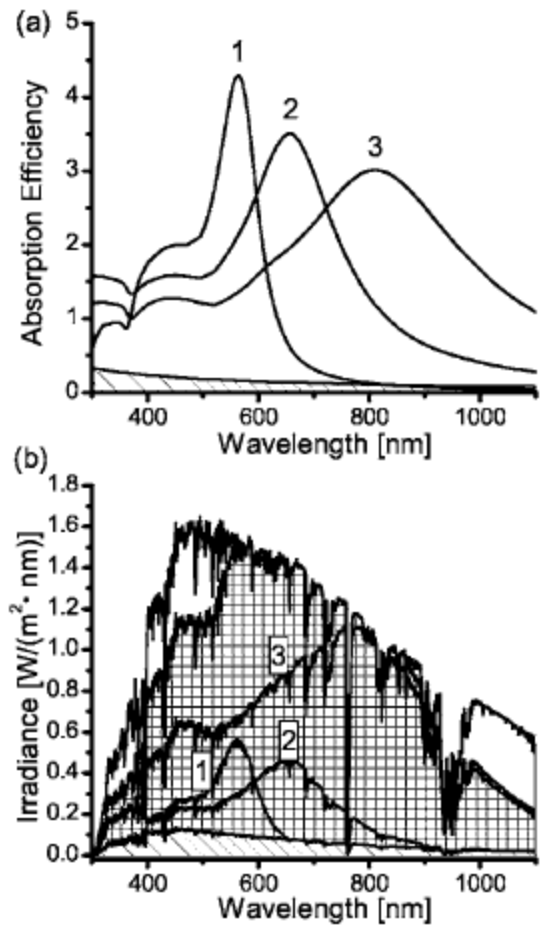


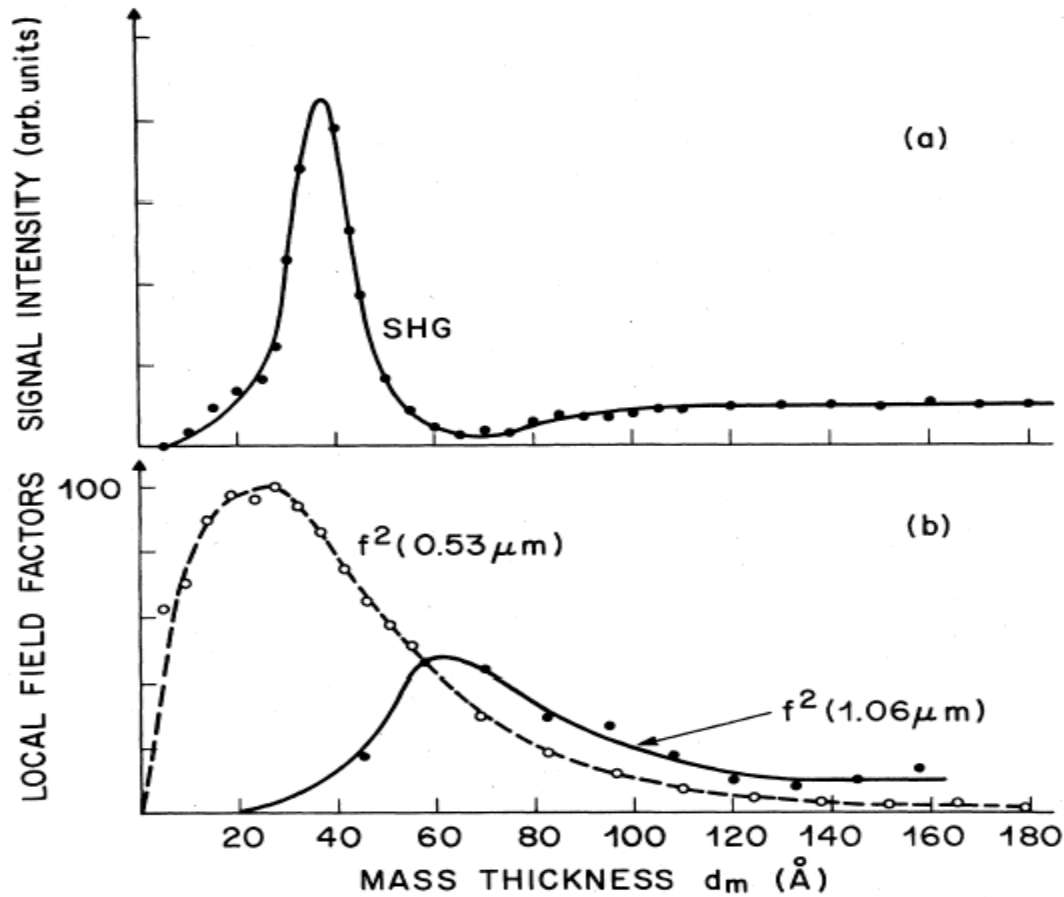
FIG. 1. Plasmon resonances of silica/Au nanoshell structures in water with $r_1=60$ nm and r_2 = (a) 80 nm, (b) 70 nm, (c) 67 nm, and (d) 65 nm, respectively.

结果：通过调节纳米金球壳的核壳比例，其SPR的吸收谱可以覆盖太阳光的区域，用于solar cell。



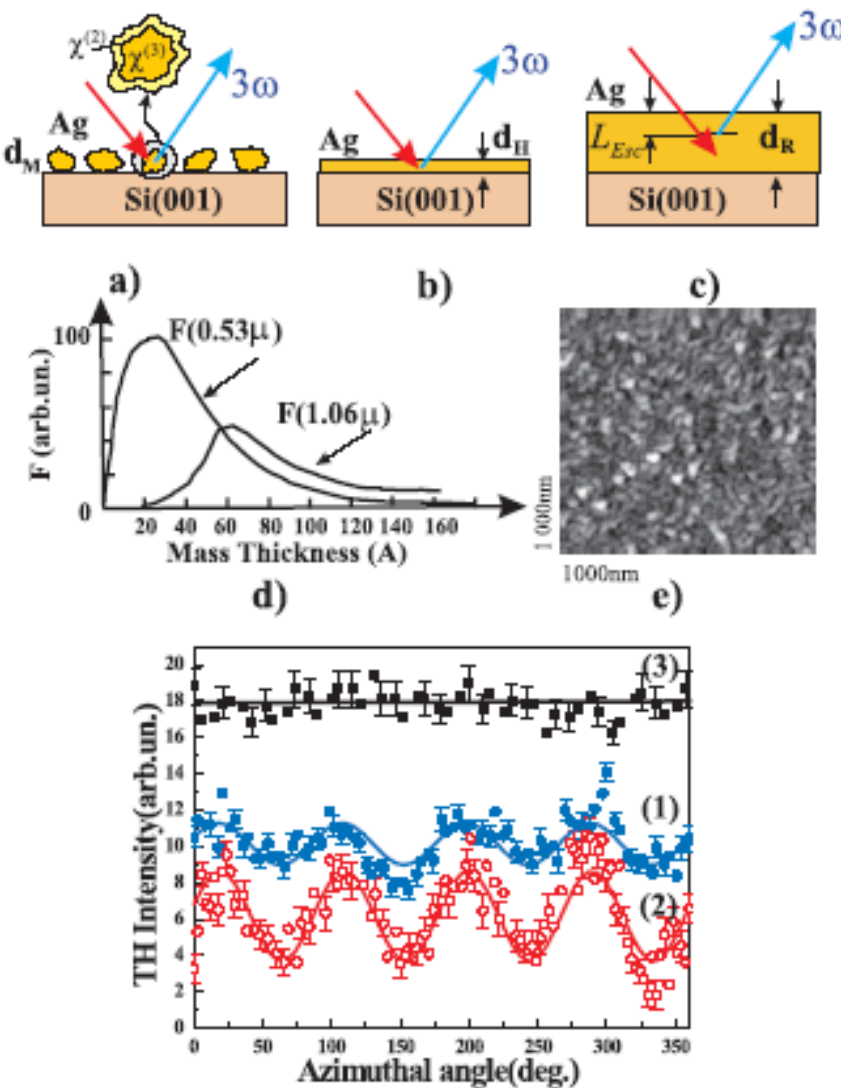
结果：将不同尺度的金或银球壳混合在一起，使其共振谱覆盖太阳光区域（200nm~1500nm），用于solar cell 能量收集。

纳米银膜上岛状结构的SPR实现二次谐波



结果：SPR用于非线性光学的典型例子。可以看到，
1060nm处激发，在530nm处产生了二次谐波。

纳米银岛上利用SPR实现三次谐波



结果：SPR用于非线性光学的又一例子。入射波长1060nm，可以看到，(d)中产生的530nm二次谐波，(f)中产生了355nm的三次谐波，厚度40nm时增益最强。

利用纳米金球的SPR耦合实现多波混频

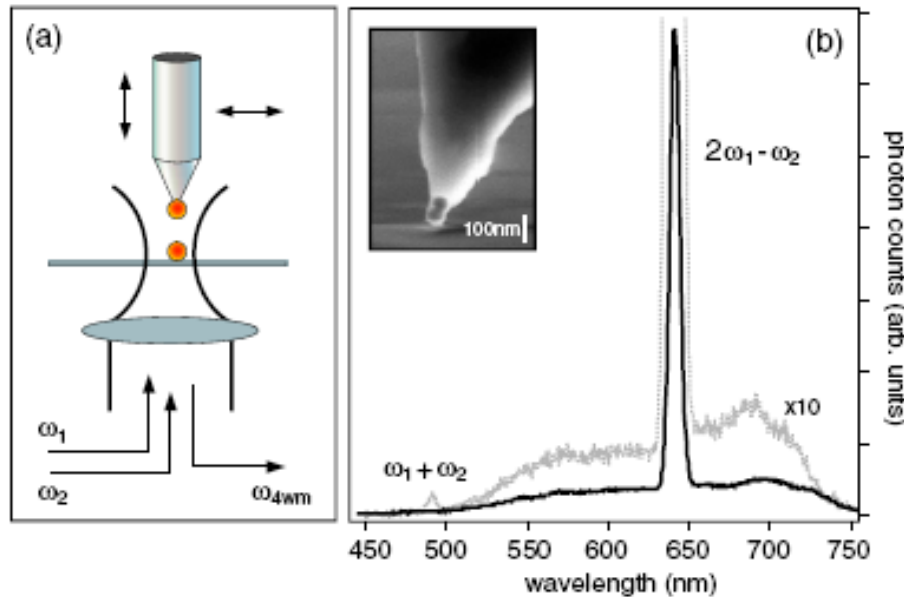
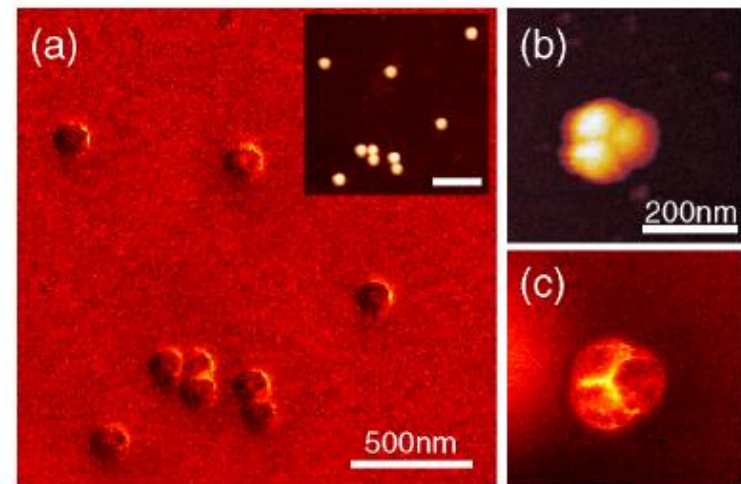
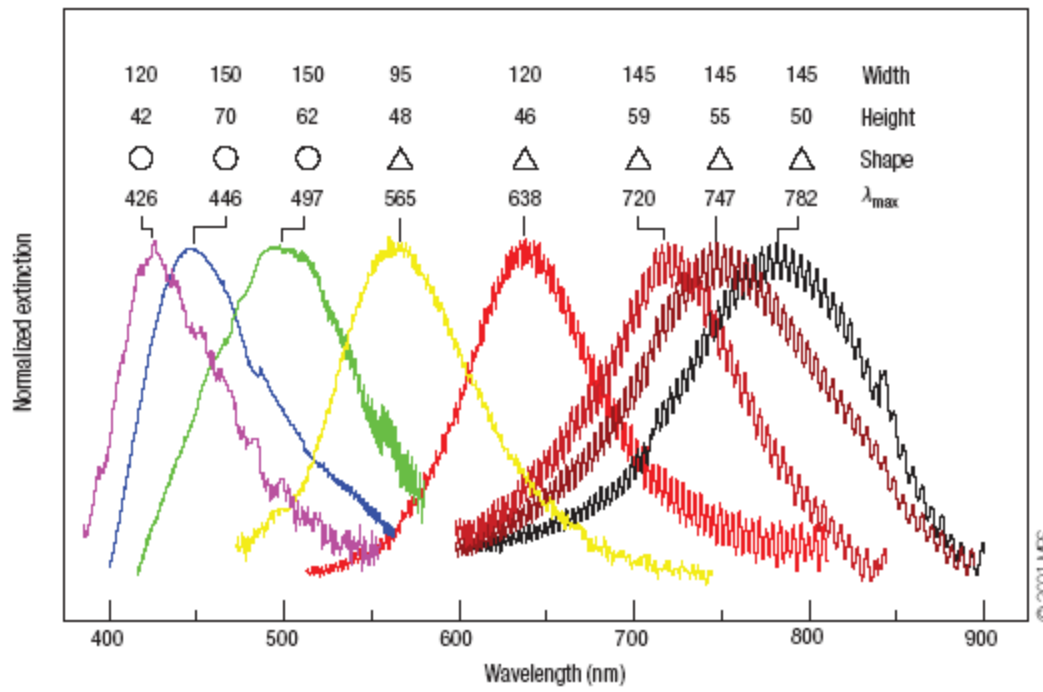


FIG. 1 (color online). (a) Sketch of the experiment. The non-linear signal at frequency $2\omega_1 - \omega_2$ is measured as a function of the relative position between individual gold nanoparticles. (b) Emission spectrum from a dimer of two identical particles (60 nm diameter), excited with pulsed lasers of wavelength $\lambda_1 = 830$ nm and $\lambda_2 = 1185$ nm. The superimposed dotted curve shows the spectrum for two particles of unequal size (60 nm and 100 nm diameter). The inset shows an SEM image of two gold particles attached to a pointed optical fiber.



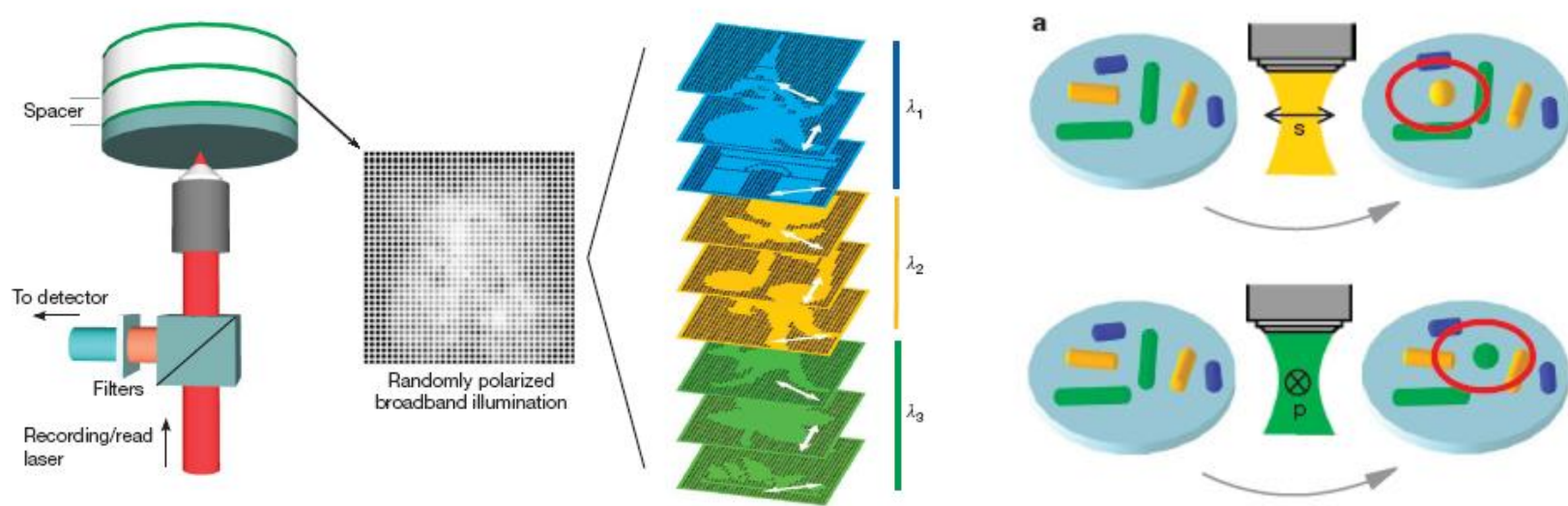
结果：SPR用于非线性光学
的例子。实现多波混频。

利用纳米金属颗粒SPR实现生物传感

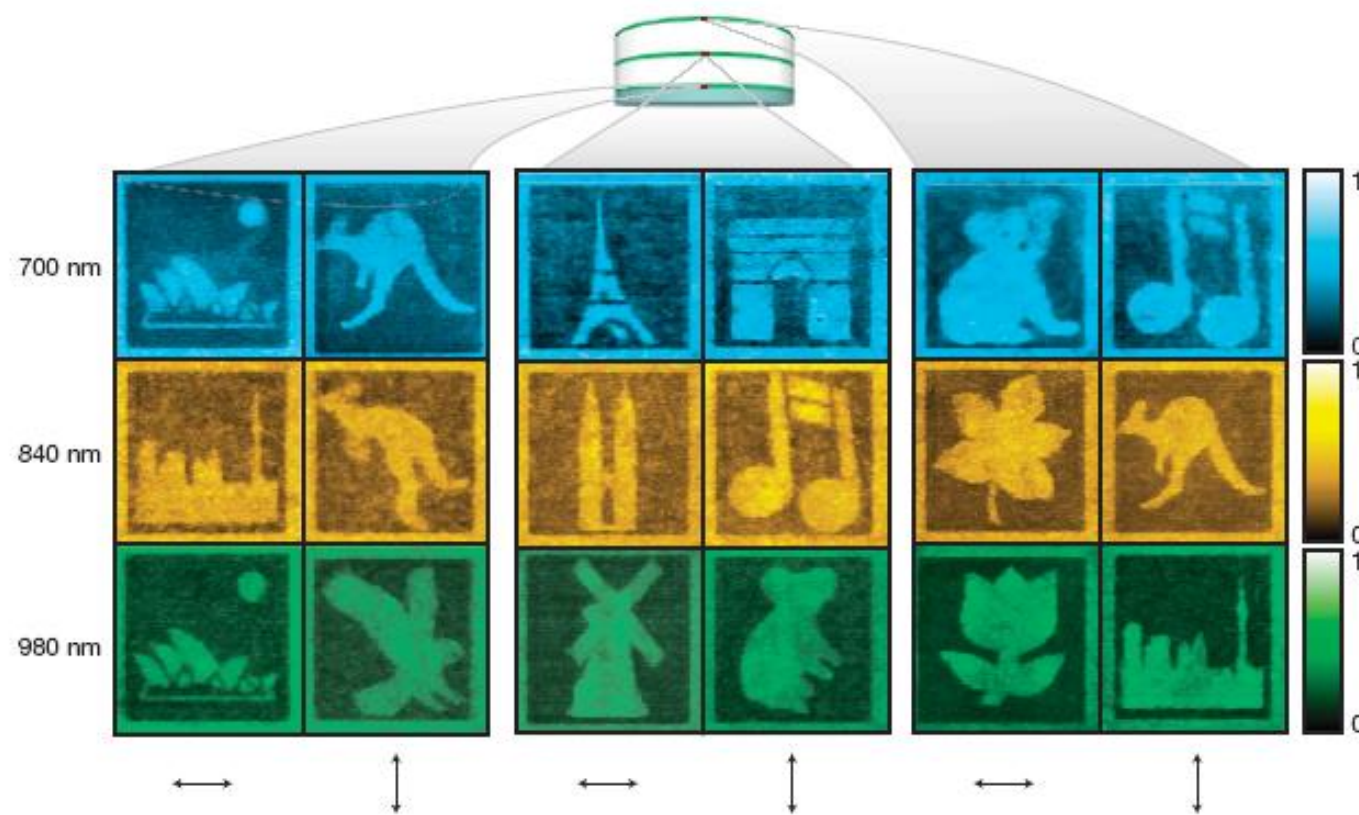


用纳米近颗粒的SPR实现数据存储

Aim to: minimize the recording storage by multiplexing:
wavelength, polarization, and spatial dimensions



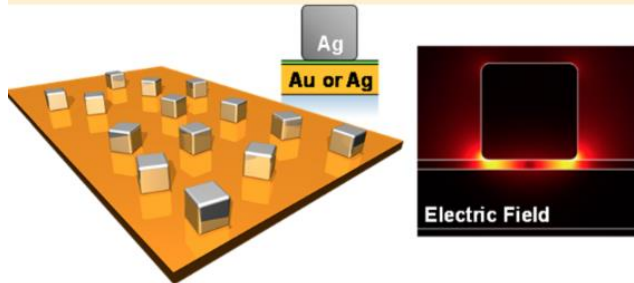
Results:
realizing five-dimensional data recording by SPR



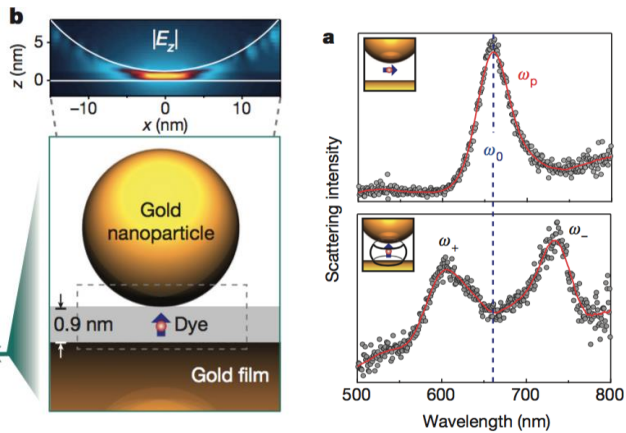
Results:

realizing five-dimensional data recording by SPR

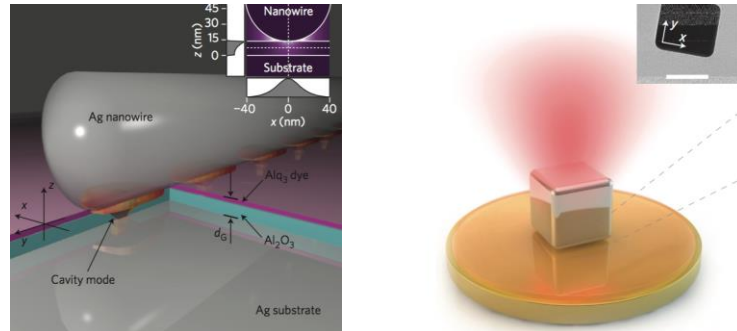
间隙表面等离激元及应用



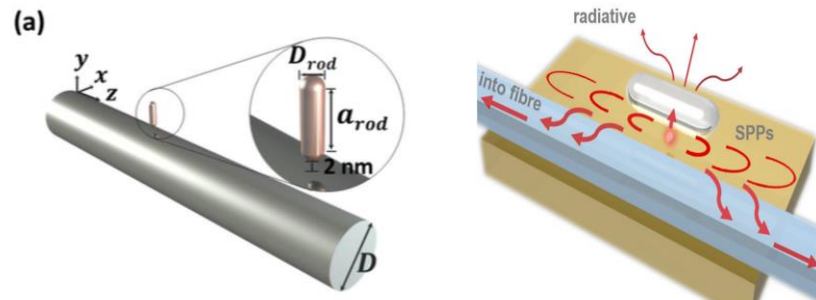
Gap surface plasmon
Nano Lett. 13, 5866 (2013)



Strong coupling
Nature 535, 127 (2016)



Enhanced spontaneous emission
Nat. Photon. 6, 459 (2012)
Nat. Photon. 8, 835 (2014)



Weak: Single photon collection
PRL 114, 193002 (2015)

Strong: Evanescent vacuum
PRL 118, 073604 (2017)



4.3 周期性结构中SPP性质

Comparisons

Photonic crystals:

spatially periodic dielectric structures

Photonic band gaps with a period \sim wavelength

To transmit and reflect light within specific frequencies

Properties tunable by the periodicity or refraction index

Polaritonic crystals: (periodical metallic nanostructure)

periodic arrangement of defects on a metal-dielectric interface

SPP band gaps with surface structure \sim wavelength of SPP

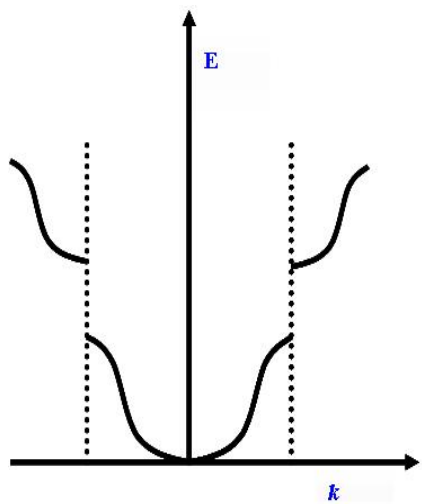
Scattering of SPP into SPP or SPP into light

(Extraordinary transmission from visible to microwave)

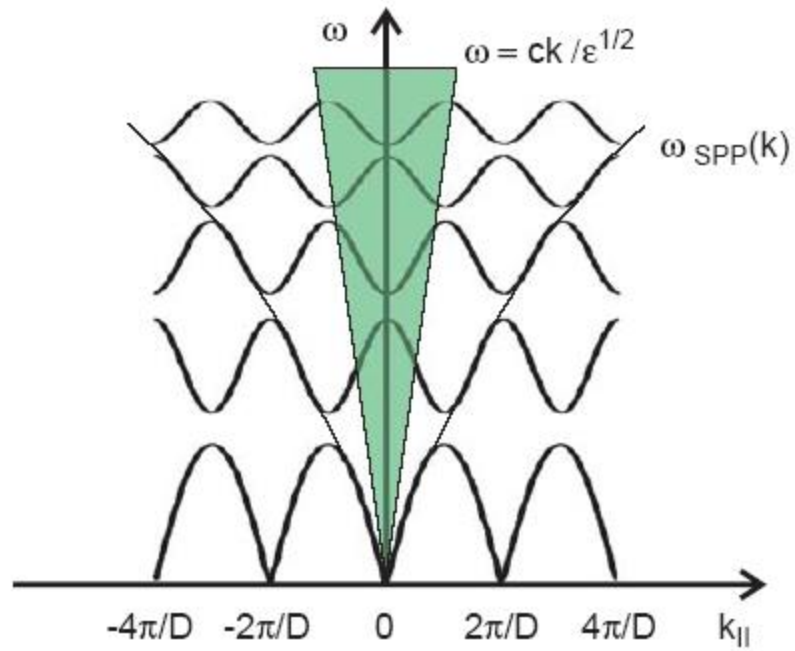
Properties tunable by the surface features

Dispersion relations

Photonic crystals:



Polaritonic crystals:



$$k_{sp} = k_x \pm nG_x \pm mG_y \quad G_x = G_y = 2\pi/a_0$$

Ebbesen Group's work

Extraordinary transmission though subwavelength hole array

T. W. Ebbesen *et al.*, Nature (London) **391**, 667 (1998);
H. F. Ghaemi *et al.*, Phys. Rev. B **58**, 6779 (1998); T. J. Kim *et al.*, Opt. Lett. **24**, 256 (1999); D. E. Grupp *et al.*, Adv. Mater. **11**, 860 (1999).

Experiments

L. Martín-Moreno, et al, PRL **86** 1114 (2001)

Theory

Beaming light from a subwavelength aperture

H J Lezec; et al, *Science*, **297** (5582) , 820 (2002)

Hole array + aperture, Hole array + molecular, SPP guiding

PRL **90**, 167401 (2003)

PRL **90**, 213901 (2003)

PRL **92**,107401(2004)

PRB **71**,035424 (2005)

PRL **95**,046802(2005)

Review Article
Nature **424**,824 (2003)

Extraordinary optical transmission through sub-wavelength hole arrays

Bottleneck: low light transmittivity of apertures smaller than the wavelength of incident photon

Hole arrays in silver film:
metal film thickness t
Periodicity of holes a_0
Scale of holes d

Results:
Extraordinary transmission
Maximum at $\lambda/d \sim 10$
Influence of t (in APL)

Explanation:
Coupling of light and plasmons

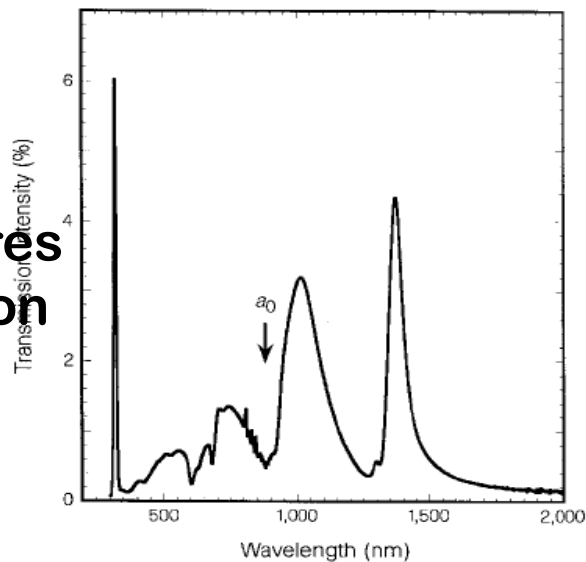
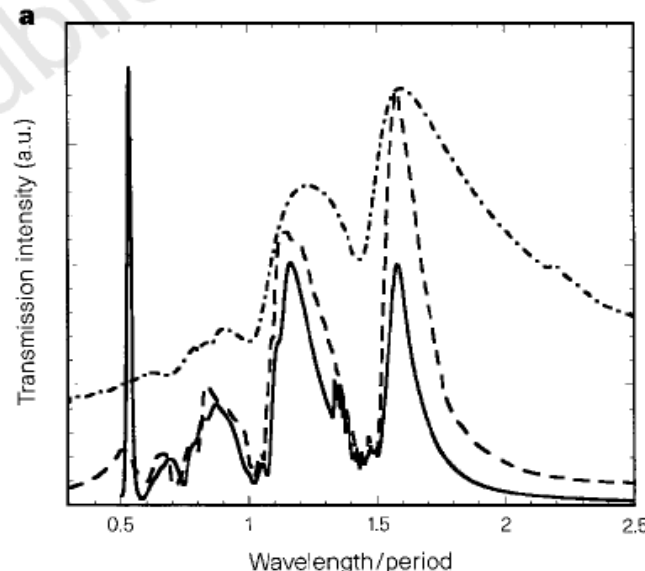


Figure 1 Zero-order transmission spectrum of an Ag array ($a_0 = 0.9 \mu\text{m}$, $d = 150 \text{ nm}$, $t = 200 \text{ nm}$).



Dispersion relations

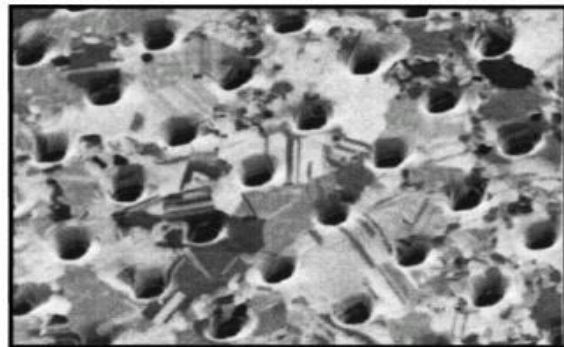
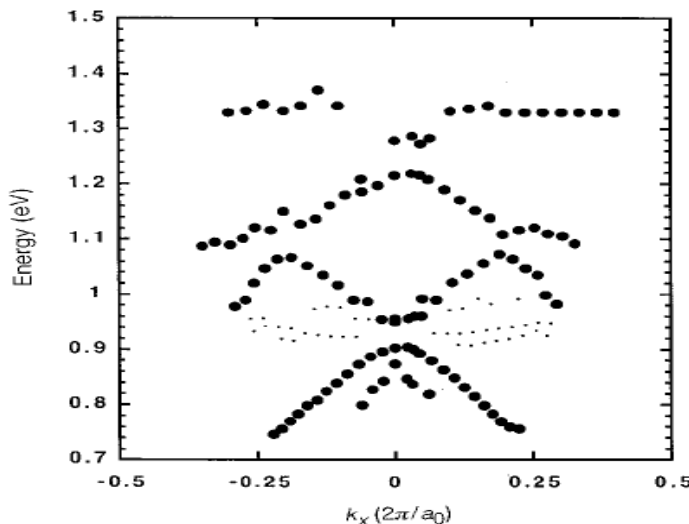
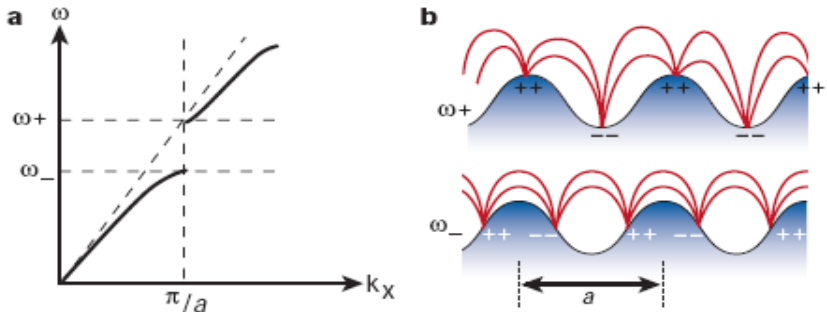


FIG. 1. Focused ion beam image of a two-dimensional hole array in a polycrystalline silver film, with film thickness $t=200$ nm, hole diameter $d=150$ nm, and period $a_0=900$ nm.



Box 3

Surface plasmon bandgaps



Periodic texturing of the metal surface can lead to the formation of an SP photonic bandgap when the period, a , is equal to half the wavelength of the SP, as shown in the dispersion diagram (a). Just as for electron waves in crystalline solids, there are two SP standing wave solutions, each with the same wavelength but, owing to their different field and surface charge distributions, they are of different frequencies. The upper frequency solution, ω_+ , is of higher energy because of the greater distance between the surface charges and the greater distortion of the field, as shown schematically in b. SP modes with frequencies between the two band edges, ω_+ and ω_- , cannot propagate, and so this frequency interval is known as a stop gap. By providing periodic texture in two dimensions, SP propagation in all in-plane directions can be blocked, leading to the full bandgap for SPs. At the band edges the density of SP states is high, and there is a significant increase in the associated field enhancement.

Theory of Extraordinary Optical transmission

surface impedance boundary condition $\lambda \geq L \gg d.$

Theory agrees experiments well, parameters are reasonable

Enhanced transmission is due to tunneling through surface plasmons.

For small thickness h , the photon then goes back and forth several times inside the hole, building up coherent constructive interference in the forward direction much as would occur in electron resonant tunneling.

For larger h , the photon can make fewer round-trips inside the hole before being radiated to infinity, and the concept of plasmon molecule becomes less well defined.

For even larger h , the process is more like sequential tunneling, where the incoming photon gets trapped in a SP, tunnels to the SP at the other interface, and then couples to the outgoing radiative mode and exits.

Effects of hole depth on light transmission

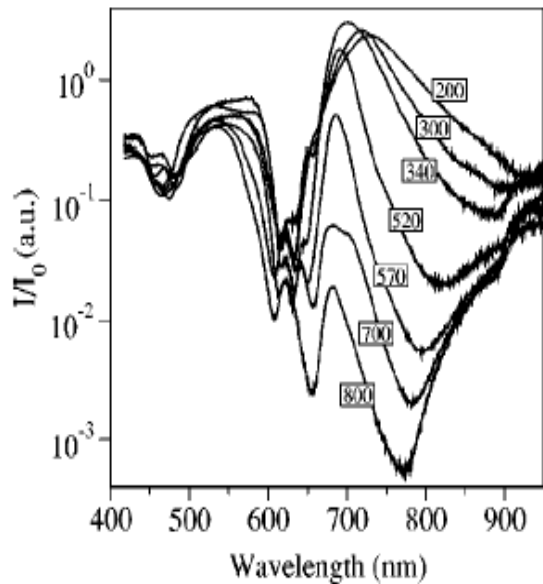


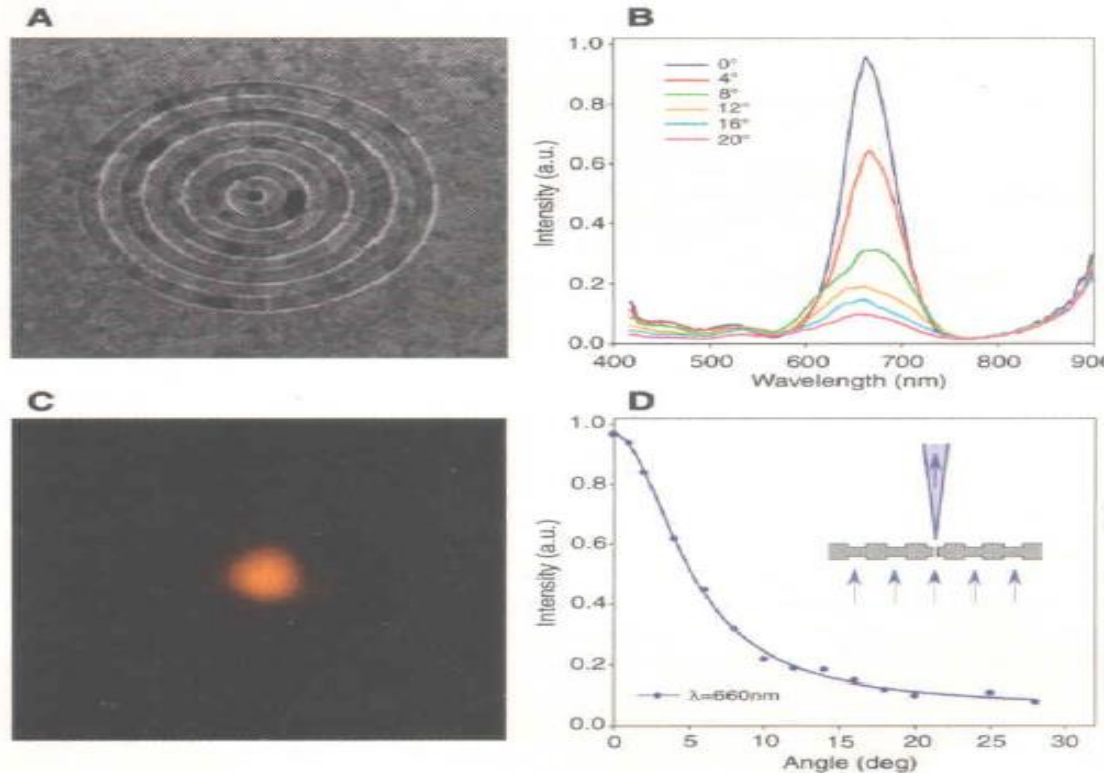
FIG. 1. Zero-order transmission spectra at normal incidence for square arrays of cylindrical holes ($d=300$ nm, $P=600$ nm) for a range of hole depths h , as indicated on each curve.

$$I(h, \lambda_p, d) \propto \exp\left[-\frac{4\pi h}{\lambda_p} \sqrt{\left(\frac{\lambda_p}{1.7d}\right)^2 - 1}\right].$$

For shallow holes, two SPs modes couple as the resonant passage of light through the array.
For deeper holes, the uncoupled SP modes therefore transmission falls exponentially as the film gets thicker.

Beaming light from a subwavelength aperture

Fig. 1. (A) FIB micrograph image of a bull's eye structure surrounding a cylindrical hole in a suspended Ag film (groove periodicity, 500 nm; groove depth, 60 nm; hole diameter, 250 nm; film thickness, 300 nm). (B) Transmission spectra recorded at various collection angles for a bull's eye structure on both sides of a suspended Ag film (groove periodicity, 600 nm; groove depth, 60 nm; hole diameter, 300 nm; film thickness, 300 nm). The tail above 800 nm is an artifact of the spectral measurement. The structure is illuminated at normal incidence with unpolarized collimated light. The spectra were measured using a Nikon TE200 microscope coupled to an Acton monochromator and a Princeton Instruments CCD (charge-coupled device) camera. (C) Optical image of the sample of (A) illuminated from the back at its wavelength of peak transmission ($\lambda_{\max} = 660$ nm) using a 50-nm band-pass filter. (D) Angular transmission-intensity distribution derived from the spectra of (B) at λ_{\max} . (Inset) Schematic diagram of the structure and the beam divergence and directionality of the transmitted light at λ_{\max} in the far field.



Highly Directional Emission from a Single Subwavelength Aperture Surrounded by Surface Corrugations

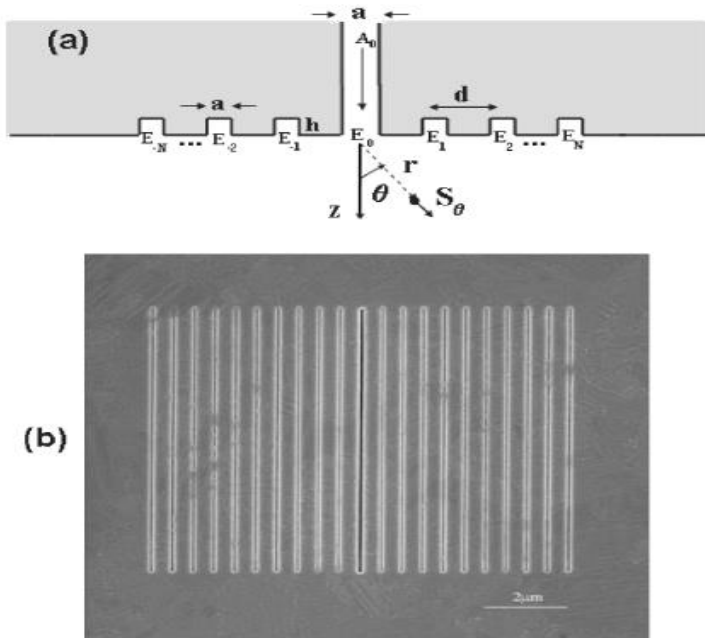


FIG. 1. (a) Schematic picture for the system analyzed: single slit surrounded in the exit surface by a finite array of grooves. In this paper all indentations have width a , and grooves have depth h . (b) Focused-ion-beam image of the exit surface of a slit in a Ag film, with $N = 10$ grooves at each side, and nominal values $a = 40$ nm, $d = 500$ nm, and $h = 100$ nm.

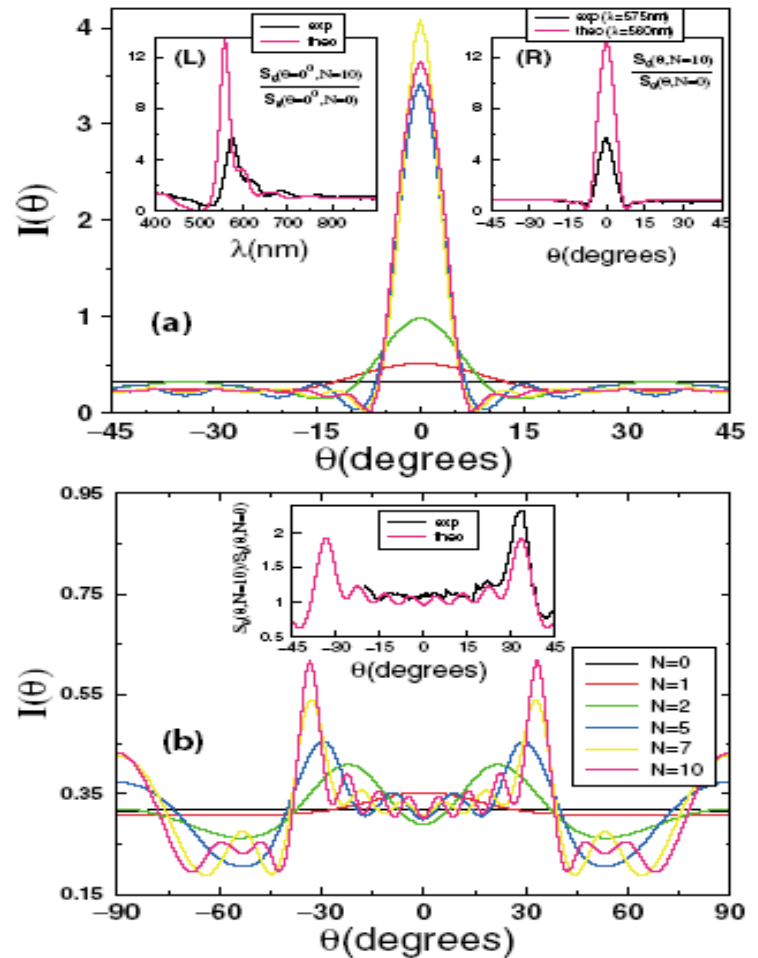


FIG. 2 (color). Calculated angular transmission distribution, $I_N(\theta)$, for $\pm N$ grooves surrounding a central slit. Geometrical parameters as in Fig. 1(b). (a) $\lambda = 560$ nm; (b) $\lambda = 800$ nm. Insets show the comparison between measured and calculated $\Delta S(\theta) = S_\theta(\theta, N = 10)/S_\theta(\theta, N = 0)$. (L): $\Delta S(0)$ vs λ . (R): $\Delta S(\theta)$ at maximum forward beaming ($\lambda^{\text{theo}} = 560$ nm, $\lambda^{\text{exp}} = 575$ nm). Inset to (b): $\Delta S(\theta)$ for $\lambda = 800$ nm.

PRL 90, 167401 (2003, ebbesen)

PRL 90, 213901 (2003)(subwavelength slit)

Role of SPP in subwavelength hole arrrys

Transmittance maxima are associated with both reflectance minima and absorption maxima

(i) Incident light couples to an SPP mode supported by the surface facing the incident light. The enhanced field associated with an SPP mode increases the probability of transmission through the holes, where it is again scattered by the periodic array to produce light. (ii) Incident light cannot couple to an SPP mode on the incident side, instead matching conditions allow light that is weakly transmitted through the array to couple to an SPP mode on the far side; the enhanced electric field associated with the SPP mode increases the probability of transmission, and subsequent scattering again results in transmitted light. (iii) Matching conditions allow processes (i) and (ii) to take place simultaneously.

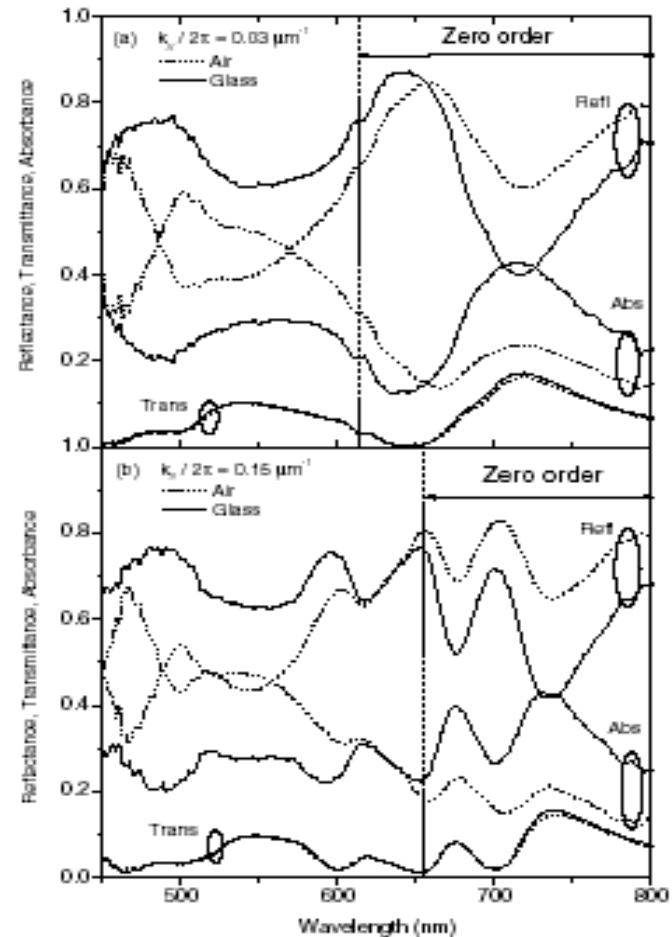


FIG. 4. Transmittance, reflectance, and inferred absorbance spectra for p -polarized incident light at in-plane wave vectors of $0.03 \mu\text{m}^{-1}$ (a) and $0.15 \mu\text{m}^{-1}$ (b).

Sambles Group's work

Full Photonic Band Gap for Surface Modes in the Visible

PRL 77,2670(96) 94 experiment

PRB 54 6227(96) 96 theory and a good review

Influence of depth of grating on band gaps

PRL 79, 3978 (97)

PRL 80, 5667 (98)

PRB 65,125415(02) theory and experiment

Extraordinary transmission in microwave region

APL 77,2789 (00)

PRL 89,063901 (02)

APL 84,849 (04)

Other works

Full Photonic Band Gap for Surface Modes in the Visible

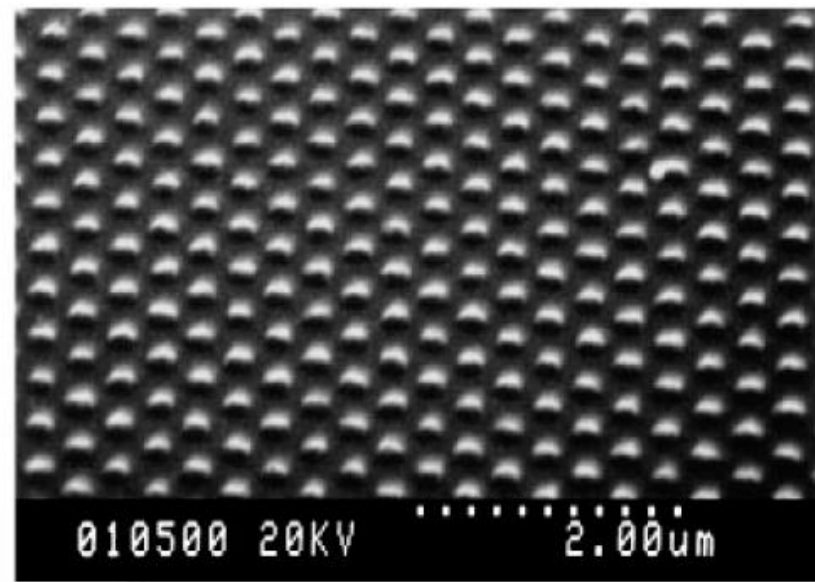
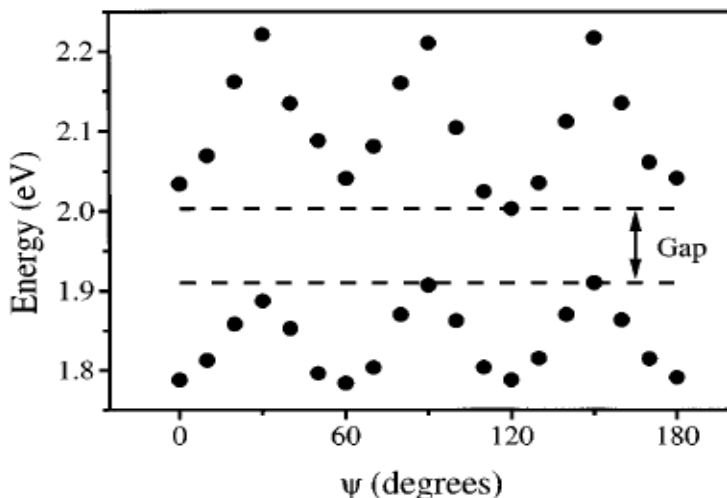
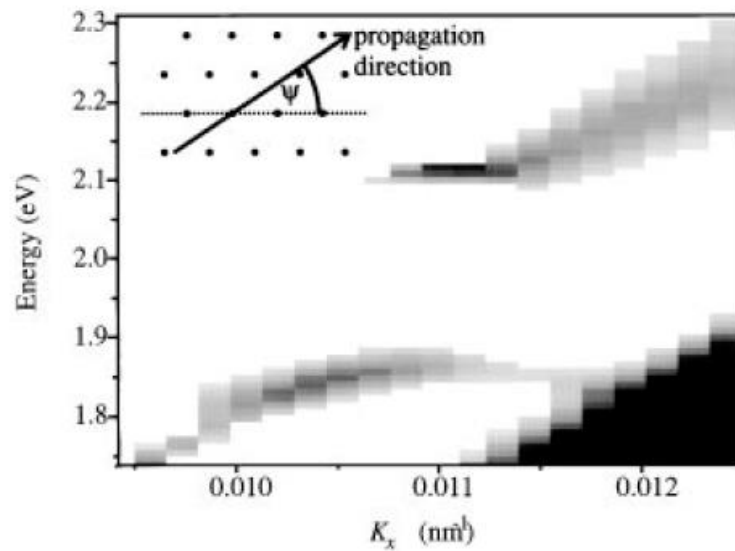


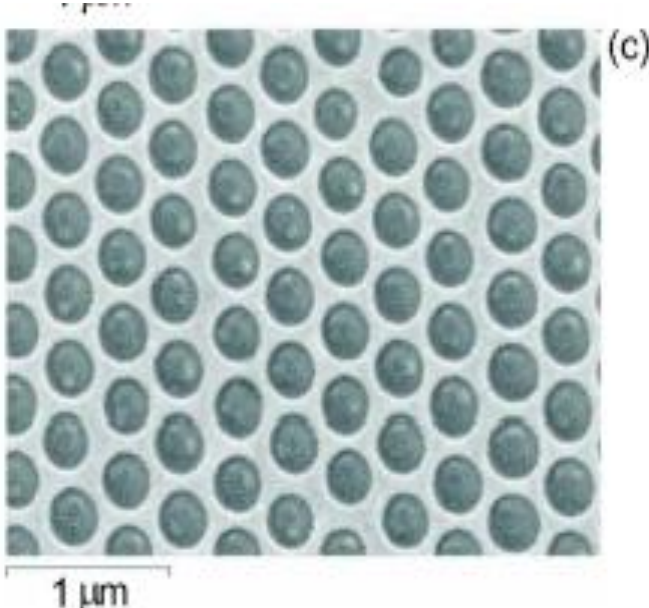
FIG. 1. A scanning electron micrograph of the hexagonal array of dots. The dots are composed of photoresist on a glass substrate. The surface has been coated with a thin film of silver to support the propagation of SPPs.

Period **300nm**
Dot radius **100nm**
Silver film **40nm**

Other several works

Transition from localized surface plasmon resonance to extended surface plasmon-polariton as metallic nanoparticles merge to form a periodic hole array

Main results



For individual metallic nanoparticals,
Localized SPPs dominate.

For adjacent metallic nanoparticals,
A small gap appears.

For a continues metallic thin films,
Extended SPPs dominate.

Transmission of Light through a Single Rectangular Hole

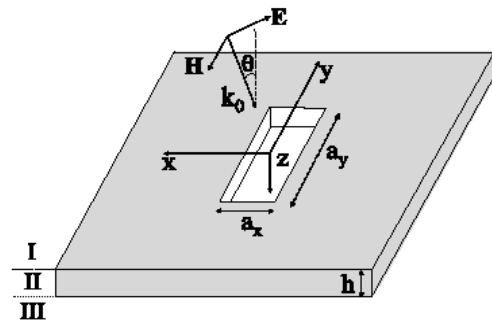


FIG. 1. Diagram of a single rectangular hole of sides a_x and a_y perforated on a metal film of thickness h . The structure is illuminated by a p -polarized plane wave with its angle of incidence with respect to the normal being θ .

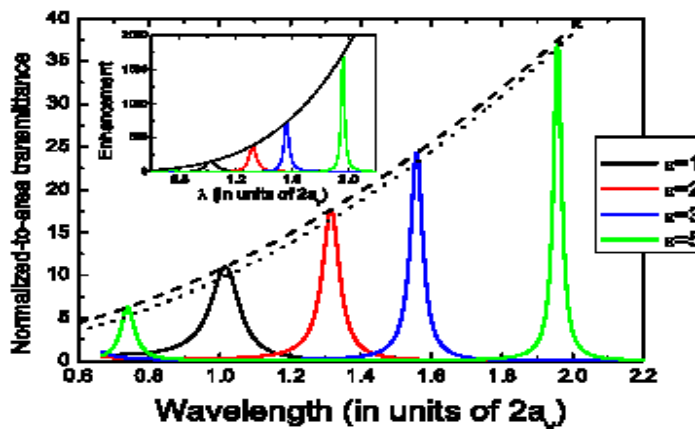


FIG. 3 (color online). T for a normal incident plane wave versus wavelength for a rectangular hole with $a_y/a_x = 10$ and different values of ϵ inside the hole. Metal thickness is $h = a_y/3$. Dashed and dotted lines show the behavior of Eqs. (5) and (6), respectively. Inset: enhancement of the E -field intensity obtained for the previous cases; black curve renders Eq. (7).

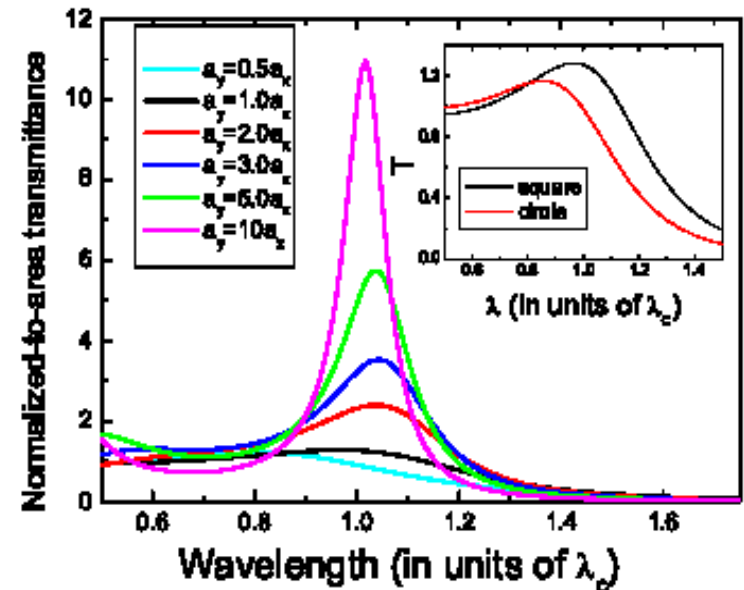


FIG. 2 (color online). Normalized-to-area transmittance (T) versus wavelength (in units of the cutoff wavelength, $\lambda_c = 2a_y$), for a normal incident plane wave impinging on a rectangular hole, for different ratios a_y/a_x . Metal thickness is $h = a_y/3$. For comparison, the inset shows T versus wavelength for a single square (black line) and circular (red line) holes.

Theory

111

纳米金椭球链中的超窄几何共振

参数：

金颗粒尺寸： $60 \times 40 \times 15 \text{ nm}^3$

折射率 $n=1.46$, 周期 $h=519 \text{ nm}$

原理：

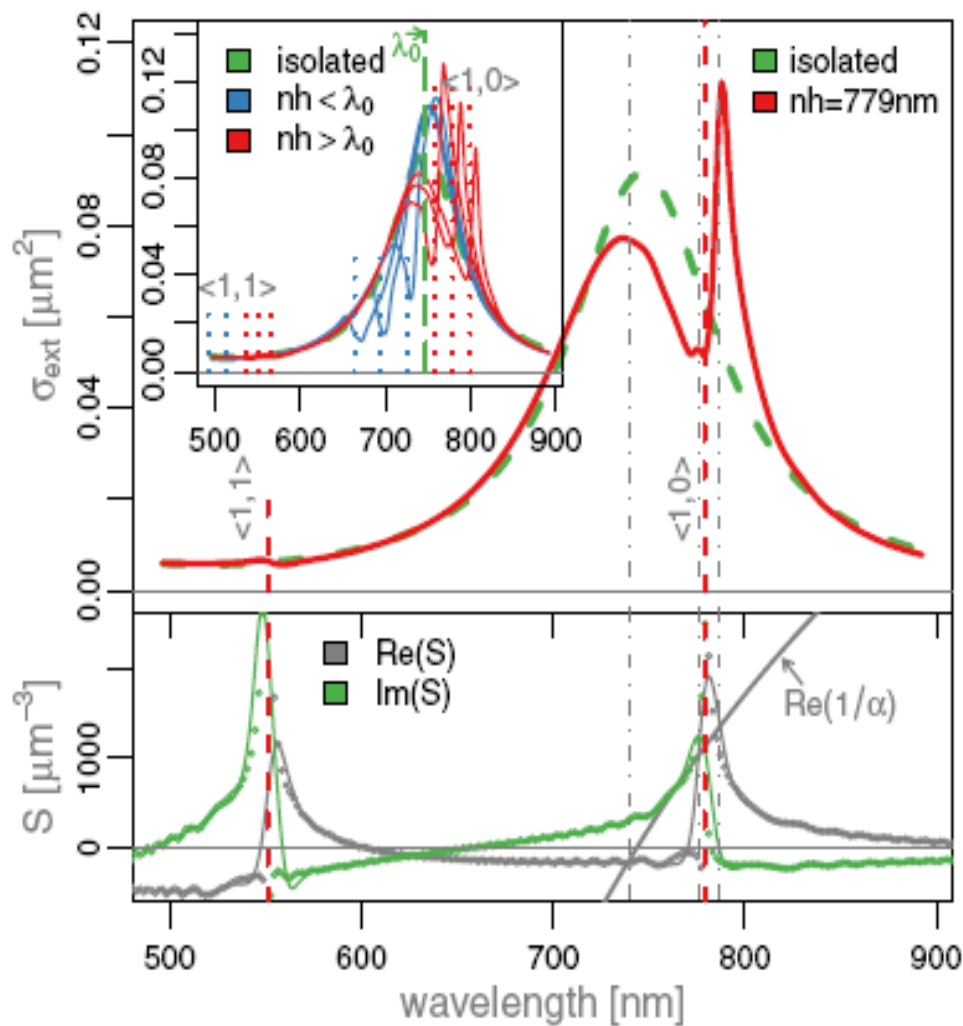
超窄几何峰的出现是由于近场的衍射效应造成。

极化率： $\alpha^* = \frac{1}{1/\alpha - S}$

$$S = \sum_{\text{dipoles}} e^{ikr} \left[\frac{(1 - ikr)(3\cos^2\theta - 1)}{r^3} + \frac{k^2 \sin^2\theta}{r} \right],$$

$$\sigma_{ext} \propto k \operatorname{Im}(\alpha^*)$$

$1/\alpha$ 与 S 实部的交点导致消光极大。



本章总结：

一方面：从历史发展的角度，看到SPP的发展历程、前沿和里程碑工作，从而对plasmonics有个全面的了解

另一方面：以波导、individual结构和周期性结构为线索，梳理plasmonics 在特定方向的重要进展

